MECHANISM-BASED INHIBITION OF BACTERIAL AND MITOCHONDRIAL TRYPTOPHANYL-TRNA SYNTHESASES IS POTENTIATED BY MG^{2+}•ATP

Tishan L. Williams

A dissertation submitted to the faculty of the University of North Carolina at Chapel Hill in partial fulfillment of the requirements for the degree of Doctor of Philosophy in the Department of Biochemistry and Biophysics, School of Medicine.

Chapel Hill
2015

Approved by:

Charles Carter, Jr.

Hengming Ke

Howard Fried

Lorena Beese

ABSTRACT

Tishan L. Williams: Mechanism-based Inhibition of Bacterial and Mitochondrial Tryptophanyl-tRNA Synthesases is Potentiated by Mg^{2+}•ATP
(Under the direction of Charles W. Carter, Jr.)

Eukaryotes have distinct nuclear genes for tryptophanyl-tRNA synthetase (TrpRS) enzymes targeted by N-terminal sequence variations to the cytoplasm (H_c) and mitochondria (H_{mt}) that share only 14% sequence identity. Indolmycin, a natural tryptophan analog, competes with tryptophan for binding to tryptophanyl-tRNA synthetase (TrpRS) enzymes. Although bacterial and eukaryotic cytosolic TrpRSs have comparable affinities for tryptophan, K_M ~2 μM, eukaryotic cytosolic TrpRS enzymes are able to evade inhibition by indolmycin. Tryptophan binding to *Bacillus stearothermophilus* (Bs) TrpRS is largely promoted by hydrophobic interactions and recognition of the indole nitrogen by the side chain of Asp 132. By contrast, H_cTrpRS complements non polar interactions for tryptophan binding with electrostatic and hydrogen bonding interactions, which we show by modelling are inconsistent with indolmycin binding. Our crystallographic and inhibition kinetics data show the non-reactive analog indolmycin can recruit unique polar interactions to form an active-site metal coordination that lies off the normal mechanistic path, enhancing affinity to BsTrpRS and other prokaryotic TrpRS enzymes by 1500-fold over its tryptophan substrate. The Mg^{2+} ion in the inhibited complex forms significantly closer contacts with triphosphate oxygen atoms of ATP and three water molecules than occur in the catalytically-competent pre-transition state (preTS). Indolmycin binding also leads to weakened interactions between ATP and active-site lysine side-chains. Confirmation of our interpretation of structural consequences of indolmycin binding comes from a 1.82 Å crystal

structure of an indolmycin-inhibited H_{mt}TrpRS complex. This structure unequivocally demonstrates the use of similar determinants by mitochondrial and bacterial TrpRS enzymes to bind both ATP and indolmycin, with the mitochondrial enzyme forming similar ATP-enzyme, ATP-metal and indolmycin-enzyme interactions. Indolmycin binds H_{mt}TrpRS ~700-times tighter than tryptophan and Mg^{2+}•ATP leads to an ~80-fold enhancement in indolmycin binding affinity. The oxazolinone- Mg^{2+}•ATP interaction contributes ~-2.2 kcal/mol to the Gibbs free energy of the fully-liganded indolmycin inhibited H_{mt}TrpRS complex. Together, our complementary structural, kinetic and thermodynamic characterization of BsTrpRS and H_{mt}TrpRS establish a shared mechanism for indolmycin inhibition of mitochondrial and prokaryotic TrpRS enzymes, which bind indolmycin 10^5-10^6-fold tighter than eukaryotic cytosolic homologs.

ACKNOWLEDGEMENTS

I would like to thank Charlie for his support, encouragement and mentorship. I am grateful to my committee members and lab mates for aiding in the successful completion of my dissertation. Thanks to Vita, Li, Martha, and Niranj for creating a productive and intellectually-stimulating lab environment. I thank you for your contributions and for allowing me to contribute to your research. I am appreciative of the various people and labs that shared knowledge, resources, reagents and equipment. I am grateful to D. Söll and to J. Sello for discussions and for unpublished data on indolmycin-resistant mutants of *E. coli* and indolmycin-resistant TrpRS variants in *S. griseus*. Shubin Liu kindly performed quantum-mechanical simulations of Mg^{2+}•ATP.

Finally, I would like to acknowledge my friends and family. Thanks to Ozgun for sharing in my accomplishments and frustrations. We have shared so much over many cups of tea and endless hours of knitting. Thank you for being a great friend. I am grateful for the love and support of my family, especially that of my grandmother Alice and my siblings. You are my eight favorite people and my success is your success.

I dedicate this work to my siblings, Steven, Lamont, Tyrone, Lenny (in memoriam), Brandon, Shantel, and Bryson.

TABLE OF CONTENTS

LIST OF FIGURES

LIST OF TABLES

LIST OF ABBREVIATIONS

aa	Amino acid
aa-AMP	Aminoacyl-adenylate
aaRS	Aminoacyl-tRNA synthetase
AI	Auto-induction
CD	Circular dichroism
DSF	Differential scanning fluorimetry
Hc	Human cytosolic
Hmt	Human mitochondrial
IND	Indolmycin
IPTG	Isopropyl β-D-1-thiogalactopyranoside
ITC	Isothermal titration calorimetry
LF	Ligand-free
LTN	Tryptophanamide
OXA	Methylamino-substituted oxazolinone
PCR	Polymerase chain reaction
PEI	Polyethylenimine
PPi	Pyrophosphate
preTS	Pre-transition state
SEC	Size exclusion chromatography
Sol	Soluble fraction
TEV	Tobacco Etch Virus
TLC	Thin-layer chromatography

Tm	Melting temperature
Trp	Tryptophan
TrpRS	Tryptophanyl-tRNA synthetase
TYM	Tryptophanyl-5’AMP
Wcl	Whole-cell lysate
WT	Wild-type

CHAPTER I: INTRODUCTION

The never-ending cycle of drug development and antibiotic resistance

Antibiotic selective pressure ensures that only microbes that have either acquired or evolved methods by which to evade drug action will survive and propagate. Adaptive responses by pathogenic bacteria over time and following prolonged use of anti-infectives to treat infected individuals allow bacteria to develop resistance. Despite the great variety among bacterial species and antibiotics, resistance emerges primarily via three well-characterized mechanisms; i) enzyme-catalyzed inactivation of antibiotic (1-3), ii) reduced affinity for antibiotic by reprogramming of drug target structure (4, 5), and iii) reduced intracellular drug concentration due to increased efflux or decreased cellular import (6-8). The accumulation of resistance through genomic alterations in pathogenic organisms necessitates the perpetual development of new anti-infective therapeutics. A common method employed to increase the available arsenal of antibiotics is to chemically modify existing compounds that bind to exploited targets but can, due to the modification, counteract current resistance mechanisms.

One over-utilized target for anti-infective action is the ribosome (Table 1). Drugs targeting the ribosome have been around since the beginning of the antibiotic era with the latest drug class targeting the 50S ribosomal subunit becoming clinically-relevant in 2000. The emergence of resistance in response to compounds from each class belies the need for new compounds targeting other essential translation components (9). Divergent evolution between proteins involved in prokaryotic and eukaryotic translation yields a number of attractive targets

for selective inhibition of prokaryotic translation (10-13). One validated but under-exploited class of targets is the aminoacyl-tRNA synthetase family (14).

Drug Class	Year of Clinical Introduction	Target
Aminoglycosides	1946	30S ribosomal subunit
Phenicols	1948	50S ribosomal subunit
Macrolides	1951	50S ribosomal subunit
Tetracyclines	1952	30S ribosomal subunit
Streptogramins	1999	50S ribosomal subunit
Oxazolidinones	2000	50S ribosomal subunit

Table 1: Antibiotics targeting the translation pathway. Many antibiotics make use of divergent elements involved in prokaryotic and eukaryotic translation for selective inhibition of the prokaryotic pathway. The 30S and 50S ribosomal subunits are the targets of multiple drug classes.

aaRS as antibiotic targets

Protein synthesis is essential for life and fidelity of the genetic code depends on the specific pairing of tRNA with cognate amino acid by the suite of aminoacyl-tRNA synthetases (aaRS). Organisms in all kingdoms of life utilize aaRS enzymes to catalyze the following two-step tRNA-charging reaction:

1. Amino acid activation: aaRS + ATP + aa ⇄ aaRS•aa-AMP + PPi
2. Aminoacyl transfer: aaRS•aa-AMP + tRNA ⇄ aaRS + aa-tRNA + AMP

In the first step, aaRS binds both ATP and the amino acid (aa) for which it is selective such that the nucleophilic carboxylate of the amino acid can attack the ATP α-phosphate. Pyrophosphate (PPi) is released in the process and the enzyme retains an aminoacyl-adenylate (aa-AMP) intermediate to be used as a substrate for the second step. Aminoacyl transfer occurs when either the 2’ or 3’ hydroxyl of the terminal tRNA adenosine attacks the α-carbonyl of aa-AMP. An

ester bond links the amino acid to the 3' adenosine of tRNA (aa-tRNA) and AMP is released. While all aaRS bind ATP, they utilize distinct structural and sequence motifs that allow for their grouping into one of two classes. Class I synthetases employ HIGH and KMSKS signature sequences contained within a characteristic Rossmann fold to bind ATP in an extended configuration. TRNA-charging by members of this class occurs exclusively via the 2'hydroxyl. Class II aaRS have three signature sequences, Motifs 1-3, and bind a bent ATP conformer at an active site that consists of anti-parallel β-sheets (15, 16).

It is evident that targeted inhibition of aaRS enzymes can be achieved by blocking either step of the two-step charging reaction. Amino acid activation of all aaRSs should be inhibited by non-reactive ATP analogues whereas individual aaRS can be targeted by amino acid analogues as is the case for TrpRS inhibition by indolmycin (17-19). Similarly, structural analogues of the aminoacyl-adenylate intermediate are potent aaRS inhibitors. Mupirocin, used in the treatment of methicillin-resistant *Staphylococcus aureus* (MRSA) infections, inhibits Isoleucyl-tRNA synthetase (IleRS) by blocking the isoleucyl-adenylate (Ile-AMP) binding site (10). Sequence variation among prokaryotic and eukaryotic IleRS homologs in active-site residues allows for selective inhibition of bacterial over eukaryotic IleRS by mupirocin (10). Mupirocin validates the aaRS enzyme family as a druggable target for antibiotic development and demonstrates the pivotal role of structural and sequence differences between eukaryotic and prokaryotic aaRS in achieving selective inhibition of prokaryotic synthetases by novel anti-infective therapeutics.

Prokaryotic versus eukaryotic TrpRS

Differential structural responses to ligand binding

Extensive structural and kinetic characterization of tryptophanyl-tRNA synthetases from prokaryotic and eukaryotic organisms has uncovered conserved and divergent features utilized in

the catalysis of tryptophan activation (17, 20-25). Comparison of primary TrpRS sequences identified N-terminal eukaryote-specific (ESE) and vertebrate-specific extensions (VSE) that are absent from all bacterial TrpRS enzymes (25). Furthermore, two lysine residues (Lys 111 and Lys 195) and an aspartic acid (Asp 132) shown to interact with the PPi leaving group of ATP and NE1 atom of tryptophan by Bacillus stearothermophilus (Bs)TrpRS, respectively, are missing from eukaryotic TrpRS. Together, these sequence variations point to the use of non-conserved active-site residues in the recognition and binding of both substrates by eukaryotic TrpRS.

The structural changes accompanying tryptophan activation (Trp + ATP → TYM + PPi) by BsTrpRS are well-characterized (Fig. 1A). In the absence of ligands (1D2R), the enzyme exists in an open conformation (26). This same open state is observed when either ATP (1MAW) or tryptophan (1MB2) separately occupies the active site (22). Induced-fit closing of the active site to form the pre-transition state (preTS) results from full-ligation with ATP and tryptophan (1MAU; (22)). The transition from open to closed is facilitated by movements of the mobile loop containing Lys 111 (~3 Å), the specificity helix (~3 Å), GxDQ (~1.5 Å), HIGH (~3 Å) and the KMSKS loop (~4 Å). At high concentrations ATP can drive closing of the active site to form the pre-transition state (1M83).

In contrast, human cytosolic (H_c) TrpRS, which does not engage residues in the specificity helix for tryptophan recognition, adopts a closed state in response to tryptophan binding (2QUH; (23)). The apo (1O5T; (27)) and tryptophan-bound H_cTrpRS complexes differ by 0.8 Å (316 Cα pairs) compared to the 0.3 Å RMSD (301 Cα pairs) for the corresponding BsTrpRS structures (Fig. 1B). Structural changes accompanying tryptophan binding include movements toward the active site by the KMSAS loop (0.8 Å), GxDQ (~2 Å) and the loop containing Arg 162 (~1.2 Å). Superposition of the tryptophan- and tryptophanamide+ATP-bound (2QUI; (23)) H_cTrpRS

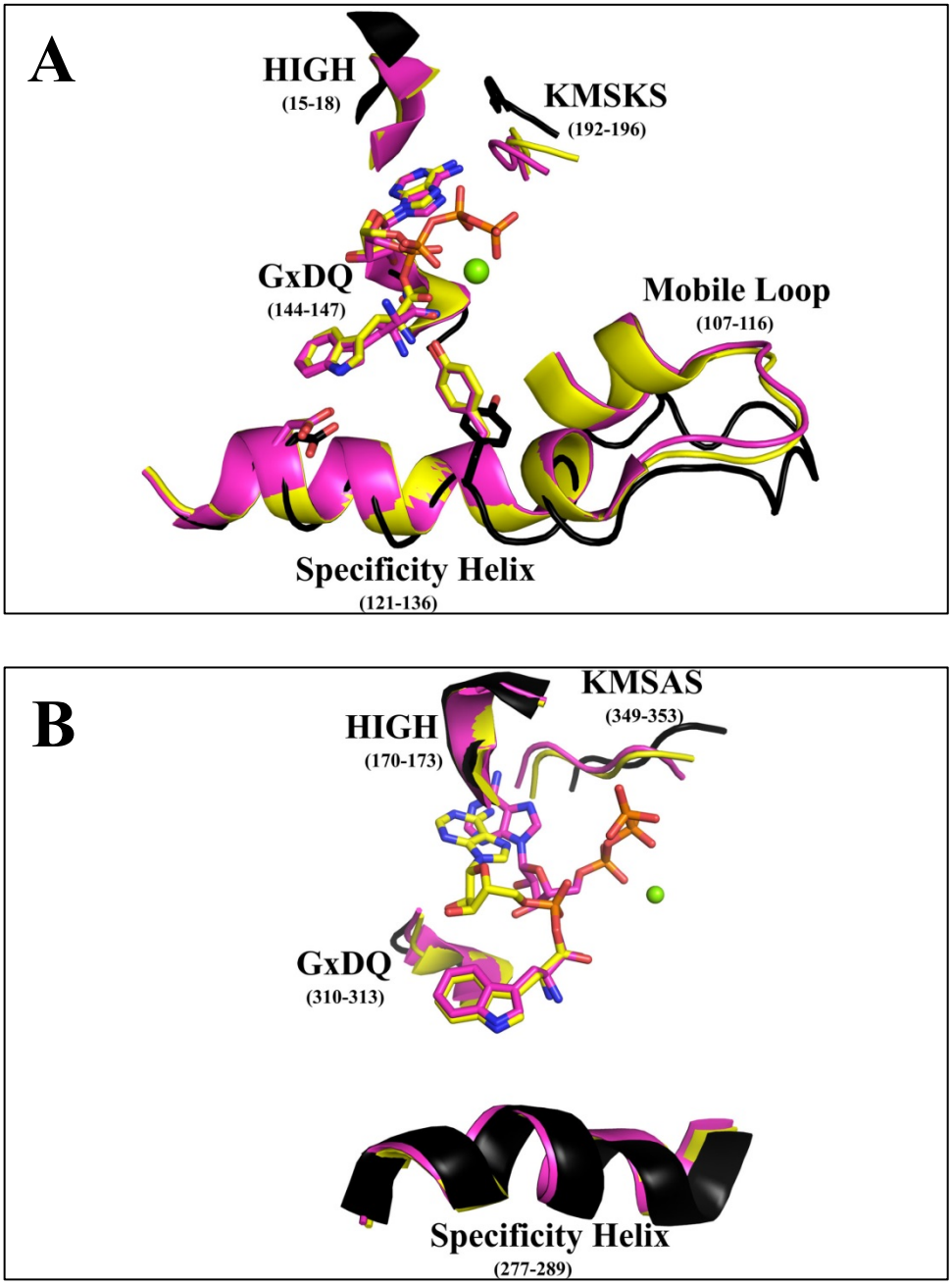

Figure 1: Varied structural consequences of substrate binding to prokaryotic and eukaryotic TrpRS. (A) BsTrpRS resides in an open state conformation in the absence of ligands (black) and transitions to a closed, preTS conformation when both ATP and tryptophan(amide) are bound (pink). Tryptophan activation is accompanied by a slight opening of the KMSKS loop (yellow). (B) Smaller global movements occur when H_cTrpRS goes from open (apo; black) to closed, preTS (pink) to closed, product (yellow) conformation. Tryptophan-bound BsTrpRS favors the open apo-BsTrpRS structure whereas tryptophan-HcTrpRS favors the closed, preTS HcTrpRS complex.

complexes showed a high degree of structural similarity with an RMSD of 0.3 Å for 298 Cα pairs. The addition of ATP in the H_cTrpRS preTS complex closes the KMSAS loop by an additional 2 Å. Overall, less dramatic structural changes accompany the transition from open, ligand-free state to closed, pre-transition state by H_cTrpRS (0.7 Å) than BsTrpRS (2.5 Å).

Tryptophan recognition

Tryptophan binds in a hydrophobic pocket within the BsTrpRS active site (Fig. 2A). BsTrpRS utilizes the carboxylate side-chain of Asp 132 to recognize the indole nitrogen of substrate tryptophan. Other stabilizing interactions include hydrophobic van der Waals (Ile 8, Val 40, Val 141, Val 143, Ile 133, and Ile 151), π-π (Phe 5) and π-sulfur (Met 129) interactions. In contrast, H_cTrpRS relies more heavily on hydrogen bonding interactions with Tyr 159 and Gln 194 for tryptophan recognition (Fig. 2B). Additional direct polar interactions with four active-site side-chains (Glu 199, Lys 200, Gln 284 and Gln 313) and π-π (Phe 317 and Tyr 159) interactions promote tryptophan binding to H_cTrpRS.

Bent versus extended ATP configuration

H_cTrpRS and BsTrpRS bind different ATP conformers, with BsTrpRS binding the extended conformer that is characteristic for Class I aminoacyl-tRNA synthetases. BsTrpRS engages three active-site lysine residues to stabilize the triphosphate group of ATP. Two of these lysines (192 and 111) compete with the catalytic Mg^{2+} ion electrostatically coupled to each phosphate group for negatively charged oxygen atoms in the eventual PPi leaving group. Lysine 195 forms a salt bridge with an α-phosphate oxygen atom. While Lys 192 is conserved in all TrpRS enzymes, Lys 111 and Lys 195 are missing from eukaryotic cytosolic TrpRSs. Instead, H_cTrpRS uses Lys 349 (KMSAS; Lys 195_{BS}) to stabilize an α-phosphate oxygen atom, while Ser 351, Ser 353 and Ser 165 form hydrogen bonding interactions with β-phosphate oxygen atoms.

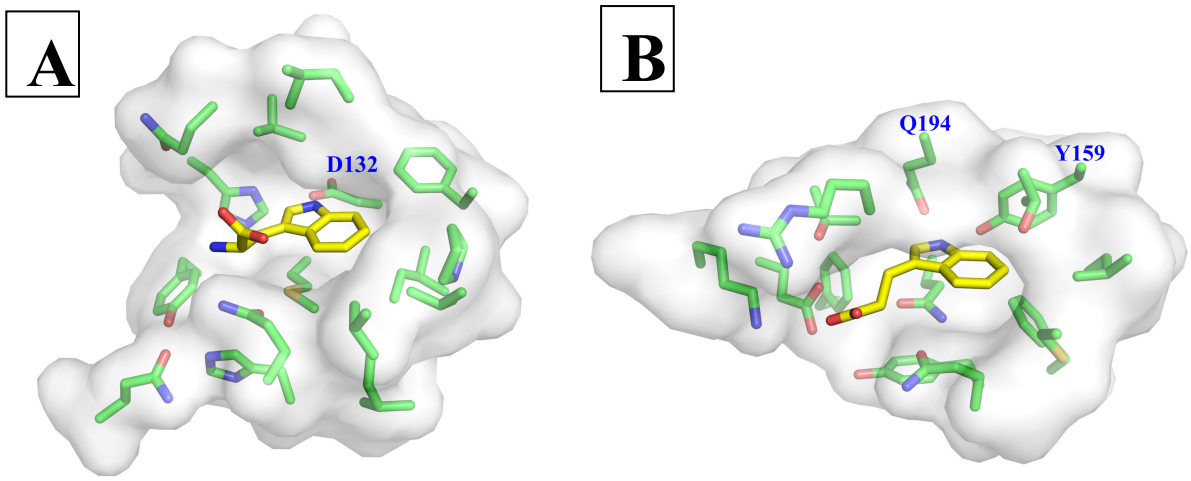

Figure 2: Differential modes of tryptophan recognition. (A) Prokaryotic TrpRS enzymes use a strictly conserved aspartic acid to recognize the NE1 atom of tryptophan. (B) The tryptophan binding pocket of eukaryotic cytosolic TrpRS is more polar and less hydrophobic than that of prokaryotic homologs.

The γ-phosphate group interacts with Arg 162 and His 173 (HIGH) side-chains. Arg 162 is close in sequence to the eukaryotic-specific extension (ESE) which Yang et al. showed was involved in ATP binding (25). Deletion of the ESE reduces ATP binding ~25-fold.

Pre-transition states and Mg^{2+} coordination

From Figure 1 it is clear that BsTrpRS-bound ATP and tryptophan need minimal movements for nucleophilic attack of the α-phosphate by the tryptophan carboxylate; i.e. the indole and AMP moieties occupy similar positions in the pre-transition state and product state structures. Induced-fit closing of the active site in response to ATP binding is responsible for the proper placement of the ATP for catalysis to proceed. Contrastingly, the preTS complex for H_cTrpRS, which closes in response to tryptophan instead of ATP binding, shows the ATP α-phosphate must move closer to tryptophan by ~5 Å before catalysis can occur. Interestingly, ATP movement is not facilitated by H_cTrpRS structural changes.

In addition to differences in ATP conformation and ATP-enzyme interactions, comparison of the bacterial and eukaryotic pre-transition state complexes reveals a distinct difference in Mg^{2+} ion placement and coordination. In H_cTrpRS, the metal lies between the α- and β-phosphate groups. The bent ATP configuration places the γ-phosphate group too far away for electrostatic coupling of this group with Mg^{2+}. The coordination sphere for the Mg^{2+} ion consists of oxygen atoms from the α- and β-phosphate groups, the side-chain hydroxyl group of Ser 165 and a stable water molecule. The precise role of Mg^{2+} in assisting tryptophan activation by H_cTrpRS and other eukaryotic TrpRS enzymes remains undefined.

Contrastingly, BsTrpRS does not form any direct interactions with Mg^{2+} and the metal forms electrostatic interactions with an oxygen atom from each phosphate group of ATP and one stable water molecule. As will be discussed in Chapter II the placement and coordination of the Mg^{2+} ion within the BsTrpRS active site is dependent on ATP and the identity of the ligand occupying the tryptophan binding pocket. BsTrpRS couples the metal to an allosteric center remote from the active site called the D1 switch (20, 21). Side-chain rearrangements between residues of the D1 switch are responsible for activating the catalytic metal. Activation involves movement of Mg^{2+} toward the eventual PPi leaving group, allowing for stabilization of the negative charge during the catalytic transition to tryptophanyl-5'AMP formation.

Indolmycin Inhibition

Varied modes of substrate binding, utilization of non-conserved residues in substrate recognition, and differential catalytic assist by Mg^{2+} all point toward tryptophan activation proceeding via different mechanisms for bacterial and eukaryotic cytosolic TrpRS enzymes. These differences can be exploited to selectively inhibit prokaryotic TrpRS with small molecule

inhibitors, thereby making TrpRS a suitable target for novel anti-infective therapies to treat infected individuals. The relatively minor structural differences between tryptophan and indolmycin (Fig. 3), a naturally-occurring prokaryotic-specific TrpRS inhibitor produced by *Streptomyces griseus*, allow for comparable tryptophan affinities but drastically different indolmycin affinities between prokaryotic and eukaryotic cytosolic TrpRS homologs (19). Binding of indolmycin to prokaryotic and eukaryotic cytosolic TrpRS enzymes differs by six orders of magnitude (18, 19).

In addition to cytosolic TrpRS, eukaryotes express a second TrpRS required for translation of the mitochondrial genome. Mitochondrial TrpRS is nuclear-encoded and translated in the cytosol prior to mitochondrial import (28). Any potential clinically-useful TrpRS inhibitors need to avoid inhibition of both cytosolic and mitochondrial TrpRS to prevent deleterious side-effects. Lack of structural information about mitochondrial TrpRS has hindered our understanding of the binding determinants used for substrate recognition by these enzymes. Sequence comparison shows conservation among ATP- and tryptophan-interacting residues between human mitochondrial TrpRS and BsTrpRS. A shared mode of tryptophan recognition and binding might be indicative of shared susceptibility to inhibition by indolmycin.

The following chapters detail our efforts to uncover the structural and mechanistic basis for selective inhibition of bacterial TrpRS over eukaryotic TrpRS, accounting for the 10^6-fold difference in affinity. Specifically, we account for the 10^3-fold stronger preference of BsTrpRS for indolmycin than its tryptophan substrate and uncover potential means employed by eukaryotic cytosolic TrpRS to evade inhibition by indolmycin. Finally, we establish mitochondrial TrpRS as a target for indolmycin inhibition via a shared inhibition mechanism with BsTrpRS.

CHAPTER II: SELECTIVE INHIBITION OF BACTERIAL TRYPTOPHANYL-TRNA SYNTHETASES BY INDOLMYCIN IS MECHANISM-BASED[1]

Introduction

The accumulation of resistance in pathogenic organisms over time and with prolonged drug use necessitates the continued development of new anti-infective therapeutics. Such developments can include modifications to current drugs that are active against exploited targets while counteracting current resistance mechanisms or novel compounds targeted against underexploited targets. One group of enzyme targets that has been validated but remains underexploited is the class of aminoacyl-tRNA synthetases (aaRS). Aminoacyl-tRNA synthetases maintain the fidelity of the genetic code by ensuring the charging of tRNA with its cognate amino acid via the following two- step reaction:

1) aaRS + ATP + aa → aaRS•aa-AMP + PPi

2) aaRS•aa-AMP + tRNA → aaRS + aa-tRNA +AMP.

All aaRS enzymes bind ATP and activate a specific amino acid by catalyzing the formation of an aminoacyl-5'adenylate (aa—AMP) during the first step. This is followed by transfer of the activated amino acid to the 3' end of the correct tRNA. Structural and mechanistic differences among the different aaRS enzymes as well as orthologs of individual synthetases make it possible to selectively modulate the activity of specific synthetases; e.g. prokaryotic over

[1] This chapter previously appeared as an article in *The Journal of Biological Chemistry*. The original citation is as follows: Williams TL, Yin WY, & Carter CW, Jr. (2015) Selective Inhibition of Bacterial Tryptophanyl-tRNA Synthetases by Indolmycin is Mechanism-Based.

eukaryotic TrpRS (19). This makes the aaRS enzymes attractive targets for novel anti-infective therapeutics.

Any compounds intended for clinical use must be much less inhibitory against the eukaryotic orthologs of its intended target. Naturally occurring aminoacyl-tRNA synthetase inhibitors include indolmycin (TrpRS), granaticin (LeuRS), mupirocin (IleRS), and ochratoxin A (PheRS) (10, 19, 29, 30). Of these, mupirocin displays the required selectivity for prokaryotic over eukaryotic IleRS and has been developed for the treatment of infections in humans (14).

Indolmycin produced by *Streptomyces griseus* displays selective inhibition for prokaryotic TrpRS (9 nM; *E. coli*) over eukaryotic TrpRS (4 mM; *B. taurus*) (31). Problems with off-target effects on tryptophan metabolism have prevented its clinical use (32). However, if we could understand the molecular basis for the observed inhibition and selectivity we could exploit this information for the rational design of antibiotics targeted against TrpRS on pathogens.

Structurally, tryptophan and indolmycin are quite similar, with a heterocyclic indole moiety at the root of each ligand (Fig. 3). Indolmycin differs from tryptophan in the following ways: i) the carbon that is functionally equivalent to Cβ is substituted with a methyl group, ii) the carbonyl carbon is part of an oxazolinone ring, iii) the hydroxyl and amine groups of tryptophan are replaced by the nitrogen and oxygen atoms of the oxazolinone ring, respectively, and iv) the -NH-CH3 moiety attached to the oxazolinone ring does not have functionally equivalent atoms in tryptophan.

BsTrpRS is one of the most extensively characterized TrpRS enzymes. Mechanistically a Mg^{2+} ion is linked to what appears to be a dissociative transition state for tryptophan activation (20) (17) (21). During catalysis the Mg^{2+} ion helps compensate for the increased negative charge that develops on the PPi leaving group, resulting from breaking the αP---O—βP bond. The Mg^{2+}

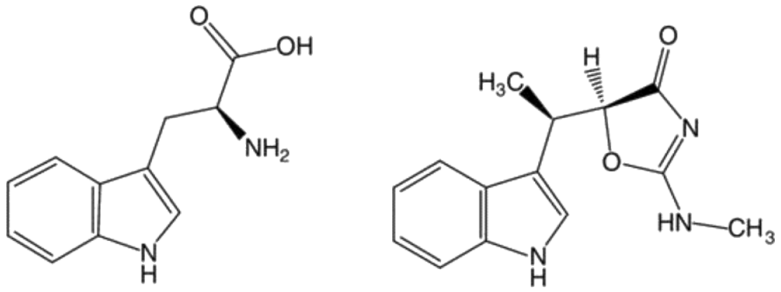

Tryptophan **Indolmycin**

Figure 3: Functional equivalences of tryptophan and indolmycin. Indolmycin differs from tryptophan in three key ways: 1) the incorporation of Cα-constituents into an oxazolinone ring, 2) a methylamino group extending from the oxazolinone ring, and 3) replacement of a hydrogen on Cβ with a hydrophobic methyl group.

ion must move to be catalytically competent, yet no protein-metal interactions have been observed in any of the BsTrpRS crystal structures determined. Instead a remote allosteric location, the D1 switch, must undergo significant conformational change in order to promote the Mg^{2+} ion to a catalytically competent position. The metal moves closer to the PPi leaving group, whose charge is further stabilized in the transition state by the KMSKS loop. ATP binding is required for the conformational switching between the open and closed states that allows for catalysis. ATP-dependent induced-fit closing of the active site brings ATP ~4 Å closer to tryptophan in a predominantly translational movement mediated by relative movement of the catalytic and anticodon-binding domains.

In the absence of ATP, tryptophan binding is promoted by hydrophobic Van der Waals interactions, π- π interactions with Phe 5 and a hydrogen bond between the indole nitrogen and Asp 132 of the specificity helix. When both substrates bind, the tryptophan substrate undergoes a rotational movement that brings the indole ring deeper into the binding pocket and results in more stabilizing interactions between tryptophan and active site residues. This change is

facilitated by the inward movement of the specificity helix that is not observed when only tryptophan is bound.

ATP-dependent induced fit rearrangement of the active site facilitates proper ATP positioning in BsTrpRS, whereas molecular dynamics simulations demonstrate that tryptophan is required to achieve the requisite movement of the αP in H_cTrpRS(22, 24). Even a modest substitution of tryptophanamide in place of tryptophan prevents the re-positioning of ATP. These findings support the idea that H_cTrpRS is intrinsically better at discriminating between tryptophan and its structural analogues than is BsTrpRS.

H_cTrpRS uses different structural elements for substrate recognition than its prokaryotic orthologs (23). Such elements include an extended N-terminus with a β1-β2 hairpin structure shown to have a role in ATP binding as well as the amino acid activation reaction in H_cTrpRS (25). In contrast to BsTrpRS, it is tryptophan binding that leads to induced-fit rearrangement of the active site in H_cTrpRS. There are a greater number of binding determinants for tryptophan recognition as eight direct and water-mediated hydrogen bonds with polar side-chains stabilize tryptophan in the active site. It has been proposed that amino acid activation proceeds via an associative transition state in H_cTrpRS with an unclear role of Mg^{2+} in the catalytic transition state (24). However, comparison of the pre-transition (2QUI) and product states (2QUJ) shows that, as with BsTrpRS, the Pα of ATP must move 5.3 Å to be in a position for nucleophilic attack by tryptophan.

Despite mechanistic and structural differences, BsTrpRS and H_cTrpRS have comparable tryptophan binding affinities. Yet, these inherent differences between prokaryotic and eukaryotic TrpRS enzymes promote the binding of indolmycin to prokaryotic TrpRSs ~1500 fold while protecting eukaryotic TrpRSs from such inhibition by a comparable amount. Determining the

structure of BsTrpRS bound by Mg^{2+}•ATP and indolmycin allowed us to probe the structural basis for indolmycin inhibition and selectivity. Specifically, we examined this structure along with the catalytically-relevant structures of BsTrpRS and H_cTrpRS deposited in the Protein Data Bank to answer the following questions: 1) what are the structural consequences of binding indolmycin; 2) why is indolmycin a tight inhibitor of prokaryotic TrpRS; and 3) why isn't indolmycin an inhibitor of eukaryotic cytosolic TrpRSs?

Experimental procedures

Construction of pet28-His-BsTrpRS vector

The full-length BsTrpRS sequence was pcr-amplified from a pet11 construct made previously in the lab. Pcr primers contained restriction sites for BamHI and HindIII. The resultant pcr product was digested with BamHI and HindIII. A three-way ligation between the pcr product (BamHI/HindIII), dsoligo encoding for the TEV site (NdeI/BamHI) and pet28b (NdeI/HindIII) yielded an expression vector for His-tev-BsTrpRS.

Expression and Purification of His-BsTrpRS

BsTrpRS was expressed by auto-induction with BL21(DE3)pLysS cells at 37°C (33).The cells were pelleted at 4500 rpm for 30 minutes, resuspended in lysis buffer and frozen at -20°C. Upon thawing cells were sonicated and centrifuged (16000 rpm, 4°C, and 1 hour). His-BsTrpRS was captured from the lysate on Ni-NTA resin and eluted with 0.3 M imidazole. Purified protein was cleaved overnight with TEV while dialyzing out the imidazole. The cleaved protein mixture was passed back over a Ni-NTA column to capture both uncleaved protein and his-TEV protease.

Active Site Titration

Active sites were titrated by following the loss of ATP to determine the fraction of molecules competent for catalysis (34, 35). The reaction was performed at 37°C in a final reaction mix containing 50 mM Hepes pH 7.5, 5000 cpm/µl (γ^{32}P)-ATP, 10 µM ATP, 0.5 mM tryptophan, 5 mM $MgCl_2$ and 0.05 U/µl pyrophosphatase. The reaction was initiated with enzyme at a final concentration of 3 µM. At various time points between 10 seconds and 30 minutes, 3 µl of the reaction were added to 6 µl of quench buffer (sodium acetate pH 5.3, 1% SDS) and placed on ice. Three microliters of each quenched reaction were spotted onto a cellulose-PEI TLC plate and run in 0.75 M KH_2PO4 pH 3.5 with 4 M urea to separate ^{32}Pi and (γ^{32}P)-ATP. Plates were developed using a Typhoon Imager and analyzed with ImageJ (36) and JMP (37).

Michaelis-Menten Kinetics

The incorporation of (^{32}P)-PPi into ATP was tracked either by TLC or filter-binding after purification on charcoal (35). Reactions contained (^{32}P)-PPi (5000 cpm/µl for TLC and 400 cpm/µl for filter assay), 0.1 M Tris pH 8.0, 70 mM BME, 5 mM $MgCl_2$, 10 mM KF, 2 mM PPi, 2 mM ATP and tryptophan ranging from 0.3 – 100 µM. Reactions were initiated with enzyme at a final concentration of 30 nM.

Indolmycin Inhibition Assays

Inhibition assays were performed as described above; Michaelis-Menten experiments for tryptophan were performed in the presence of stoichiometric amounts of indolmycin to enzyme. Indolmycin to enzyme ratios of 1:5, 1:1 and 5:1 were used and results fitted to a competitive inhibition model (1) using JMP (37). Non-linear regression to eq. (1) allowed for determination of Km for tryptophan and Ki for indolmycin.

$$Rate = \frac{[Tryptophan] * k_{cat}}{\left(1 + \frac{[Indolmycin]}{K_i} + [Tryptophan]\right)} \quad \textbf{(1)}$$

Differential scanning fluorimetry (DSF; Thermofluor)

The effects of ATP, tryptophanamide (LTN), and indolmycin on the thermal stability of BsTrpRS were assessed by Thermofluor. We showed separately (Weinreb, V, Weinreb, G, unpublished) that DSF detects a conversion of TrpRS into a molten globule form that fully denatures only at higher temperature. The following saturating ligand concentrations were used to ensure a predominance of conformations corresponding to those observed in crystal structures: 5 mM ATP, 5 mM $MgCl_2$, 10 mM LTN, and 600 μM indolmycin. All reactions contained 8 μM BsTrpRS, 50 mM NaCl, 5 mM BME, 50 mM Hepes pH 7.5, and 0.15% Sypro-Orange in a final volume of 20 μl. Fluorescence intensities were determined using an Applied Biosystems 7900HTFast Real Time (RT)PCR instrument, and data were analyzed with MATLAB (Mathworks) with routines developed by Visinets, Inc. The software was built as a pipeline of several m-files, connected to provide full analysis of the data, including thermodynamic characterization and presentation of statistics. Fluorescence at each data point along a melting curve is assumed to be the sum of contributions from two states with probabilities P_1, P_2 established by thermodynamic equilibrium between the two states:

$$F(t) = (a_1 + b_1 T) * P_1 + (a_2 + b_2 T) * P_2 \quad \textbf{(2)}$$

where a_1, and a_2 are adjustable parameters representing intercepts and b_1 and b_2 the slopes of the linear dependences of the initial and final states, and T is the Kelvin temperature. The pipeline consists of three parts:

A. Reading the data from high-throughput, 384 well, RT PCR) files and transforming them into a matrix consisting of four columns: i) number of the well from which temperature-dependent readings were taken; ii) an index representing the protein variant; and finally the data, iii) temperature and iv) fluorescence readings;

B. Fitting the Thermofluor data to a thermodynamic model (eq. 3, 4).

$$F = F_0 + \frac{a_1 + b_1 T + (a_2 + b_2 T) e^{-\Delta G(T)/RT}}{1 + e^{-\Delta G(T)/RT}}$$

$$= F_0 + (a_2 + b_2 T) + \frac{(a_1 - a_2) + (b_1 - b_2) T}{1 + e^{-\Delta G(T)/RT}} \quad \textbf{(3)}$$

where ΔG is the Gibbs energy difference between the two states, and $e^{-\Delta G(T)/RT}$ is the Boltzmann factor that determines the state probabilities, P_1 and P_2:

$$\Delta G = \Delta H(T_m) + \Delta C_p * (T - T_m) - T\left[\Delta S(T_m) + c_p \ln\left(\frac{T}{T_m}\right)\right] \quad \textbf{(4)}$$

where ΔH and ΔS are the enthalpy and entropy changes between the states, c_p is the heat capacity at temperature T and Δc_p is the heat capacity change between the two states at the melting temperature, T_m.

C. Independent determination of T_m assuming that the state probabilities, P_1, P_2 can be estimated from distances between the intersection of the melting curve with vertical lines connecting the extrapolated linear final and initial slopes. Data initially worked up using both methods (B) and (C) agreed closely, and the analysis reported here follows (C).

Crystallization, Data Collection, Structure Determination

Crystals of seleno-Met- substituted BsTrpRS in complex with ATP, Mg^{2+}, and indolmycin were grown by vapor diffusion against a reservoir of 1.4 M potassium citrate and 0.1 M Hepes pH 7.4. Crystals were cryoprotected in Fomblin-Y and passed in a nitrogen airstream

before plunging into liquid nitrogen. Data were collected remotely at SER-CAT (Beamline ID-22) using inverse beam geometry at 0.979 Å to obtain experimental phases from the Bijvoet differences, and processed with XDS (38). Phenix (39) and Coot (40) were used for phase determination, to interpret the map, and iteratively refine the final structure (PDB accession code 5DK4).

Results

BsTrpRS binds indolmycin ~1500x more tightly than tryptophan

Indolmycin is a competitive inhibitor of *Bacillus stearothermophilus* and other bacterial TrpRS enzymes that competes with tryptophan for binding to the enzyme's active site. By conducting Michaelis-Menten experiments at increasing tryptophan concentrations in the presence of different indolmycin concentrations and fitting all 64 data points simultaneously to Eq. (1) we were able to determine $K_{M,\ tryptophan}$, 3 μM, and $K_{i,\ indolmycin}$, 2 nM (Table 2). As these experiments were carried out under exchange conditions (41), we determined the standard free energy, $\Delta G° = -RTlnK$, at 310 K for tryptophan and indolmycin binding to be 7.8 and 12.3 kcal/mol, respectively. This translates to a free energy difference of 4.5 kcal/mol between the affinities of the catalytic and inhibited complexes for the indole-containing ligand. In order to determine what factors account for the observed difference in binding free energy we determined the structure of the BsTrpRS•ATP•indolmycin ternary complex and then conducted differential scanning fluorimetric experiments in the presence of various ligands.

k_{cat} (s^{-1})	ΔG_{kcat} (kcal/mol)	$K_{M,tryptophan}$ (M)	ΔG_{Km} (kcal/mol)	$K_{i,indolmycin}$ (M)	ΔG_{Ki} (kcal/mol)	$K_{M,tryptophan}$/ $K_{i,indolmycin}$
31.6 +/- 0.8	-2.1 +/- 0.01	3.0E-06 +/- 6.4E-07	7.8 +/- 0.1	2.0E-09 +/- 5.2E-10	12.3 +/- 0.1	1.5E+03

Table 2: Steady-state kinetic analysis of indolmycin inhibition. PPi exchange assays performed in the presence of saturating Mg^{2+}•ATP with varying concentrations of tryptophan and indolmycin show BsTrpRS binds indolmycin ~1450 times tighter than tryptophan. The difference in free energy between the catalytic and inhibited complexes is ~4.5 kcal/mol.

Indolmycin and ATP form a ternary complex with BsTrpRS

Extensive crystallization studies conducted on BsTrpRS have revealed three distinct conformational states; an open conformation (ligand-free, tryptophan, low ATP (22, 26)), a closed pre-transition state [high ATP, ATP + tryptophanamide; (17, 22)], and a closed product conformation [Trp-5'AMP; (42, 43)]. A previously unpublished structure of BsTrpRS bound to Mg^{2+}•ATP and indolmycin was never deposited (44). Nevertheless, that structure was the first example of a series of subsequently solved structures that have been described as "Pre-transition state" (PreTS) structures (1MAU, 1M83; (22)). In these structures the initial ATP binding site in the small domain composed of the N-terminal alpha helix and the anticodon-binding domain closes on the remainder of the Rossmann fold, bringing the nucleotide alpha phosphate from 6.7 Å away to within van der Waals contact distance of the tryptophan carboxyl oxygen (22).

The new structure presented here is at higher resolution (1.9 Å vs 2.4 Å) and the experimental phases greatly enhanced the quality of electron density maps (Table 3, Fig. 4). Details of the new structure, such as the orientation of the ribose and the metal position, are quite similar to those observed in deposited PreTS structures, 1MAU and 1M83. Detailed differences that appear functionally relevant are discussed below.

Indolmycin induces new contacts with active-site side-chains

Indolmycin makes contacts with the side chains of His 43, Asp 132 and Gln 147 as well as two water molecules (Fig. 5A). The interaction between OD2 of Asp 132 in the specificity helix and the nitrogen atom of the indole ring is observed when tryptophan (3.1 Å), tryptophanamide (3.0 Å), or indolmycin (2.9 Å) is bound. The addition of the oxazolinone group to the ligand allows for stabilizing interactions with His 43, Gln 147, with functionalities on either side of the ring, which have the effect of fixing the rotation of the ring (Fig. 5B). ND1 of His 43 can donate and/or accept a hydrogen bond from N2 (methylamino group) of indolmycin. In addition to these hydrogen bonds His 43 can form a salt bridge with OD2 of Asp 132 (2.8 Å). The amide group of Gln 147 forms two hydrogen bonds, one with the carbonyl oxygen of the oxazolinone ring (3.0 Å) and another with OD2 of Asp 146 (3.0 Å). OD1 of D146 makes a highly conserved hydrogen bond with the 2'OH group of ATP (2.7 Å). These side-chain interactions in the conserved GEDQ motif link the indolmycin and ATP binding sites, while reinforcing the linkage between opposite sides of the indole-binding pocket.

Structurally, indolmycin binding also prevents the Tyr 125 rotamer switch that occurs upon the enzyme going from its open to closed conformation (Fig. 6A, B). During the catalytic cycle Tyr 125 changes hydrogen-bonding partners from His 150 (2.7 Å) in the open conformation to the alpha amino group (2.4 Å) of the tryptophan substrate in the closed PreTS. The tryptophanyl-adenylate intermediate is stabilized by two polar contacts with the hydroxyl group of Tyr 125 (1I6K). The inhibited state maintains the side-chain interaction between Tyr 125 and His 150 (2.8 Å) observed in the open state.

Data Collection	
Space group	$P4_32_12$
Cell Constants	62.04 Å 62.04 Å 219.06 Å
a, b, c, α, β, γ	90.00° 90.00° 90.00°
Resolution (Å)	43.02 – 1.9
Completeness (%)[a]	99.7 (97.9)
CC1/2 (%)[a,b]	99.6 (93.2)
Rmeas (%)[a]	15.3 (61.9)
Mean I/σI [a]	12.6 (3.3)
Number of Observations	464942
Multiplicity	15.5
Refinement	
R_{work}/R_{free} (%)	16.6/18.7
Fo, Fc correlation	0.96
RMS (bonds)	0.005
RMS (angles)	0.994
Ramachandran favored (%)	97.0
Ramachandran outliers (%)	0.0
Average B, all atoms ($Å^2$)	32.0
Clash score	2.2
PDB Entry ID	5DK4

[a]Highest resolution shell is shown in parentheses.

[b]CC1/2 is the percentage of correlation between intensities from random half-datasets.

Table 3: Data collection and refinement Statistics. Crystallographic data, including experimental phases, of seleno-methionylated BsTrpRS crystals were collected on Beamline ID-22. The final structure was determined to 1.9 Å resolution and refined to an R_{work}/R_{free} of 16.9/18.9%.

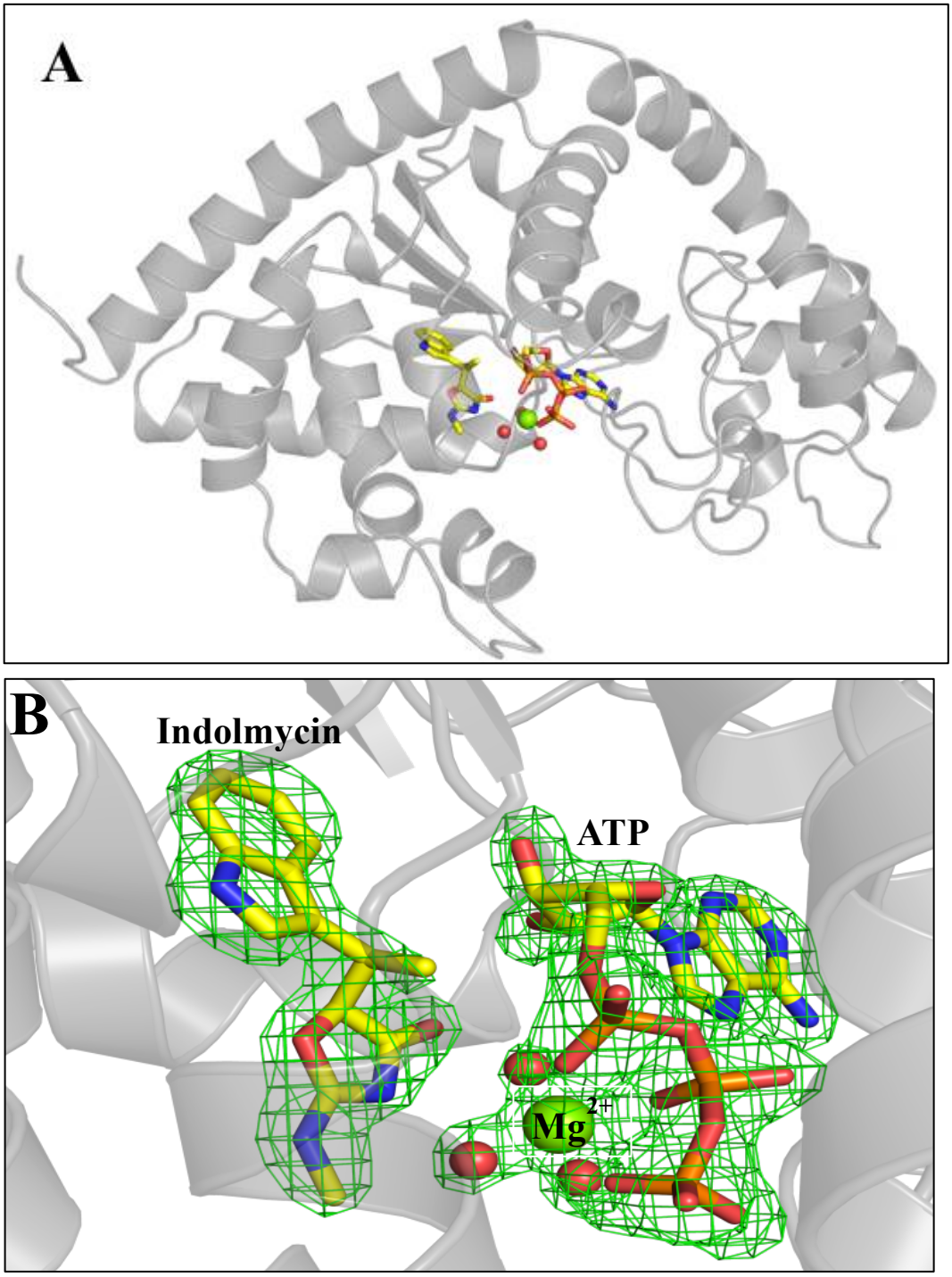

Figure 4: BsTrpRS forms a ternary complex with indolmycin and Mg^{2+}•ATP in a closed conformation. (A) Functionally dimeric BsTrpRS crystallizes with one monomer in the asymmetric unit. (B) In addition to indolmycin and ATP, the active site contains a Mg^{2+} ion and three stable water molecules. The Fo-Fc omit map, derived by omitting indolmycin, ATP, Mg^{2+} and three water molecules from a final round of refinement, contoured to 4.0 σ is depicted in green.

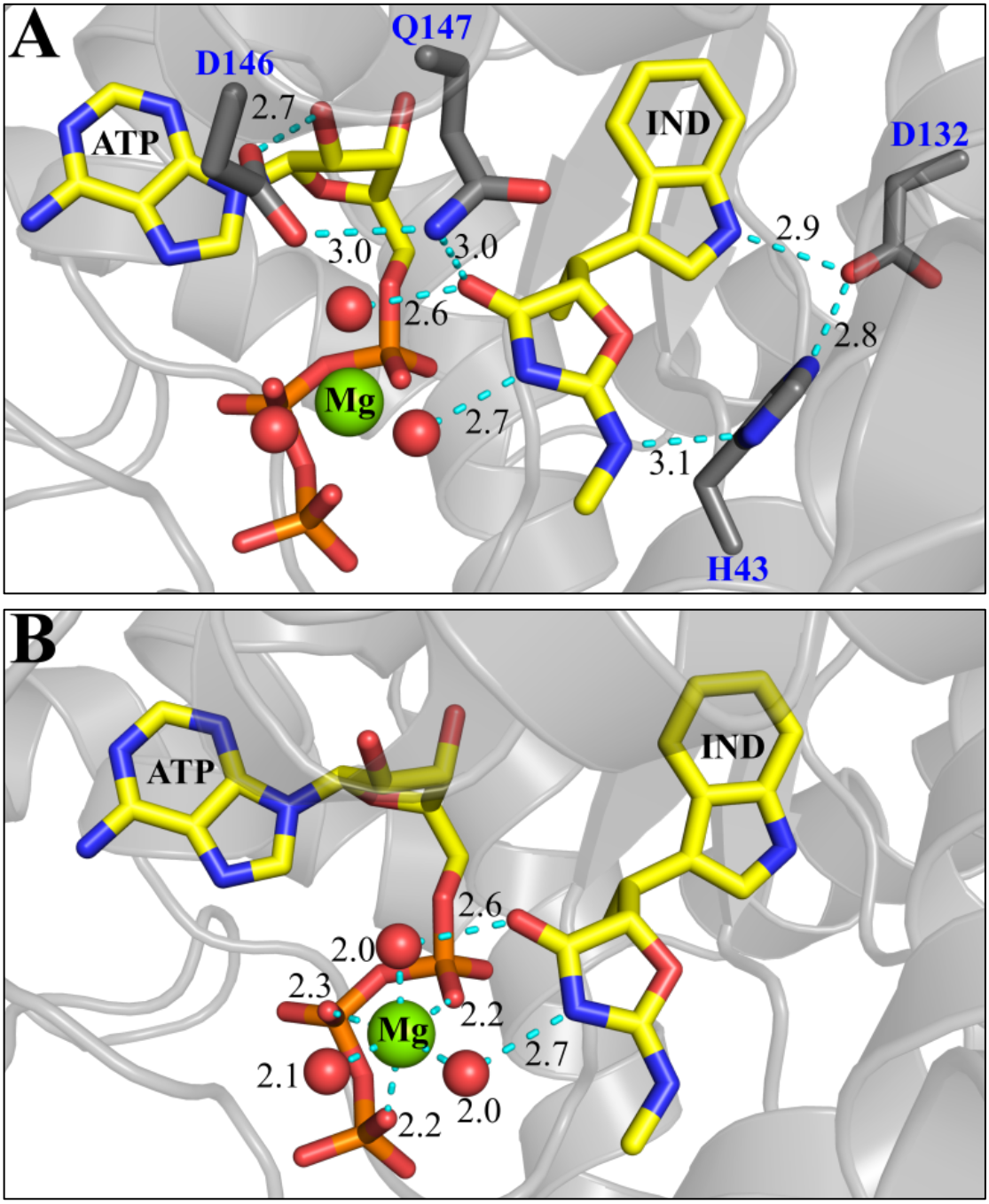

Figure 5: Hydrogen bonding and electrostatic interactions promote indolmycin binding and Mg^{2+} coordination within the active site. (A) BsTrpRS residues His 43, Asp 132, and Gln 147 make stabilizing contacts with indolmycin (IND) via side-chain atoms. The ATP and indolmycin binding subsites are linked via a hydrogen bond (2.7 Å) between Asp 146 and Gln 147 of the conserved GxDQ motif. (B) Mg^{2+} forms tight electrostatic interactions (2.0-2.3 Å) with three water molecules (red spheres) and an oxygen atom from each phosphate group of ATP. Two of these water molecules are within hydrogen bonding distance (2.6 and 2.7 Å) of indolmycin.

Structural modifications induced by indolmycin to the Mg^{2+}•ATP configuration

Superposition of the inhibited structure onto the closed PreTS structure (1MAU) gives a root mean-square deviation of 0.28 Å for 323 Cα pairs. For comparison the two closed PreTS structures, 1MAU and 1M83, have an RMSD 0.17 Å for 328 Cα pairs. The greatest structural difference between the PreTS and inhibited states occurs around Glu 103 – Ala 120, with an RMSD of 0.63 Å for these 18 residues. This mobile loop, which contains Gln 107 and Lys 111, is more open by ~0.5 Å in the inhibited structure, as measured from the γP of ATP to the alpha carbons of residues Gln 107, Lys 111, and Lys 115. The carbonyl oxygen of the Gln 107 side-chain accepts a hydrogen bond from the water molecule coordinated to the Mg^{2+} ion (2.8 Å) and another from NE2 of Gln 147 (3.0 Å) in the pre-transition state. Steric clashing with the constrained Tyr 125 rotamer prevents Gln 107 from switching rotamers in the inhibited state. As such, the interaction with Gln 147 is not observed. Instead, the side-chain of Gln 107 accepts a hydrogen bond at OE1 from a water molecule (3.0 Å) and donates a hydrogen bond at NE2 to another water molecule (3.3 Å).

In the pre-transition state, the NZ atom of Lys 111 forms a salt bridge with the O1G atom of ATP (2.9 Å), which also forms a strong electrostatic interaction with the catalytic Mg^{2+} ion (2.4 Å). This interaction presumably is important for stabilizing the developing charge on the PPi leaving group released after tryptophan activation. Additionally, in the pre-transition state Lys 111 is in position to act as a hydrogen bond donor to the one water molecule coordinated to the Mg^{2+} ion (Fig. 7). The subtle opening of this loop in the inhibited state weakens the salt bridge between the Lys 111 NZ atom and the O1G atom of ATP (3.4 Å) from that observed in the preTS. Now the closest interactions are with three water molecules (2.6, 2.8, and 2.8 Å), none of which are coordinated directly to the catalytic Mg^{2+} ion and are not shown in Fig. 7.

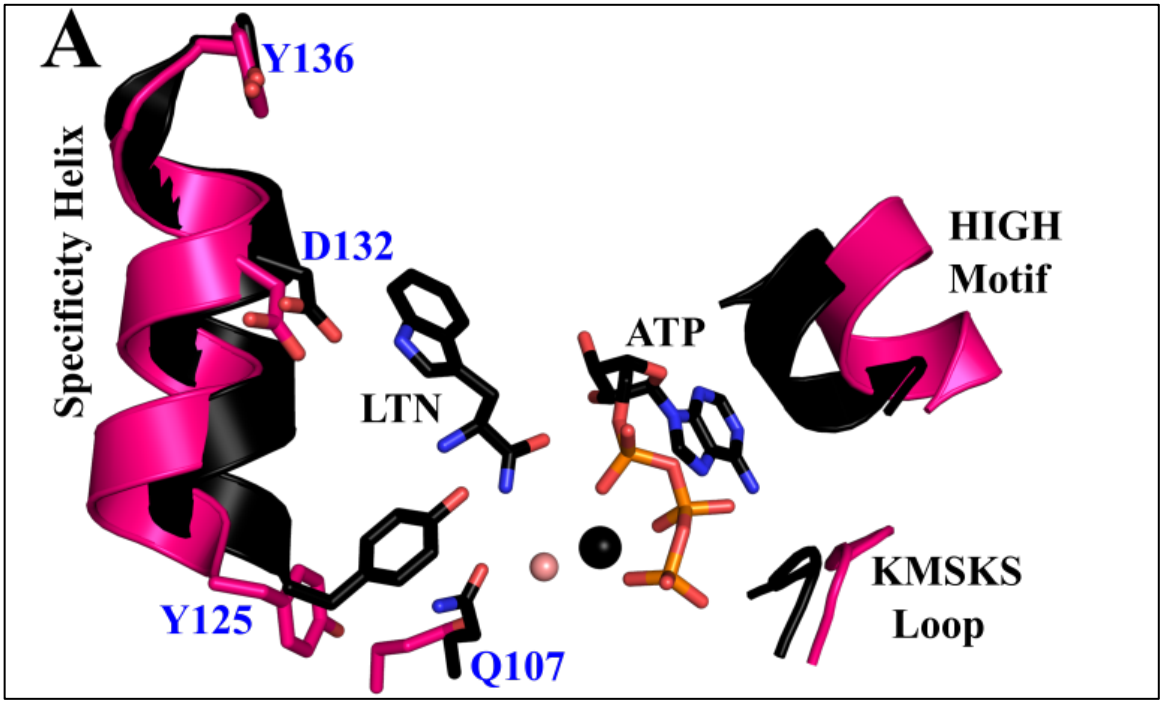
A
Y136
Specificity Helix
D132
HIGH
Motif
ATP
LTN
KMSKS
Loop
Y125
Q107

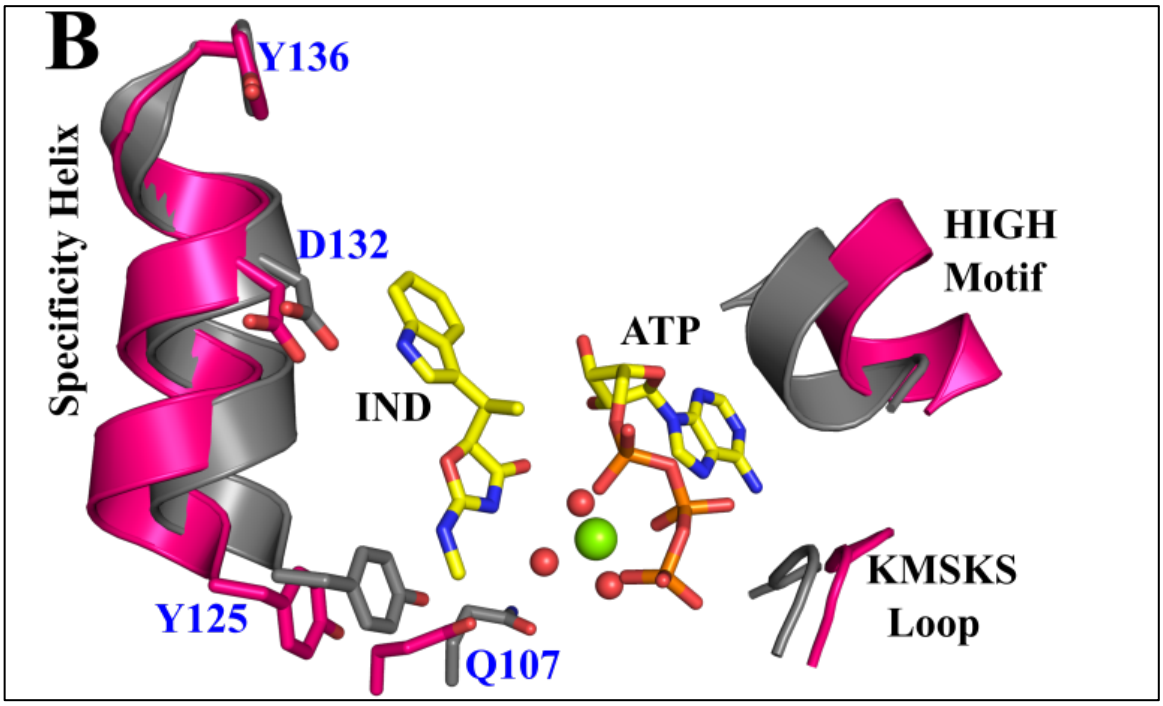
B
Y136
Specificity Helix
D132
HIGH
Motif
ATP
IND
KMSKS
Loop
Y125
Q107

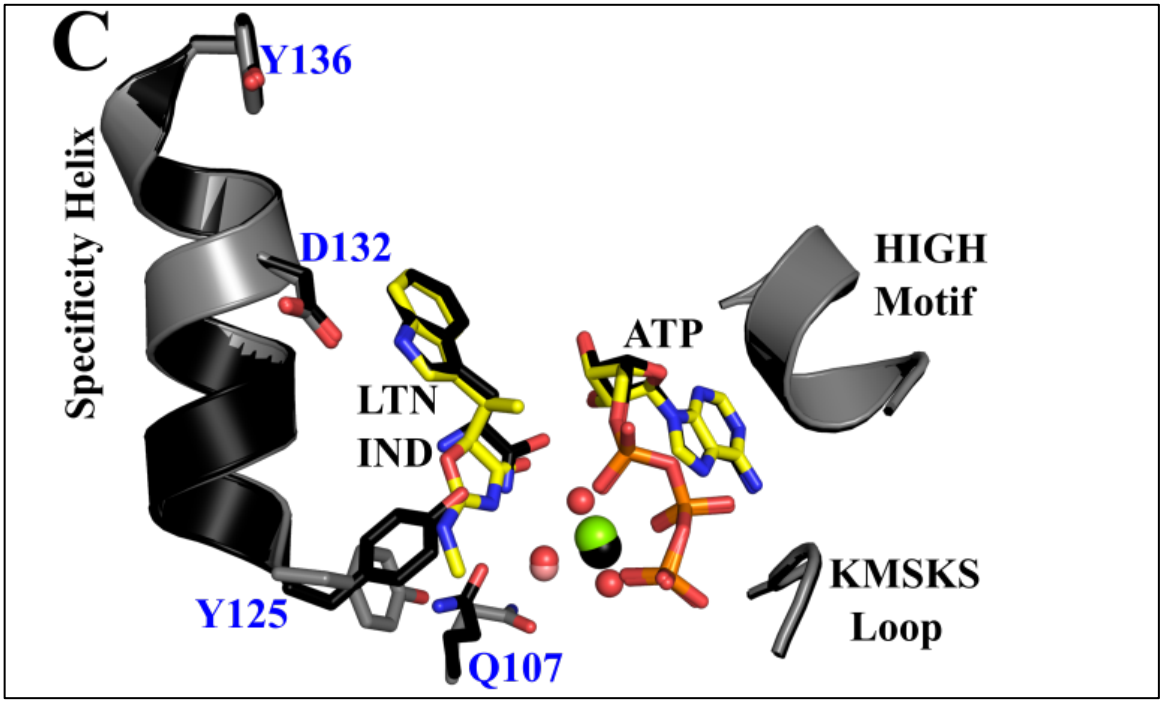

Figure 6: Comparison of ligand-free, preTS, and inhibited BsTrpRS structures. (A) Compared to the apo-form (pink; 1D2R), the fully occupied PreTS structure (black; 1MAU) assumes a closed conformation. The Cα of Tyr 125 is shifted inward by 2.4 Å and the side-chain is flipped ~45° (measured from OH-Ca-OH). A Mg^{2+} ion (black sphere) forms electrostatic interactions with ATP and one water molecule (salmon sphere). (B) Binding of indolmycin and ATP causes similar shifts in the backbone (grey) as the enzyme adopts a closed conformation. However, due to the addition of the methylamino-substituted oxazolinone ring this movement to the closed conformation is not accompanied by a rotamer change of Tyr 125 in the inhibited structure. (C) Consequently, Gln 107 is constrained and is rotated 106° around Cβ away from the specificity helix in the inhibited state compared to the pre-transition state. Finally, the Mg^{2+} (green sphere) is shifted toward the αPO4 and has hexavalent coordination to ATP and three water molecules (red spheres) as compared to the preTS structure.

Replacement of tryptophan(amide) with indolmycin in the active site alters the coordination and placement of the Mg^{2+} ion used during the activation step of the aminoacylation reaction. Presumably because its orientation is fixed by the hydrogen bonding network described above, the oxazolinone forms hydrogen bonds with two water molecules. Introduction of these two water molecules is associated with the movement of the Mg^{2+} ion into a hexavalent coordination that closely resembles stable configurations generated in quantum mechanical simulations of Mg^{2+}•ATP (Shubin Liu, unpublished).

As is also true in the PreTS structure, the Mg^{2+} ion in the inhibited BsTrpRS structure coordinates with a non-bridging oxygen from each phosphate group and three water molecules (Fig. 5B, 6B), two of which are further stabilized by the presence of indolmycin. In addition to the three electrostatic interactions with ATP only one water molecule was seen to coordinate with the Mg^{2+} ion in the PreTS structure (1MAU) (Fig. 6A, 7). The side-chain residues that accept and donate hydrogen bonds to this water molecule differ between these two states (Fig. 7). Due to the different Gln 107 rotamer and slight opening of the mobile loop around Lys 111 these two residues no longer interact with this water molecule in the inhibited state.

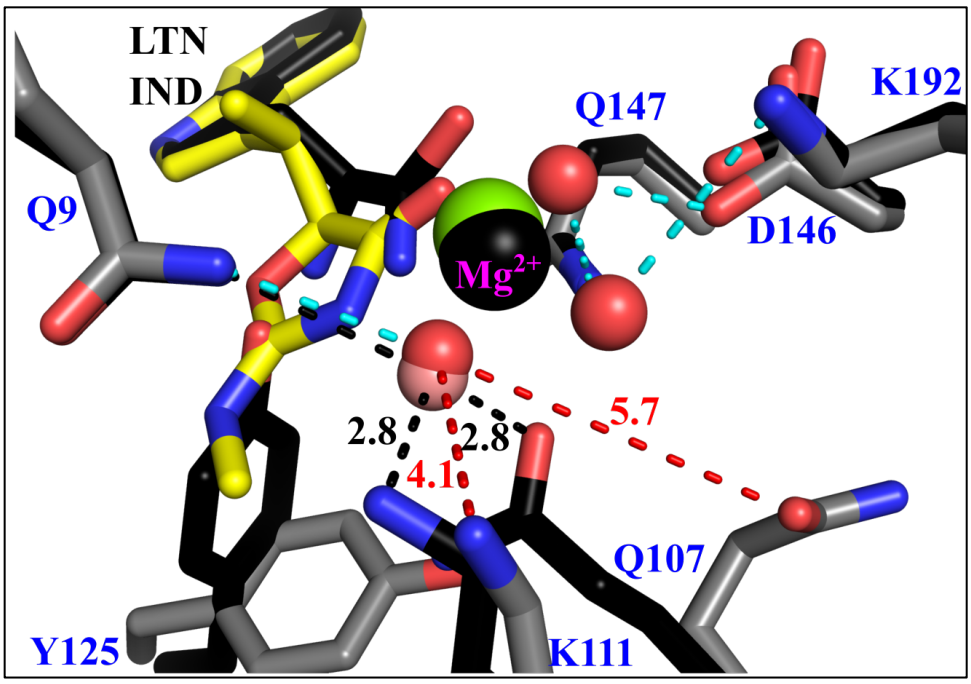

Figure 7: Differential BsTrpRS side-chain interactions with the water molecules electrostatically coordinated with Mg^{2+} in the PreTS and inhibited structures. Gln 9, Gln 107 and Lys 111 are in position to accept (Gln 107) or donate (Gln 9 and Lys 111) hydrogen bonds (black dashed lines) to the water molecule (salmon sphere) coordinated with Mg^{2+} (black sphere) in the PreTS (black sticks). As indolmycin binding leads to opening of the mobile loop containing Gln 107 and Lys 111, these residues are too far (red dashed lines) to form stabilizing interactions with the equivalent water molecule (red sphere) in the inhibited complex (grey sticks). The three water molecules (red spheres) electrostatically coordinated to Mg^{2+} (green sphere) in the inhibited complex are stabilized by interactions (cyan dashed lines) with side-chain atoms of residues Gln 9, Asp 146, Gln 147, and Lys 192.

The Mg^{2+} ion is closer and more central to the triphosphate moiety in the inhibited structure than in the PreTS structure (Fig. 6C), and makes equivalent interactions with the phosphate oxygen atoms. The significance of the differences in metal positions is evident from several measurements. (i) Metal to oxygen distances are significantly shorter (0.2 Å; P = 0.002) in the inhibited complexes. (ii) Movement of the divalent metal ion into closer contact with the ATP phosphate oxygen atoms is associated with a subtle, but statistically significant opening of the active site crevice between the N-terminal helix of the second crossover connection (the GXDQ motif), the KMSKS signature, and the mobile loop containing Lys 111.

Ligand-induced stability changes imply cooperative sources of high indolmycin affinity

The nature of the ligands within the active site has a significant effect on an enzyme's conformation and thermal stability. For small perturbations, the fractional change in melting temperature ($\Delta T_m/T_m$) induced by ligand binding is proportional to the free energy change in stability, the proportionality constant being the enthalpy change, ΔH (45). We use this implicit relationship to assess the stabilizing or destabilizing effects of various ligands on the BsTrpRS enzyme. Binding of ATP, tryptophan or tryptophanamide stabilizes the thermal transition of molten globule formation by 3%, 7% and 7%, respectively (Table 4). Indolmycin enhances the thermal stability of BsTrpRS by 20%, increasing T_m by 13.5°C. The enhanced affinity for indolmycin over tryptophan results in a shift by 8°C to higher temperature in the thermal transition due to molten globule formation in the presence of indolmycin compared to tryptophan.

The linkage between protein stability and ligand binding (46-48) implies that we can attribute differences in stability changes to binding affinity. Two of the stabilizing interactions formed between indolmycin and Mg^{2+}-coordinated water molecules are associated with a change

in the metal position, relative to the ATP phosphate oxygen atoms. A key implication of the structural observations in Fig. 5A and Fig. 6C is that binding of indolmycin to BsTrpRS should be potentiated by the presence of Mg^{2+}•ATP.

Ligand	Mg^{2+}	T_m (°C)	ΔT_m (°C)	$(\Delta T_m/T_m)*100$
LF	-	69.0 ± 0.2	n/a	n/a
ATP	-	71.1 ± 0.1	2.1 ± 0.2	3.0 ± 0.2%
TRP	-	74.7 ± 0.1	5.7 ± 0.3	8.2 ± 0.4%
LTN	-	74.1 ± 0.1	5.1 ± 0.3	7.4 ± 0.4%
LTN + ATP	-	74.7 ± 0.2	5.7 ± 0.2	8.3 ± 0.3%
IND	-	82.5 ± 0.2	13.5 ± 0.3	19.6 ± 0.5%
IND + ATP	-	83.3 ± 0.3	14.3 ± 0.4	20.7 ± 0.6%
LF	+	69.0 ± 0.1	n/a	n/a
ATP	+	71.2 ± 0.03	2.2 ± 0.1	3.1 ± 0.2%
TRP	+	74.1 ± 0.1	5.1 ± 0.1	7.4 ± 0.1%
LTN	+	74.2 ± 0.2	5.1 ± 0.2	7.4 ± 0.3%
LTN + ATP	+	76.8 ± 0.2	7.7 ± 0.1	11.2 ± 0.2%
IND	+	82.7 ± 0.04	13.6 ± 0.2	19.7 ± 0.3%
IND + ATP	+	87.5 ± 0.1	18.4 ± 0.2	26.7 ± 0.4%

Table 4: Thermofluor analysis of ligand-dependent stability. Substrates (ATP and tryptophan) and substrate analogs (LTN and IND) induce conformational changes in BsTrpRS. These changes vary with ligand type and confer varying degrees of thermal stability in the transition to molten globule formation. ATP, tryptophan, tryptophanamide, and indolmycin separately enhance the thermal stability of BsTrpRS. Mg^{2+} is required for additional stabilization by ATP of both LTN-bound and IND-bound BsTrpRS. The inhibited complex (BsTrpRS bound with IND and Mg^{2+}•ATP) is the most thermal stable, with a Tm 18.4°C and 10.7°C higher than that of ligand-free (LF) enzyme and PreTS complex, respectively.

The presence/position of Mg^{2+} in the active site is strictly dependent on ATP, because the protein makes no contacts with the metal. As no direct ATP-indolmycin interactions are observed, we therefore expected that ATP would enhance the thermal stability of the BsTrpRS-indolmycin complex by a larger amount in the presence, compared to the absence of Mg^{2+}. Additionally, we did not expect Mg^{2+} to contribute to thermal stability in the absence of ATP. As

expected, the DSF measurements show that the BsTrpRS in complex with indolmycin and Mg^{2+}•ATP has a 27% increase in melting temperature compared to ligand-free enzyme, with Mg^{2+}•ATP contributing an additional 5°C of thermal stability on top of the 13.5°C provided by indolmycin binding. By contrast, binding of indolmycin, indolmycin+Mg^{2+}, or indolmycin+ATP all elicit far smaller changes of ~20% in thermal stability, demonstrating that both Mg^{2+} and ATP are required to confer additional thermal stability to the BsTrpRS•IND complex.

The conclusion that the metal is essential to the enhanced affinity of indolmycin to the pre-transition state complex can also be derived using the 3D thermodynamic cycle of contributions to stability from ATP, the methylamino-substituted oxazolinone ring (OXA) and the presence/absence of Mg^{2+} (Fig. 8). Differences in binding and thermal stability between tryptophanamide and indolmycin were attributed to the methylamino-substituted oxazolinone ring as this is the major structural difference between these two ligands.

Stabilizing and destabilizing interactions are distinguished by positive and negative non-additivity, respectively. If thermal stability were unaffected by interactions between the ligands, then we expect the effects of binding multiple ligands, e.g. ATP and LTN, to be additive and binding one ligand not to be affected by the presence of a second ligand. Thus:

$$\Delta T_m(ATP) + \Delta T_m(LTN) = \Delta T_m(ATP + LTN) \quad (5)$$

$$\Delta T_m(LTN) = T_m(LTN) - T_m(LF) = T_m(ATP + LTN) - T_m(ATP) \quad (6)$$

An interaction between the ligands would introduce a term, $\Delta T_{m,int}$, to describe the non-additivity (49), and: $\Delta T_m(ATP) + \Delta T_m(LTN) + \Delta T_{m,\text{int}} = \Delta T_m(ATP + LTN)$ **(7)**

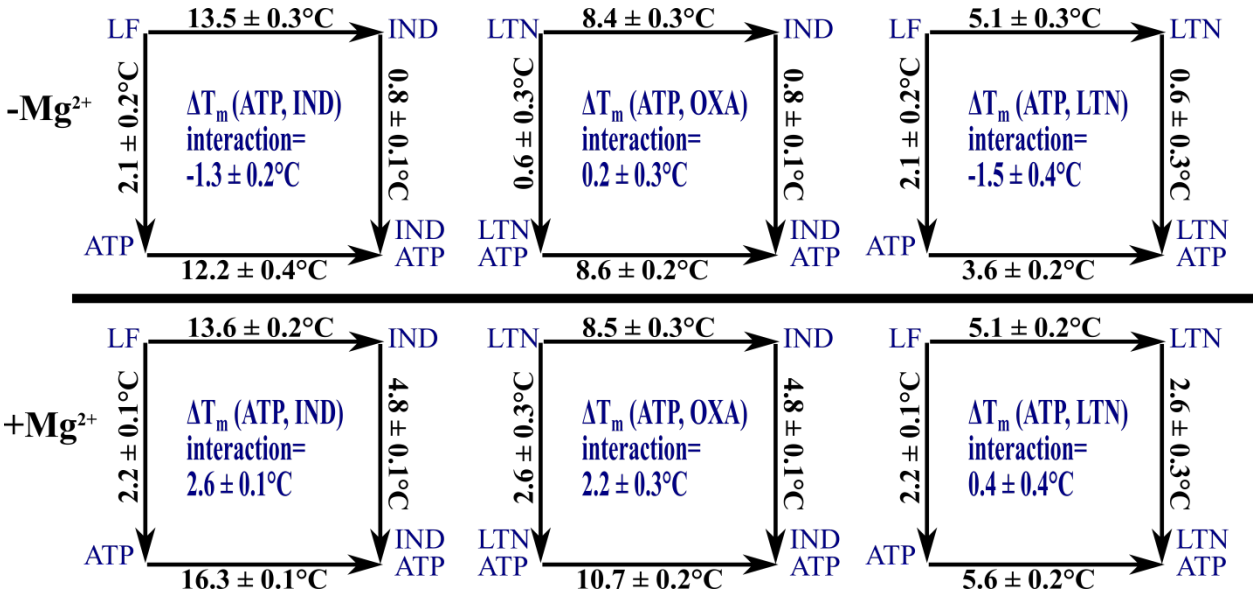

Figure 8: Contributions of Mg^{2+}, ATP, indolmycin and tryptophanamide to the thermal stability of BsTrpRS. TrpRS enzymes require a Mg^{2+} ion for tryptophan activation. While Mg^{2+} does not change the thermal stability of BsTrpRS on its own, its presence or absence significantly impacts the interaction of ATP with both tryptophanamide (LTN) and indolmycin (IND). In the absence of Mg^{2+} (top row) both the ATP-LTN and ATP-IND interactions lower the fractional change in Tm by 2% from its expected value. In the presence of Mg^{2+} (bottom row) the interaction between ATP and LTN is insignificant, while the ATP-IND interaction raises the Tm 4% higher than expected. As expected from the crystal structure, the Mg^{2+} -dependent ATP-IND interaction is mediated through the oxazolinone moiety of indolmycin.

In the absence of Mg^{2+} there is no significant ATP•OXA interaction, and binding either IND or LTN reduces the effect of ATP on T_m by ~1.5°C. The ATP•LTN and ATP•IND interactions are both destabilizing, i.e. the doubly-liganded complexes melt at lower temperatures. In contrast, addition of Mg^{2+} stabilizes the interactions of ATP with LTN and IND to varying degrees. In the case of LTN•ATP, addition of Mg^{2+} compensates for the destabilizing ATP•LTN interaction such that the interaction is no longer significant. The metal compensates for the -1.3°C destabilizing ATP•IND interaction and allows for an additional stabilizing interaction of 2.6°C. Thus, the ΔT_m (ATP•OXA) interaction is comparable to that of the ΔT_m (ATP•IND) interaction. The crystal structure suggests that the stabilizing effect of Mg^{2+} on the interaction between ATP and indolmycin is mediated through the oxazolinone ring, whose

orientation is, in turn, stabilized by hydrogen bonds to His 43 and Gln 147 as discussed in a previous section.

Mutations to residues in the D1 Switch alter the indolmycin:tryptophan selectivity ratio

Residues I4, F26, L29, Y33, C35, F37 and I140 within the D1 switch region of BsTrpRS rearrange to form new Delaunay tetrahedra during Mg^{2+}-assisted catalysis and are critical for protein-metal interactions in the transition state for tryptophan activation (50). Furthermore, mutations to these residues lead to altered tryptophan-tyrosine specificity ratios. In light of the observed stabilizing oxazolinone-ATP interaction that is mediated via Mg^{2+} we wondered if D1 switch mutants displayed differential indolmycin inhibition kinetics. Steady-state PPi-exchange assays conducted with varying indolmycin and tryptophan concentrations allowed us to determine k_{cat}, K_M tryptophan, and K_i indolmycin for four BsTrpRS variants (Table 5).

BsTrpRS	**k_{cat} (s^{-1})**	**$K_{M,\ trp}$ (M)**	**$K_{i,\ ind}$ (M)**
I4V F26L Y33F F37I	35.3 ± 1.2	2.2E-06 ± 6.0E-07	5.5E-09 ± 2.2E-09
Y33F F37I	21.6 ± 1.3	2.2E-05 ± 6.3E-06	4.5E-09 ± 1.3E-09
F26L F37I	29.9 ± 1.0	1.5E-05 ± 2.8E-06	7.0E-09 ± 1.5E-09
F26L Y33F	26.4 ± 0.6	9.0E-06 ± 2.2E-06	8.0E-09 ± 2.4E-09

Table 5: Steady-state kinetic analysis reveals differential indolmycin and tryptophan binding by D1 switch mutants.

All four variants tested had altered catalytic efficiencies compared to wild-type BsTrpRS. The Y33F F37I and I4VF26LY33FF37I mutants were the least and most efficient variants, respectively. Both double mutants containing the F37I substitution bound tryptophan an order of magnitude weaker than native BsTrpRS. While the affinity of the quadruple mutant for tryptophan did not change, its affinity for indolmycin was ~2.7 times weaker. In contrast, the

observed ~2-fold weaker indolmycin binding of the Y33F F37I BsTrpRS variant was accompanied by a 10-fold reduction in tryptophan affinity. The F26LF37I and F26LY33F double mutants had comparable changes in their affinities for tryptophan and indolmycin such that their selectivity ratio did not differ from wild-type (Fig. 9).

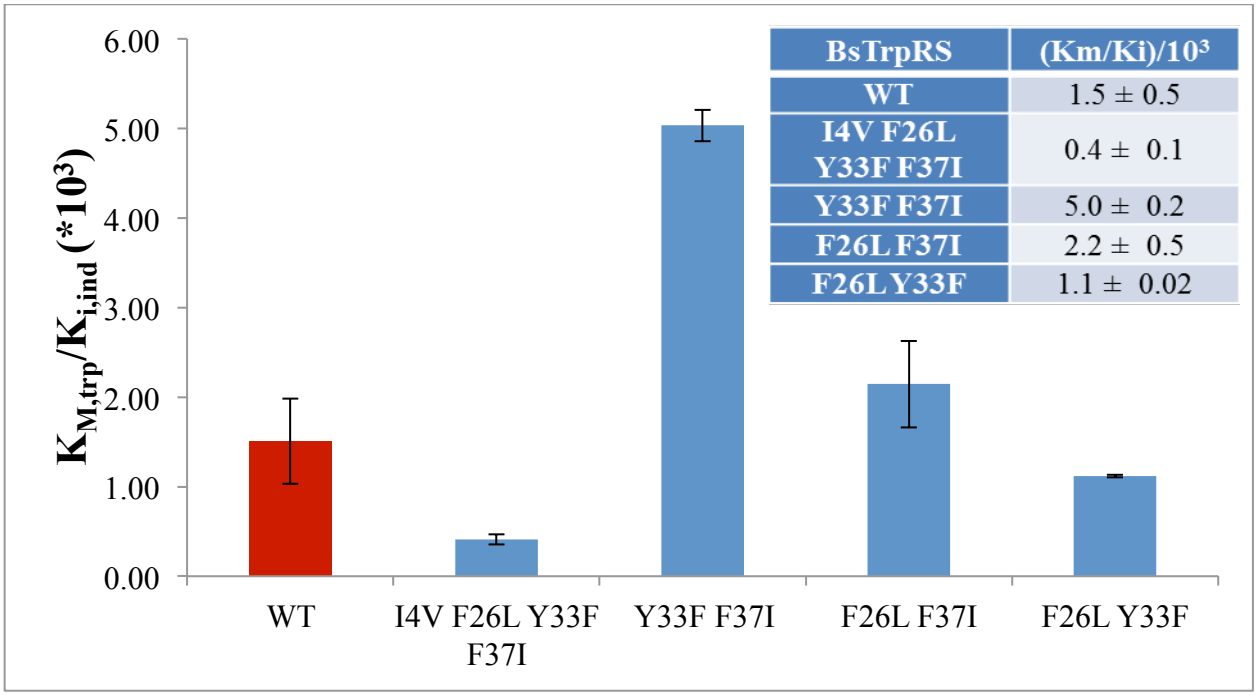

Figure 9: D1 switch residues contribute to tryptophan versus indolmycin selectivity. Compared to native BsTrpRS (WT; red bar), variants containing substitutions at residues involved in long-range coupling to the catalytic Mg^{2+} ion display differential inhibition kinetics. The Y33FF37I variant has the highest preference for indolmycin due mainly to decreased tryptophan affinity. Reduced indolmycin binding results in the quadruple mutant having the smallest (400-fold) difference between tryptophan and indolmycin affinities.

Discussion

An array of crystal structures of both BsTrpRS and H_cTrpRS provide snapshots of the enzymes along their catalytic paths and demonstrate the conformational changes that result from binding of various ligands (22, 23, 26). From these structures it is evident that H_cTrpRS uses a greater number of binding determinants for tryptophan recognition and that binding of tryptophan causes an induced-fit rearrangement of the active site in H_cTrpRS, but not BsTrpRS. Here we discuss possible structural and mechanistic reasons for the tight binding of indolmycin to BsTrpRS and the inability of indolmycin to inhibit eukaryotic TrpRSs.

Why is indolmycin a high-affinity inhibitor of bacterial TrpRS?

There are no drastic global changes between pre-transition state (1MAU) and the indolmycin-inhibited (5DK4) BsTrpRS structures. We propose that subtle, mechanistically relevant differences in the active-site metal configuration account for the ability of indolmycin to inhibit BsTrpRS as tightly as it does. We observe stronger Mg^{2+}--ATP and weaker BsTrpRS--ATP interactions (Fig. 8), as well as altered Mg^{2+} coordination and placement in the inhibited state (indolmycin + Mg^{2+}•ATP; Figs. 5B, 6), compared to the pre-transition state (tryptophanamide + Mg^{2+}•ATP) structure. We attribute these differences to the replacement of tryptophanamide with indolmycin which varies mainly at the methylamino-substituted oxazolinone ring of indolmycin. Interactions between His 43, Gln 147, and indolmycin restrict the oxazolinone ring orientation, thereby reducing the entropy of the α-carbon mimic in the inhibited complex compared to the pre-transition state complex. This unfavorable entropy change is compensated by the enthalpy from additional hydrogen bonds formed between the Mg^{2+}-coordinated water molecules and the oxazolinone nitrogen and carbonyl oxygen atoms as well as the interaction with His 43.

These hydrogen bonds stabilize the water molecules that are also tightly coordinated to the catalytic Mg^{2+} ion. Functional groups of the α-carbon atoms of tryptophan and tryptophanamide can adopt alternative conformations that are similar in energy, none of which allow for completion of the Mg^{2+} coordination sphere. We conclude from these observations that completion of that coordination sphere allows the metal to form significantly tighter interactions with all three phosphate oxygen atoms, and hence that indolmycin stabilizes a ground-state Mg^{2+}•ATP configuration, opposing the tendency of the PreTS state to promote the metal to a high energy state that assists in transition-state stabilization.

Further, the oxazolinone ring of indolmycin, stabilized by hydrogen bonds with His 43 and Gln 147, prevents the rotamer switch of Tyr 125 in the specificity helix that is part of the structural transition from the open to closed state. To avoid a steric clash with the constrained Tyr 125 residue Gln 107 likewise does not switch rotamers in the presence of indolmycin. Gln 107 is part of a highly mobile loop that shows a subtle but significant opening in the inhibited state compared to the pre-transition state. This opening results in the weakening of ATP--BsTrpRS interactions, specifically those between Lys 111 and the γ-phosphate group.

In the catalytically-competent PreTS configuration, coordination by lysine residues of the phosphate oxygen atoms promotes the metal to an activated, less stable state with weaker interactions to the three phosphate oxygen atoms and prevents the Mg^{2+} ion from assuming a lower energy position with stronger contacts to ATP. The positively charged NZ atom of Lys 111 competes with the Mg^{2+} ion for stabilization of a negatively charged oxygen atom (Oγ) of the γ-phosphate group. In the PreTS state the Mg^{2+}--Oγ and Lys 111—Oγ distances are 2.4 Å and 2.9 Å, respectively.

Substitution by indolmycin for tryptophanamide simultaneously weakens the Lys 111—Oγ (3.4 Å) interaction and strengthens that between that oxygen atom and the Mg^{2+} ion (2.2 Å). Additionally, the 0.4 Å shift in Mg^{2+} placement along with the opening of the mobile loop around Lys 111 allows for tight, hexavalent Mg^{2+} coordination, accompanied by stronger, more nearly equivalent interactions between Mg^{2+} and the three ATP phosphate groups.

Mutation of His 43 results in indolmycin-resistance

When both tryptophanamide and ATP are bound, the His 43 side-chain switches from one rotamer to another in the transition from open to closed, PreTS state and back again in the closed, product state. This rotamer switch does not occur when the active site is bound to AMP, PPi and tryptophan (51). In the PreTS (Mg^{2+}•ATP + LTN) and inhibited (Mg^{2+}•ATP + IND) states, NE2 of His 43 interacts with OD2 of Asp 132. In all other observed states, NE2 of His 43 forms an interaction with the carbonyl oxygen of Tyr 125. His 43 also contributes to indolmycin binding via ND1. This re-orientation of His 43 appears correlated with the succession of ligands most similar to the putative catalytic reaction path, and it may thus also be functional.

Several groups have identified mutations that confer high-level indolmycin resistance (52-54). One of the mutant sites, His 43, is of direct interest in the context of the present inhibited structure, which furnishes a semi-quantitative explanation for the mutational effects at position 43. We have implicated His 43 in a hydrogen bond network that requires hydrogen bonds to both indole nitrogen atoms that stabilize the orientation of the plane of the oxazolinone ring of indolmycin. Fixing the orientation of the ring consequently allows formation of a full hexacoordinated environment for the catalytic Mg^{2+} ion, which we have shown accounts for the additional stabilization of the indolmycin•Mg^{2+}•ATP complex.

Indolmycin inhibition of the *B. stearothermophilus* TrpRS H43N mutant is weaker by 3.5 kcal/mole than that of the native enzyme (55). Depending on the stabilization energy provided by these two hydrogen bonds and their coupling, we would predict that an H43N mutant would lose 2 to 4 kcal/mol of binding energy compared to wild-type enzyme. All rotamers of an asparagine substitution at position 43 would result in the loss of two of the three hydrogen bonds observed in the network between indolmycin, His 43 and Asp 132. Similarly, the homologous H48Q mutation in *Streptomyces coelicolor* similarly appears incapable of forming both hydrogen bonds we observe for His 43 (54).

Modeling reveals why indolmycin is a weak inhibitor of eukaryotic cytosolic TrpRS

The selectivity ratio (SR) of indolmycin for cytosolic *B. taurus* (Bt)TrpRS versus BsTrpRS is 10^6-fold in favor of BsTrpRS binding. This selectivity factor far surpasses those of most therapeutic drugs, including trimethoprim (SR rat/*T. gondii* DHFR = 49) and metoprolol (SR β_2/β_1 adrenergic receptor = 6.0) which treat toxoplasmosis and cardiovascular disease, respectively (56, 57). This dramatic selectivity arises by enhancing indolmycin binding recognition by BsTrpRS as we have just shown, while reducing eukaryotic cytosolic TrpRS affinity by similar magnitudes. H_cTrpRS shares 93% sequence identity with BtTrpRS and is therefore highly likely to have a comparably weak millimolar affinity for indolmycin. Interest in developing indolmycin as a lead compound for anti-infective therapy, as well as the extensive kinetic and structural studies conducted on H_cTrpRS, led us to examine the repertoire of deposited H_cTrpRS structures with the purpose of identifying potential means by which eukaryotic cytosolic TrpRS enzymes evade inhibition by indolmycin (23, 25, 27, 58).

Whereas BsTrpRS uses an induced fit mechanism for ATP binding, H_cTrpRS uses induced fit for tryptophan binding. Binding of tryptophan to BsTrpRS is stabilized by one

hydrogen bond between the indole nitrogen of tryptophan and OD2 of Asp 132 and π-π interactions with Phe 5. Meanwhile H_cTrpRS makes seven direct and water-mediated contacts to its tryptophan substrate. The determinants for tryptophan binding to H_cTrpRS include Glu 199, which has a direct and water-mediated interaction with the α-amino group of tryptophan (Fig. 10A). Modeling of indolmycin into the amino acid binding site introduces steric clashes between indolmycin and Glu 199 (Fig. 10B). Furthermore, Glu 199 cannot adopt an alternative rotamer conformation without introducing additional clashes between Glu 199 and Thr 196, Trp 203 or Phe 280. Besides clashing with Glu 199, this indolmycin conformer would not form any of the hydrogen bonds observed when tryptophan is bound, aside from the bifurcated hydrogen bond with the indole nitrogen, Tyr 159 and Gln 194. These interactions are preserved because indolmycin was modelled into the active site by overlaying its indole moiety with that of tryptophan (2QUH).

Indolmycin can be modelled into the active site of H_cTrpRS by rotating the oxazolinone ring away from Glu 199 to an orientation perpendicular to the indole moiety (Fig. 10B). While this indolmycin conformer does not clash with active site residues, it does disrupt the hydrogen bonding pattern used by the cytosolic enzyme to identify tryptophan as the bound substrate. The α-amino group of tryptophan, which is protonated at physiological pH, is recognized by Glu 199, Gln 284 and Gln 313 (Fig. 10A). Each of these residues acts a hydrogen bond acceptor and the negatively charged carboxylate of Glu 199 forms additional electrostatic interactions with the amino group. According to our model the side chain amide group of Gln 284 would act as a hydrogen bond donor for the cyclic oxygen atom in indolmycin that is in the equivalent position of the α-amino group (Fig. 10B). While Glu 199 cannot form a salt bridge with indolmycin it can

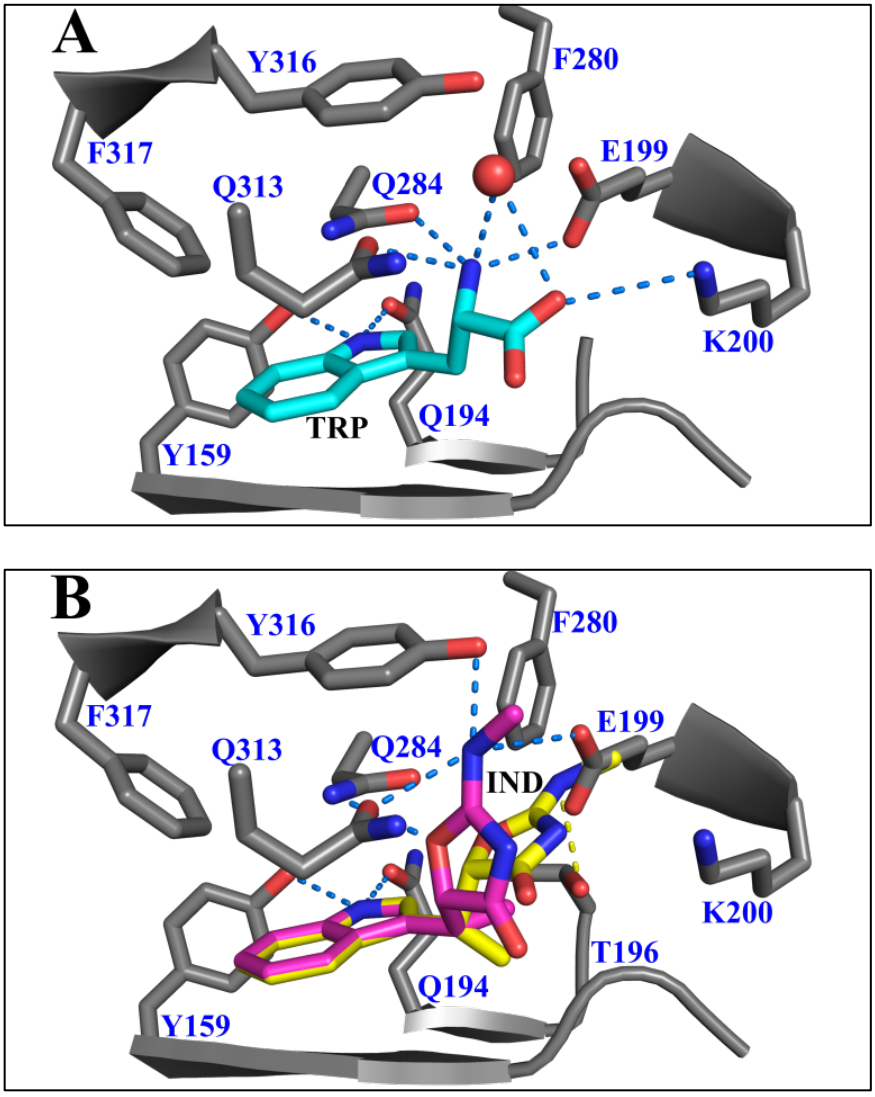

Figure 10: Steric hindrance and altered hydrogen bonding pattern allow H_cTrpRS to discriminate between tryptophan and indolmycin. (A) The electrostatic and hydrogen bonding interactions that facilitate specific recognition and binding of tryptophan (TRP) to H_cTrpRS (2QUH) are shown in yellow dashes. (B) Indolmycin (IND; yellow and pink sticks) from the BsTrpRS complex was modelled into the tryptophan binding site of H_cTrpRS (2QUH) so the indole moieties superimposed. This maintained the H-bonding interactions between the indole nitrogen and Tyr 159 and Gln 194. Rigid-body modelling shows none of the interactions important for tryptophan substrate recognition/binding can form between active site residues and indolmycin (yellow sticks). Additionally, rotating the oxazolinone ring away from Glu 199 eliminates a prominent steric clash between the methylamino group of indolmycin and the side chain carboxylate group of Glu 199. This alternate indolmycin conformation (pink sticks) allows for more hydrogen bonding interactions between indolmycin and active-site residues, though the nature of these interactions is different from those observed upon tryptophan binding. Modelling suggests that these altered interactions allow H_cTrpRS to reject indolmycin as a substrate.

instead share a bifurcated hydrogen bond from the methylamino group nitrogen with Gln 313. This nitrogen can accept a hydrogen bond from the hydroxyl group of Tyr 316.

Finally, Lys 200 cannot form a salt bridge with indolmycin as it does with the tryptophan carboxylate. This electrostatic interaction is also missing when tryptophanamide is bound in place of tryptophan and appears to be critical for progression from the pre-transition state to transition state, as this is the only interaction used for tryptophan substrate recognition and binding that cannot form when tryptophanamide occupies the active site. Indolmycin differs from tryptophan by a greater degree than does tryptophanamide. The inability of indolmycin to fully retain the tryptophan-H_cTrpRS side-chain interactions, including the salt bridge with Lys 200, allows H_cTrpRS to discriminate between tryptophan and the inhibitor. For these reasons a stable H_cTrpRS •ATP•indolmycin complex is ~1000 less likely to form than that of H_cTrpRS •ATP•tryptophan. Contrastingly, BsTrpRS, which has a 10^3-fold higher affinity for indolmycin over tryptophan, is ~1500 more likely to form a stable, inhibited complex than a catalytically-competent tryptophan-bound complex.

Conclusion

In this work, we determined the structural basis for high-affinity inhibition of BsTrpRS by indolmycin. The simultaneous binding of indolmycin and Mg^{2+}•ATP results in i) movement of the Tyr 125 and Gln 107 side chains, ii) opening of the mobile loop containing Lys 111, iii) displacement of the Mg^{2+} ion by 0.4 Å, iv) hexavalent metal coordination, v) stronger, nearly equivalent electrostatic interactions of Mg^{2+} with an oxygen from each phosphate group of ATP, and vi) weaker coordination of phosphate group oxygen atoms by active-site lysine residues. These changes are reinforced by the hydrogen bonding interactions of Gln 147, His 43, and Mg^{2+}-coordinated water molecules with indolmycin. We propose that weaker coordination by

lysine residues of the phosphate oxygen atoms and stronger Mg^{2+}--ATP interactions induced by indolmycin binding allow the Mg^{2+} ion to settle into a lower energy state, thereby significantly increasing affinity by preventing activation of the metal required for use in amino acid activation.

Author contributions—CWCjr and TLW conceived the experimental plan, based on previous work by WYY. TLW carried out all experimental work, analyzed the data and wrote the paper in consultation with CWCjr and WYY.

CHAPTER III: HUMAN MITOCHONDRIAL TRYPTOPHANYL-TRNA SYNTHETASE UTILIZES CONSERVED ELEMENTS TO BIND INDOLMYCIN AND ATP

Introduction

Increasing drug resistance places great demand on the development of antibiotics active against novel targets. Successful candidates should be assessed for off-target effects including the potential for deleterious interactions with mitochondrial proteins. Mitochondrial dysfunction is often a detrimental consequence of prolonged antibacterial and antiviral therapeutics due, in part, to unintended drug interactions with host mitochondrial homologs of the pathogenic target proteins (59-61). Mitochondria have retained many conserved proteins, pathways and processes from their prokaryotic ancestors. Dysregulation or inactivation of mitochondrial enzymes, most of which are nuclear-encoded, has great potential for debilitating ATP production.

One under-utilized target for antibacterial action is tryptophanyl-tRNA synthetase. We demonstrated in Chapter 2 that mechanistic differences allow indolmycin, a natural TrpRS inhibitor, to selectively bind *Bacillus stearothermophilus* (Bs) TrpRS 10^6-fold over eukaryotic cytosolic TrpRS (18). Specifically, BsTrpRS uses an acidic residue, Asp 132, to recognize the indole nitrogen and bind indolmycin (and substrate tryptophan) to a largely hydrophobic pocket. In the presence of bound tryptophan a catalytic Mg^{2+} ion electrostatically coupled to each phosphate group of ATP becomes activated for participation in catalysis (17, 20, 21). The methylamino-substituted oxazolinone ring of indolmycin prevents Mg^{2+} activation due to stable, hexavalent Mg^{2+} coordination, stronger Mg^{2+}•ATP interactions, and weaker TrpRS•ATP

interactions (18). Sequence variations, specifically alanine substitution for the second lysine of the conserved KMSKS motif and shifting of catalytically-important residues to the N-terminal extension, altered ATP binding and Mg^{2+}•ATP coordination, as well as a greater number of binding determinants for tryptophan recognition prevent indolmycin from being a tight-binding inhibitor of H_cTrpRS (23, 25, 27).

Although the human mitochondrial (H_{mt}) TrpRS enzyme was identified and kinetically characterized over 15 years ago, structural information about the enzyme remains lacking (28). As such, little is known about how the enzyme recognizes its substrates. Based solely on primary sequence comparison, we know that H_{mt}TrpRS has retained the aspartic acid residue of the specificity helix shown to recognize tryptophan in BsTrpRS while showing sequence variation at positions involved in tryptophan binding by H_cTrpRS (Fig. 11). Additionally, H_{mt}TrpRS has the canonical KMSKS sequence important for ATP binding and lacks the N-terminal extension acquired by H_cTrpRS (Fig. 11). From this we expect H_{mt}TrpRS to utilize similar determinants as BsTrpRS for tryptophan and ATP binding and to, similarly, be targeted for inhibition by indolmycin.

Here, we provide structural, kinetic and thermodynamic evidence that indolmycin is a tight-binding inhibitor of H_{mt}TrpRS. Additionally, we use the sole structure of H_{mt}TrpRS determined as part of this work to describe structural details which support a shared mechanism for indolmycin inhibition between H_{mt}TrpRS and BsTrpRS as well as utilization of conserved elements in the recognition/binding of ATP and indolmycin that imply a shared mechanism for tryptophan activation.

Experimental procedures

Construction of H_{mt}TrpRS expression plasmids and mutagenesis

The codon-optimized gene for human mitochondrial (H_{mt}) tryptophanyl-tRNA synthetase (TrpRS) was purchased from GenScript in the puc57 plasmid. Translation of this gene yields a protein that lacks the putative mitochondrial targeting sequence, residues 1-18, identified by Jorgensen et al (28). To facilitate purification we decided to add an N-terminal 6x-His tag that could be removed by Tev protease. This was achieved via a three-way ligation with EcoRI/HindIII digested pet28a, HindIII digested pcr product of HmtTrpRS amplified from puc57 plasmid with primers L19-F and Hmt-Hd3-R, and the annealed Tev-F and Tev-R oligos (Table 6). This construct was used as a template to introduce amino acid substitutions such as H48T and K226A along with the primers listed in Table 6 in accordance with the Invitrogen GeneTailor Site-Directed Mutagenesis System. The Δ 1-33 variant was created by three-way ligation as described above following pcr amplification with primers K34-F and Hmt-Hd3-R. Finally, codons corresponding to residues 1-18 were added to the original Δ 1-18 gene via three successive pcr amplifications using the primers MTS1-3 and Hmt-Hd3-R. The final pcr product digested with BamHI and HindIII was ligated with pet28. The sequences for all constructs were confirmed by DNA sequencing.

Heterologous Expression of 6xHis-H_{mt}TrpRS

All 6xHis-H_{mt}TrpRS variants were co-expressed in BL21(DE3) cells with chaperones GroEL/ES and induced by auto-induction (33). First, BL21(DE3) cells bearing the pGro7 plasmid (Takara) were made competent by $CaCl_2$ treatment. The pGro7 plasmid allows for arabinose-induced expression of GroEL/ES chaperones and confers chloramphenicol resistance. Next, 50µl of these cells were freshly transformed with plasmid DNA. Following a 1 hour

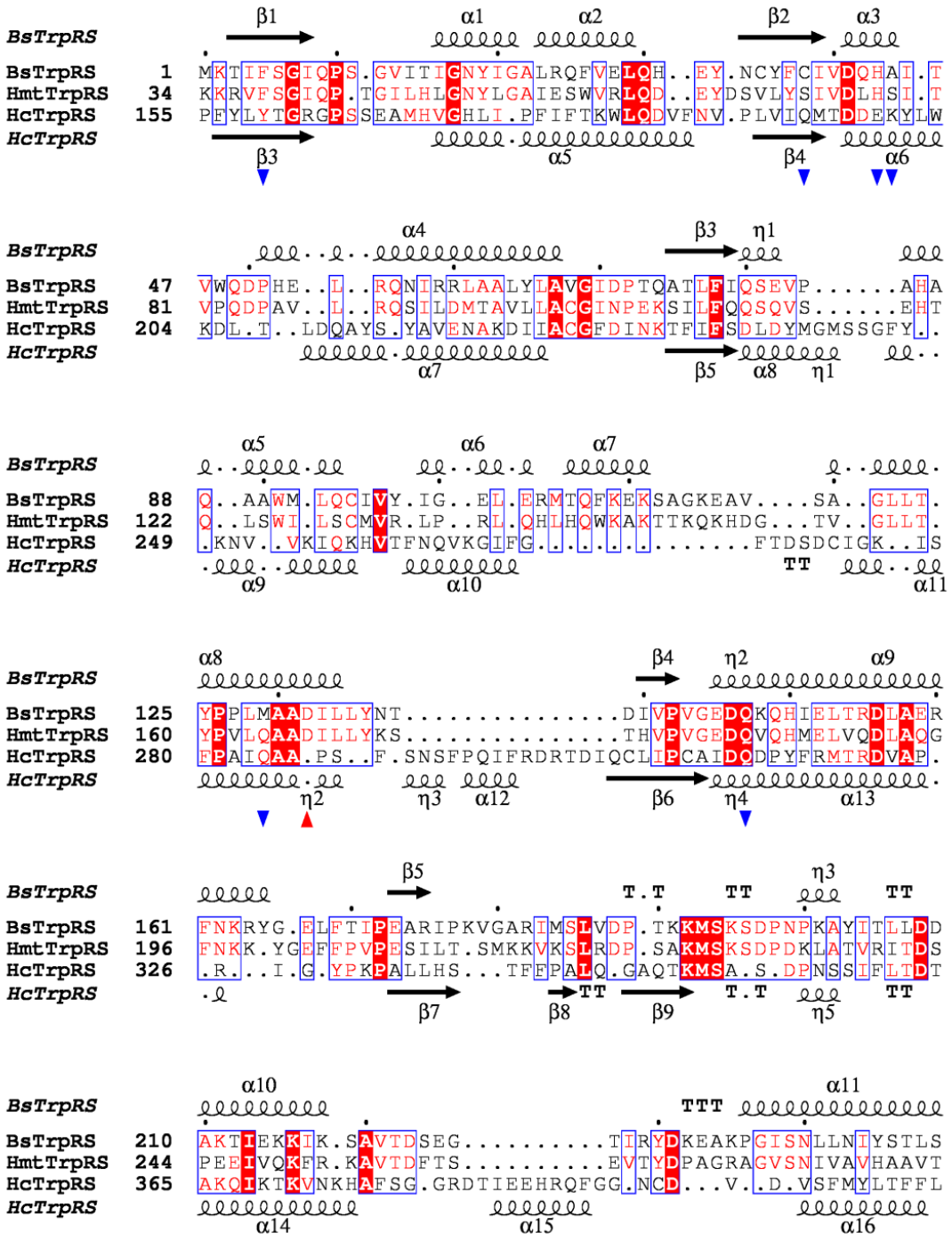

Figure 11: Structure-based sequence alignment of BsTrpRS, H_{mt}TrpRS and H_cTrpRS. Following superimposition of relevant BsTrpRS, H_{mt}TrpRS and H_cTrpRS structures USCF Chimera was used to generate a structure-based sequence alignment of the three enzymes. This alignment facilitates comparison of residues used for substrate binding. The red and blue triangles point to residues that interact with tryptophan when tryptophan alone is bound to BsTrpRS and H_cTrpRS, respectively. The final image was generated using ESPript 3.0.

Designation	Sequence 5'→ 3'	Purpose
Tev-F Tev-R	aattcgagaacctctacttccagggc gccctggaagtagaggttctcg	Add TEV cleavage site by oligo-annealing
L19-F	ctgcataaaggtagcgcggcg	Amplify HmtTrpRS gene
Hmt-Hd3-R	gattacgccaagcttatcactacaggaaac	Introduce HindIII site after stop codon
K34-F	aaaaaacgtgtgttctctggcattcaaccg	Remove codons for residues 19-33
MTS1 MTS2 MTS3	tggtccttcatcagggcgttgcataaaggtagcgcggcgggc atgaggaaggcaagggagaggtggtccttcatcagggcgttgcataaaggt gaacggatccatggcactgcacagcatgaggaaggcaagggagaggtggtccttcatc	Add mitochondrial targeting sequence by pcr in three reactions
Q42A-F Q42A-R	gtgttctctggcatt**GCA**ccgacgggcat aatgccagagaacacacgttttttgg	Mutate glutamine to alanine at position 42
H48T-F H48T-R	ccgacgggcattctg**ACT**ctgggcaact cagaatgcccgtcggttgaatgccag	Mutate histidine to threonine at position 48
K145A-F K145A-R	caccaatggaaagcc**GCA**accacgaaac ggctttccattggtgcagatgctgc	Mutate lysine to alanine at position 145
K145Q-F	caccaatggaaagcc**CAA**accacgaaac	Mutate lysine to glutamine at position 145
D181A-F D181A-R	gtcccggtgggtgaa**GCT**caggtccaac ttcacccaccgggacatgggtgctt	Mutate aspartic acid to alanine at position 181
K226A-F K226A-R	cgtgatccgtcggcc**GCA**atgagcaaatc ggccgacggatcacgcagtgattta	Mutate lysine to alanine at position 226
K226Q-F	cgtgatccgtcggcc**CAA**atgagcaaatc	Mutate lysine to glutamine at position 226
K229A-F K229A-R	tcggccaaaatgagc**GCA**tctgatccgg gctcattttggccgacggatcacgc	Mutate lysine to alanine at position 229
K229Q-F	tcggccaaaatgagc**CAA**tctgatccgg	Mutate lysine to glutamine at position 229
K226AK229A	cgtgatccgtcggcc**GCA**atgagc**GCA**tctgatccggac	Mutate lysine to alanine at positions 226 and 229
K226QK229Q	cgtgatccgtcggcc**CAA**atgagc**CAA**tctgatccggac	Mutate lysine to glutamine at positions 226 and 229

Table 6: Primers and oligos used for gene amplification and mutagenesis by pcr.

recovery with shaking at 37°C, transformed cells were allowed to grow overnight in 4 mL of ZYM-505 media supplemented with 100 μg/mL kanamycin, 34 μg/mL chloramphenicol, and 0.05% arabinose. The next morning, the overnight culture was diluted 1000-fold into ZYM-5052 supplemented with 100 μg/mL kanamycin, 34 μg/mL chloramphenicol, and 0.05% arabinose. Larger cultures were shaken at 220 rpm until reaching an OD = 1, at which point the temperature was shifted from 37°C to 18°C and allowed to grow for another 16 hours. The cells were harvested at 4500 rpm for 30 minutes and bacterial pellets frozen at -20°C for at least 2 hours before lysis.

Purification of His-H_{mt}TrpRS

Upon thawing, cells were resuspended in lysis buffer (50 mM Hepes, 0.3 M NaCl, 10 mM BME, 1 M urea, 10% glycerol, 1% triton X-100, pH 8.0), sonicated and centrifuged (16000 rpm in SS34 rotor, 4°C, and 1 hour). His-H_{mt}TrpRS was captured from the lysate on Ni-NTA resin and eluted with 0.3 M imidazole. Purified protein was cleaved overnight with TEV protease while dialyzing against 50 mM Hepes, 0.2 M NaCl, 10 mM BME, pH 7.4. The cleaved protein mixture was passed back over a Ni-NTA column to capture both uncleaved protein and his-TEV protease. Size exclusion chromatography on a Superdex 200 column was used as a final purification step for H_{mt}TrpRS. Fractions containing H_{mt}TrpRS were pooled and concentrated using Amicon concentrators with MWCO 10,000.

Active Site Titration

Active sites were titrated by following the loss of (^{32}Pγ)-ATP to determine the fraction of molecules competent for catalysis as described by (34, 35). Plates were developed using a Typhoon Imager and analyzed with ImageJ (36) and JMP (37).

Michaelis-Menten Kinetics

The incorporation of (^{32}P)-PPi into ATP was tracked by TLC. Reactions contained 5000 cpm/µl (^{32}P)-PPi, 0.1 M Tris pH 8.0, 70 mM BME, 5 mM $MgCl_2$, 10 mM KF, 2 mM PPi, 2 mM ATP and tryptophan ranging from 1-1500 µM. When ATP was varied from 60 - 2000 µM tryptophan was used at a final concentration of 2 mM. Reactions were initiated with enzyme and carried out at 37°C.

Indolmycin Inhibition Assays

Inhibition assays were performed as described above; Michaelis-Menten experiments for tryptophan were performed in the presence of stoichiometric amounts of indolmycin to enzyme. Indolmycin to enzyme ratios of 1:5, 1:1 and 5:1 were used and results fitted to a competitive inhibition model (I) using JMP (37). This setup allowed for determination of K_m for tryptophan and K_i for indolmycin.

$$Rate = \frac{[Tryptophan] * k_{cat}}{\left(1 + \frac{[Indolmycin]}{K_i} + [Tryptophan]\right)} \quad \textbf{(1)}$$

Differential scanning fluorimetry (DSF; Thermofluor)

The effects of ATP, tryptophan, tryptophanamide (LTN), and indolmycin on the thermal stability of H_{mt}TrpRS were assessed by Thermofluor. The following saturating ligand concentrations were used: 10 mM ATP, 10 mM $MgCl_2$, 3 mM LTN, and 3 mM indolmycin. All reactions contained 8 µM H_{mt}TrpRS, 100 mM NaCl, 5 mM BME, 1 M guanidine hydrochloride, 50 mM Hepes pH 7.5, and 0.15% Sypro-Orange in a final volume of 20 µl. Temperature-dependent fluorescence intensities from 25-99°C were determined using an Applied Biosystems

7900HTFast Real Time (RT)PCR instrument, and data were analyzed with MATLAB (Mathworks) with routines developed by Visinets, Inc as described in the previous chapter.

Circular Dichroism (CD)

The CD spectrum of ligand-free H_{mt}TrpRS was recorded from 190-280 nm using a Jasco J-815 CD spectrometer. The sample contained 10 μM H_{mt}TrpRS, 50 mM Hepes, 1 mM BME, 150 mM NaF, pH 7.4 with and without 1 M guanidine hydrochloride in a final volume of 200 μl. Following collection of the CD spectrum, the sample was used for thermal melting analysis at 0.1 mm path length from 4-95°C.

Isothermal Titration Calorimetry (ITC)

Experiments were carried out at 37°C. The sample cell was filled with H_{mt}TrpRS in 50 mM Na_2HPO4, 150 mM NaCl, 10 mM BME, pH 7.4 with and without 10 mM $MgCl_2$ and 5 mM ATP. Using the MicroCal Auto-iTC200 system, ligands were added by a series of 20-2 μl injections with 180 seconds between each injection and a reference power of 8 μcal/sec. Twenty-seven 1.5 μl injections were used to titrate H_{mt}TrpRS pre-bound to Mg^{2+}•ATP with indolmycin. Data were analyzed using a one-site model in Origin *(OriginLab, Northampton, MA).*

Crystallization, Data Collection, Structure Determination

Crystals of H_{mt}TrpRS in complex with ATP, indolmycin and Mn^{2+} were grown by vapor diffusion against 25% glycerol, 20% Peg5000 and 0.1 M NaOAc. As the crystal growth solution was cryoprotective, crystals did not require further handling before plunging into liquid nitrogen. Data were collected at Southeast Regional Collaborative Access Team (SER-CAT) 22-ID beamline at the Advanced Photon Source, Argonne National Laboratory. Supporting institutions may be found at www.ser-cat.org/members.html. The structure (PDB accession code 5EKD) was determined using molecular replacement with the BsTrpRS structure (5DK4) as a starting model.

The initial model was improved using cycles of Coot (40) rebuilding and refinement using Phenix (39).

Results

Co-expression with GroEL/ES enhances both expression and solubility of dimeric H_{mt}TrpRS

Initial attempts to express 6xHis-HmtTrpRS in BL21(DE3)pLysS resulted in less than 5% of the H_{mt}TrpRS being soluble (Fig. 12A), with final yield of 2 mg H_{mt}TrpRS per 2 liters. Using auto-induction instead of IPTG increased total H_{mt}TrpRS expression without improving solubility (Fig. 12A). In an effort to promote the production of soluble H_{mt}TrpRS, we assessed the effect of co-expression with various chaperones on the solubility of H_{mt}TrpRS. Figure 12B shows how chaperone co-expression influenced both expression and solubility, with GroEL/ES-expressing cells producing more total H_{mt}TrpRS and the highest fraction of soluble H_{mt}TrpRS. Chaperone co-expression and auto-induction routinely resulted in ~20 mg of H_{mt}TrpRS per 1 L culture.

We employed the 6xHis-tag to isolate H_{mt}TrpRS from the soluble bacterial proteins on Ni-NTA resin. Most of the tagged-H_{mt}TrpRS bound the Ni-NTA with minor contaminants that were eliminated by size exclusion chromatography on a Superdex 200 column (Fig. 12C). The elution profile of H_{mt}TrpRS demonstrates that it passes through the Superdex 200 resin in a manner expected of a protein with a calculated molecular weight of 80 kDa. TrpRS enzymes are functional dimers and the calculated molecular weight correlates well with the expected size (76 kDa) of the H_{mt}TrpRS dimer. Active site titration experiments tracking the consumption of ATP over time show that each active site of the H_{mt}TrpRS dimer utilizes ATP to form the tryptophanyl-5'AMP (Fig. 13). If we use the dimeric enzyme concentration to calculate the fraction of active sites, we derive a number between 1.5 and 2. However, if we use the

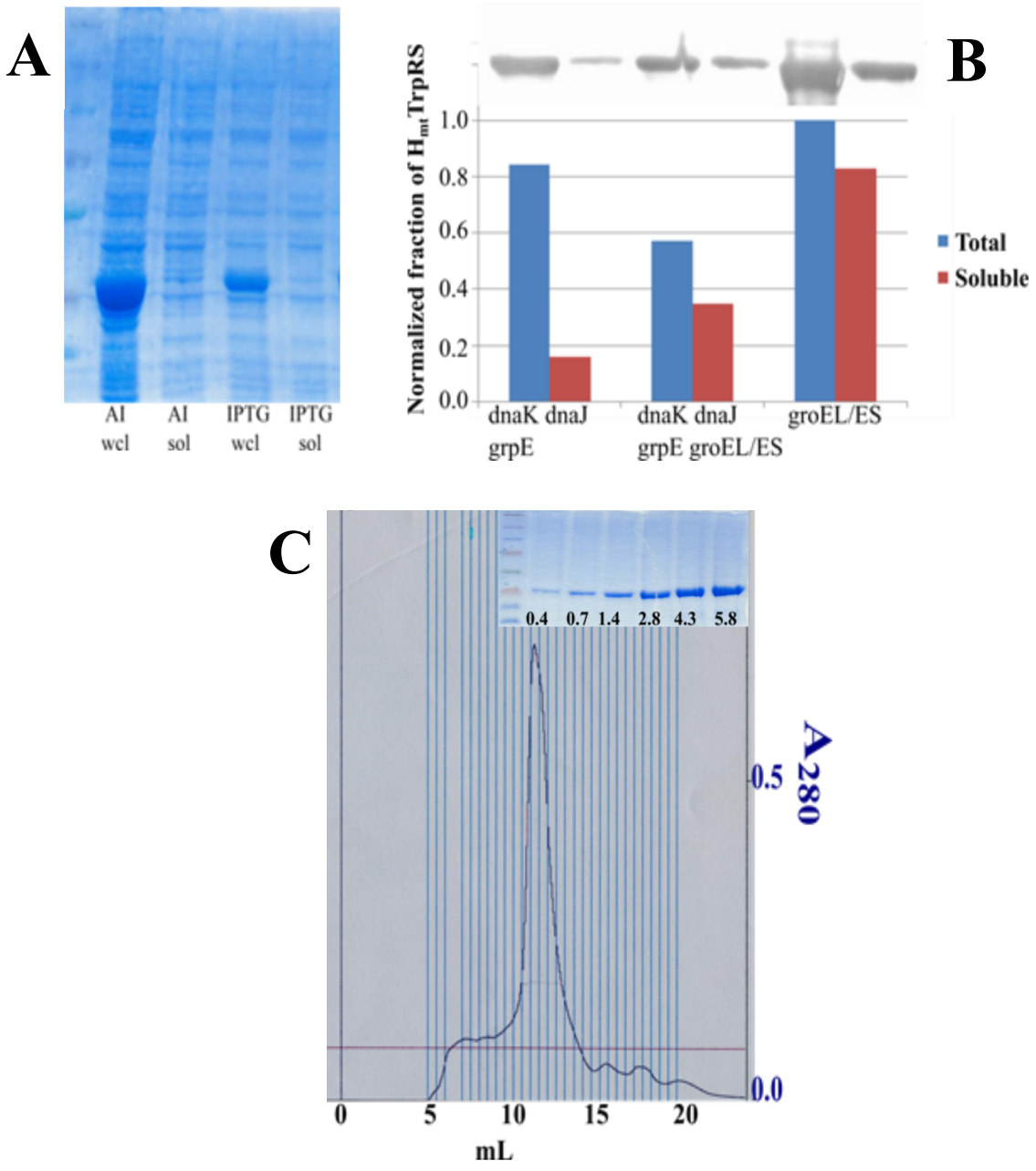

Figure 12: Auto-induction and chaperone co-expression increase the expression and solubility of dimeric H_{mt}TrpRS. A) Electrophoresis of whole-cell lysates (wcl) and soluble fractions (sol) showed that while auto-induction (AI) enhanced the overall expression of H_{mt}TrpRS it did not increase the fraction of soluble enzyme compared to the IPTG sample. B) Immunoblot analysis using an anti-His-tag antibody demonstrated that co-expression of H_{mt}TrpRS by auto-induction with the GroEL/ES yielded the highest overall expression and soluble fraction of H_{mt}TrpRS. C) Size-exclusion chromatography allowed us to determine that H_{mt}TrpRS exists as dimer in solution. Gel inset shows purity of the final protein sample. No other proteins were identified when up to ~6 µg of total protein was separated by SDS-PAGE followed by staining of the gel with Coomassie Blue (gel inset).

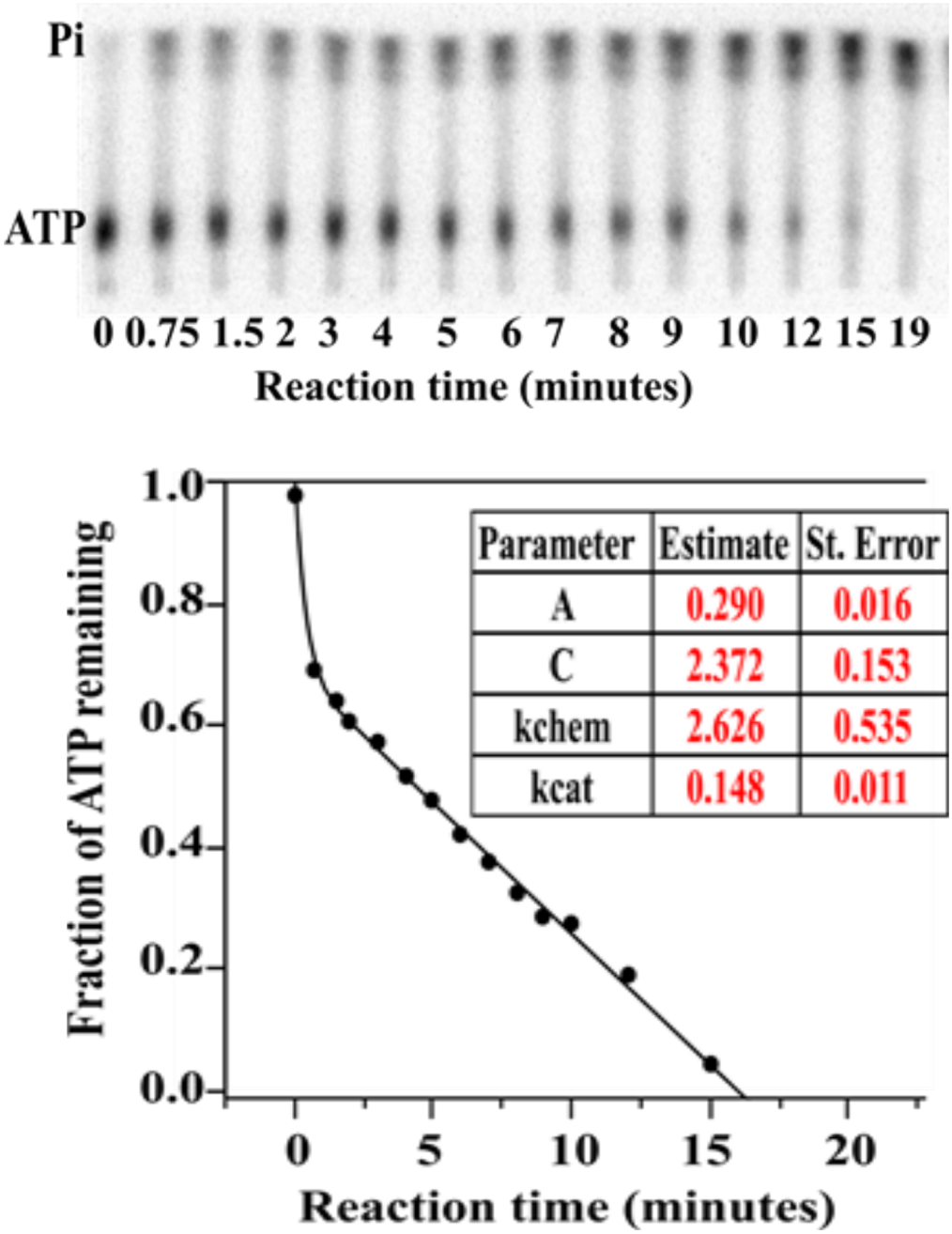

Figure 13: H_{mt}TrpRS is a dimer in solution with ~100% active sites participating in catalysis. Our purification scheme routinely produced catalytically-active H_{mt}TrpRS enzyme with 75-100% of the active sites participating in catalysis. The fraction of active sites was determined by active site titration (top; TLC plate) using 10 μM ATP, 3 μM total H_{mt}TrpRS active sites (1.5 μM dimer) and 1 mM tryptophan.

concentration of total active sites, then we routinely derive a number between 0.75 and 1. This demonstrates that both active sites of the H_{mt}TrpRS dimer are capable of participating in the tryptophan-activation reaction at comparable rates.

N-terminal truncations have minimal effect on catalytic efficiency

Jorgensen *et al.* (28) described residues 1-19 as the mitochondrial targeting signal, while MitoProt (http://ihg.gsf.de/ihg/mitoprot.html) predicted that the localization signal continues through residue 33. Michaelis-Menten kinetics for full-length, Δ1-18, and Δ1-33 variants of H_{mt}TrpRS showed comparable k_{cat}/K_M values (Table 7). As the Δ1-18 variant consistently yielded higher protein concentrations and was efficiently cleaved by TEV protease, all kinetic, thermodynamic and structural studies were carried out on this variant.

H_{mt}TrpRS	**k_{cat}/K_M (s^{-1} M^{-1})**	**$(k_{cat}/K_M)_{relative}$**
1-360	1.35E04 ± 4.57E02	1.00 ± 0.05
Δ 1-18	1.29E04 ± 7.34E02	0.96 ± 0.06
Δ 1-33	1.42E04 ± 9.01E02	1.05 ± 0.08

Table 7: Catalytic efficiency of H_{mt}TrpRS is independent of residues 1-33. Steady-state kinetics experiments tracking the incorporation of ^{32}P-PPi into ATP were performed at saturating tryptophan and variable ATP concentrations with three variants of the H_{mt}TrpRS enzyme. The data, fitted by non-linear regression modeling to simultaneously determine K_M ATP and k_{cat}, show that the three variants have statistically indistinguishable catalytic efficiencies.

Indolmycin is a tight-binding inhibitor of H_{mt}TrpRS

Table 8 summarizes our determination of the indolmycin inhibition constant by steady-state kinetics as well as the dissociation constants obtained by isothermal titration calorimetry. The human mitochondrial (H_{mt})TrpRS is about 130-fold less proficient than the bacterial enzyme, owing to roughly similar differences in both k_{cat} (7-fold smaller) and K_M (19-fold greater). Despite the extensive structural similarity between indolmycin and substrate tryptophan indolmycin selectively binds approximately 1000x tighter to BsTrpRS and H_{mt}TrpRS than the

natural tryptophan substrate. Cytosolic isoforms of eukaryotic TrpRS bind tryptophan ~1500x tighter than indolmycin. Thus, although both substrate and inhibitor share the indole ring and have similar hydrogen bonding groups associated with all three α-carbon substituents, indolmycin exploits the apparently minor differences elsewhere to enhance binding to bacterial TrpRS, yet reduce binding to the cytosolic TrpRS, leading to a discrimination between the cytosolic and bacterial forms of close to 10^6-fold.

Parameter	Indolmycin [M]	Mg^{2+}•ATP
K_i	8.45E-08 ± 1.43E-08	present
K_D	5.46E-08 ± 9.47E-09	present
K_D	4.21E-06 ± 6.22E-07	absent

Table 8: Indolmycin inhibits H_{mt}TrpRS and its binding is potentiated by Mg^{2+}•ATP. Steady-state kinetics experiments performed with saturating amounts of ATP at various tryptophan and indolmycin concentrations show indolmycin inhibits H_{mt}TrpRS with nanomolar affinity (row 1). Measuring dissociation constants (K_D) for indolmycin in the presence (row 2) and absence (row 3) of Mg^{2+}•ATP by isothermal titration calorimetry revealed an enhanced affinity of the H_{mt}TrpRS•Mg^{2+}•ATP complex for indolmycin over apo-H_{mt}TrpRS. The measured K_D in the presence of Mg^{2+}•ATP agrees with the experimentally-derived K_i.

From our studies we determined that H_{mt}TrpRS is 42-times less likely to bind indolmycin than is BsTrpRS and ~10^4-times more likely than eukaryotic cytosolic TrpRS enzymes. The reduced sensitivity of mitochondrial TrpRS relative to BsTrpRS defines a quantitative window within which it may be possible to design useful bacterio-specific anti-infective agents.

Indolmycin-induced thermal stability is not enhanced by Mg^{2+}•ATP

As revealed by differential scanning fluorimetry, apo-H_{mt}TrpRS (ΔT_m= 83.7 ± 0.5°C) is more stable than apo-BsTrpRS (ΔT_m= 69.0 ± 0.2°C) by ~15°C. As we expected ligand binding to confer additional thermal stability to H_{mt}TrpRS we modified our assay buffer to include 1 M guanidine-hydrochloride, which lowered the melting temperature of apo-H_{mt}TrpRS by ~7°C.

Surprisingly, saturating concentrations of neither ATP nor tryptophan have strong effects on the thermal stability of H_{mt}TrpRS (Table 9). Indolmycin was the only ligand tested that altered the thermal stability, shifting T_m by ~9°C. In contrast to the results of similar experiments using BsTrpRS, the presence of Mg^{2+}•ATP did not alter the stabilizing effect of indolmycin on H_{mt}TrpRS (Table 9).

Ligand	T_m (°C)	Stdev T_m
LF	76.69	0.55
Mg^{2+}•ATP	77.00	0.56
Trp	77.12	0.66
TNH	77.28	0.46
TNH + Mg^{2+}•ATP	77.34	0.44
IND	85.95	0.89
IND + Mg^{2+}•ATP	85.51	0.75

Table 9: Ligand-dependent thermal stability of H_{mt}TrpRS. Neither substrates (ATP or tryptophan) nor the substrate analog tryptophanamide contributed to the thermal stability of H_{mt}TrpRS in the transition to molten globule formation. Similarly, full occupancy of both the ATP and tryptophan binding sites (with either Trp or LTN) did not the enzyme's thermal stability profile. Indolmycin binding enhanced thermal stability by ~9°C. Unlike was observed for BsTrpRS, there was no additional stability conferred by having both indolmycin and Mg^{2+}•ATP bound to the active site.

Indolmycin affinity is enhanced by Mg^{2+}•ATP binding

Isothermal titration calorimetry experiments showed 1:1 binding of indolmycin to each active site of the functional H_{mt}TrpRS dimer with a dissociation constant (K_D) of 4.2 ±0.6 μM (Fig. 14A and Table 8). Pre-loading the enzyme with Mg^{2+}•ATP results in ~77-fold tighter binding of indolmycin and a K_D of 54.6 ±9.5 nM (Table 8, Fig. 14B). This value correlates well with our kinetically-derived K_i of 84.5 ±14.3 nM. Based on our inhibition studies we expected a difference of approximately -4 kcal/mol between the Gibbs free energies, ΔΔG, of the fully-

liganded inhibited (IND + Mg^{2+}•ATP) and catalytic (Trp + Mg^{2+}•ATP) complexes. Titration of H_{mt}TrpRS•Mg^{2+}•ATP with indolmycin and tryptophanamide, a non-reactive tryptophan analog shown to preserve most, if not all, of the tryptophan-TrpRS interactions, yielded a ΔΔG of -3.1 kcal/mol (Fig. 15A, B, C).

Oxazolinone-Mg^{2+}•ATP interaction stabilizes the indolmycin-inhibited complex

If we consider tryptophan and indolmycin as both having an indole moiety while tryptophan lacks the methylamino-substituted oxazolinone ring (OXA), then we can describe tryptophan(amide) as +indole, -OXA and indolmycin as +indole, +OXA (Fig. 15A). Any differences in Gibbs free energy between the H_{mt}TrpRS•tryptophanamide, ΔG = -6.80 ± 0.10 kcal/mol, and H_{mt}TrpRS•indolmycin, ΔG = -7.67 ± 0.11 kcal/mol, complexes are attributed to OXA (Fig. 15B). Bearing this in mind we determined that the added OXA moiety provides 0.87 kcal/mol ($\Delta\Delta G_2$) of stabilization energy upon binding to apo-H_{mt}TrpRS (Fig. 15C). Given our previous result that Mg^{2+}•ATP enhances the affinity of H_{mt}TrpRS for indolmycin with the H_{mt}TrpRS•Mg^{2+}•ATP•IND complex being more stable than the H_{mt}TrpRS•IND complex by 2.65 kcal/mol ($\Delta\Delta G_3$) we wanted to know if Mg^{2+}•ATP has a similar impact on the energetics of tryptophan binding.

Interestingly, the H_{mt}TrpRS•Mg^{2+}•ATP•LTN and H_{mt}TrpRS•LTN complexes only differ by 0.46 kcal/mol ($\Delta\Delta G_1$), suggesting that the oxazolinone moiety of indolmycin is critical for the Mg^{2+}•ATP-dependent stabilization. These four measurements allowed us to construct a thermodynamic cycle in which tryptophanamide, used in lieu of tryptophan to prevent catalysis, was the starting point (upper left corner), Mg^{2+}•ATP was varied from top (absent) to bottom (present), and OXA was varied from left (absent) to right (present) (Fig. 15C). Subtracting left

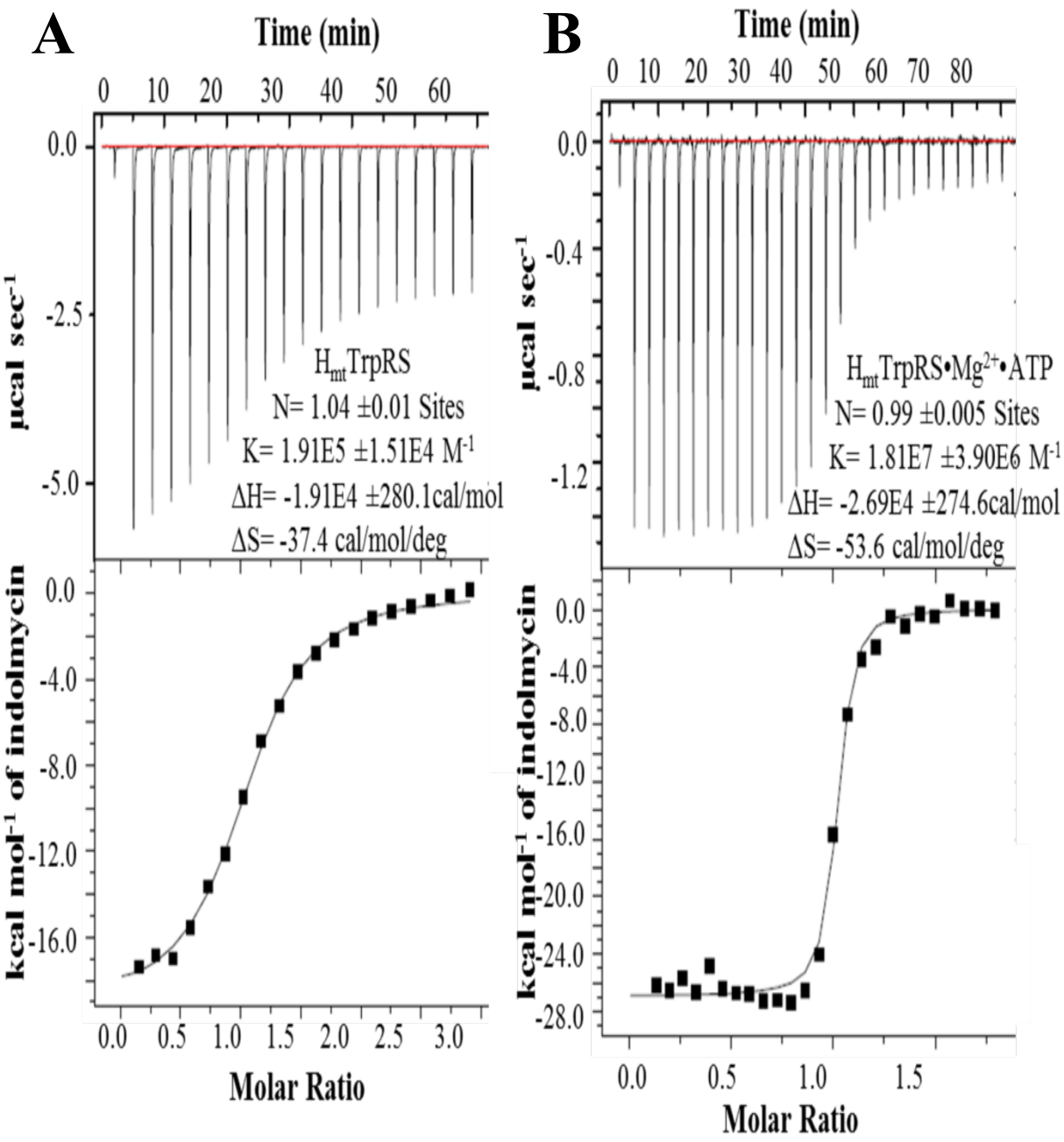

Figure 14: Pre-binding with Mg^{2+}•ATP enhances the affinity of H_{mt}TrpRS for indolmycin. Isothermal titration calorimetry experiments revealed a 1:1 binding stoichiometry of indolmycin:H_{mt}TrpRS active site both in the absence (A) and presence (B) of Mg^{2+}•ATP. Apo-H_{mt}TrpRS binds indolmycin ~77-times weaker than does Mg^{2+}•ATP-bound H_{mt}TrpRS.

from right and top from bottom gives the difference in Gibbs free energy (ΔΔG) due to the addition of OXA and Mg^{2+}•ATP, respectively. Non-equivalence of ΔΔG for opposing faces of the cycle, resulting from non-additivity of the energetic contributions of OXA and Mg^{2+}•ATP, is indicative of an interaction between OXA and Mg^{2+}•ATP in the H_{mt}TrpRS•Mg^{2+}•ATP•IND complex. It is evident from this thermodynamic cycle that the effect of adding both OXA and Mg^{2+}•ATP is greater than the sum of their individual effects; i.e. the stabilizing effect of one is dependent on the presence of the other. The non-additivity of the energetic contributions of Mg^{2+}•ATP and the OXA moiety reveals a $\Delta\Delta G_{interaction}$ of -2.20 kcal/mol in the H_{mt}TrpRS•IND•Mg^{2+}•ATP complex. The difference in Gibbs free energy for this complex and H_{mt}TrpRS•LTN is -3.5 kcal/mol or $\Delta\Delta G_1 + \Delta\Delta G_2 + \Delta\Delta G_{int}$ (Fig. 15C).

Indolmycin binds to H_{mt}TrpRS as a ternary complex with ATP

Unlike the closed-state crystal structures of BsTrpRS, all of which have a monomer in the asymmetric unit, H_{mt}TrpRS crystallized in space group C121 with a dimer in the crystallographic asymmetric unit and diffracted to 1.82 Å (Fig. 16A and Table 10). Each monomer contains ATP, Mn^{2+} and indolmycin in the active site at essentially full occupancy. Mn^{2+} was used in replacement of Mg^{2+} because we hoped to use the Mn^{2+} anomalous signal to derive experimental phase information. Although the signal was too weak for phasing, the anomalous signal did allow us to definitively identify the metal binding site. There was no electron density in which to place N-terminal residues 19-33 and 19-28 in monomers A (grey) and B (purple), respectively.

Using areaImol (62, 63), monomer A has a solvent-accessible area of 13957.4 and 15918.3 $Å^2$ in the presence and absence of monomer B, respectively. The solvent-accessible area for monomer B alone is 15642.4 $Å^2$ and 13695.5 $Å^2$ in the dimer. The calculated buried surface

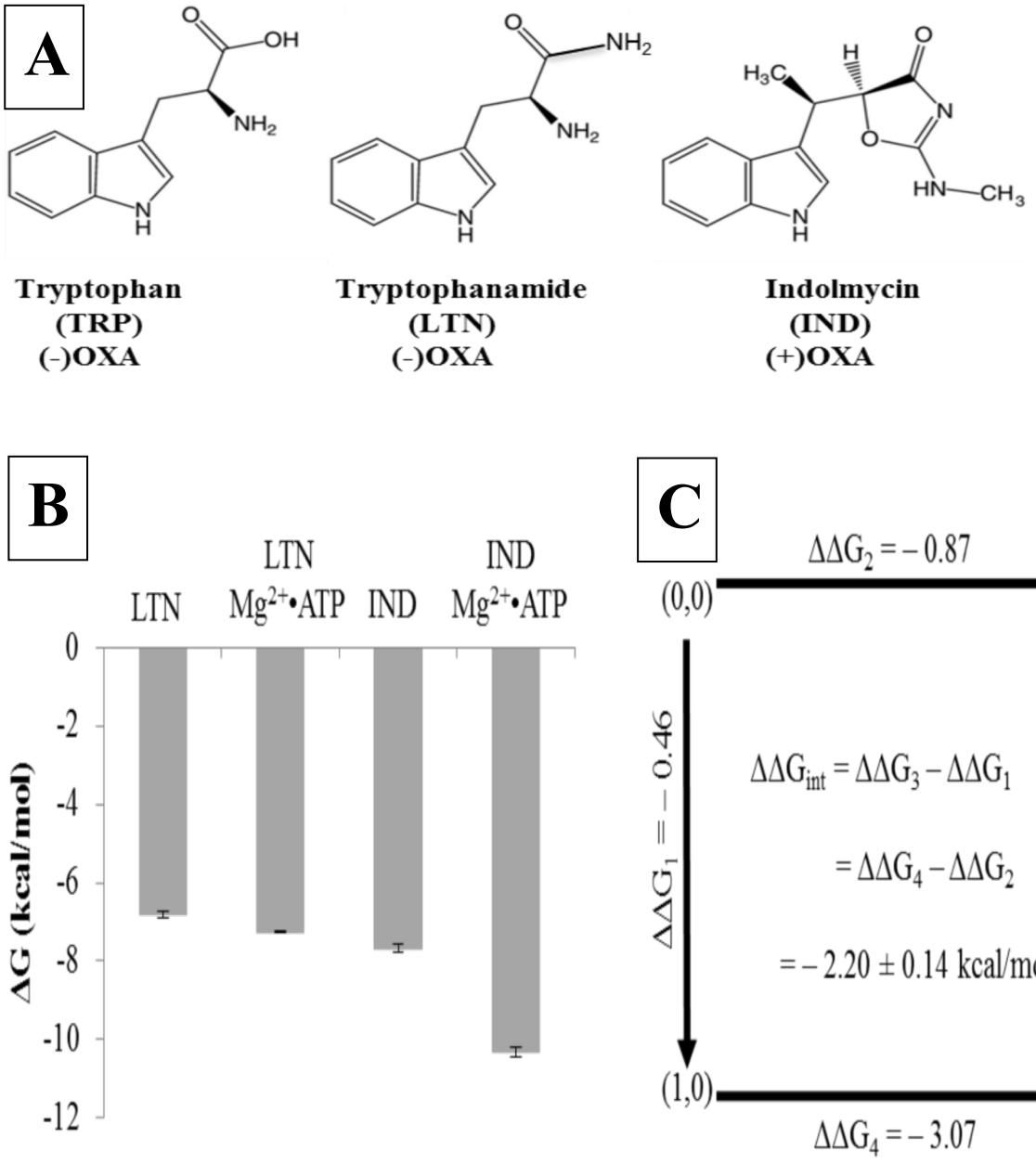

Figure 15: The potentiation effect of Mg^{2+}•ATP is mediated via the methylamino-substituted oxazolinone (OXA) moiety of indolmycin. (A) LTN is a conservative substitute for the tryptophan substrate in which the sole difference is replacement of a carboxylate oxygen atom by an amine group. Both have an indole moiety and lack the oxazolinone ring present in indolmycin. (B) The relative stability of four H_{mt}TrpRS complexes were assessed using thermodynamic measurements obtained from replicate ITC experiments. With a difference in Gibbs free energy of 3.5 kcal/mol the LTN and IND•Mg^{2+}•ATP complexes are the least and most stable, respectively. (C) The structural differences between LTN and IND account for a $\Delta\Delta G_2$= -0.87 kcal/mol. This stabilizing effect more than triples to -3.07 kcal/mol ($\Delta\Delta G_4$) in the presence of Mg^{2+}•ATP due to an interaction energy ($\Delta\Delta G_{int}$) between the methylamino-substituted oxazolinone moiety and Mg^{2+}•ATP of -2.20 kcal/mol. (0,0) = -OXA, -ATP; (0,1) = +OXA, -ATP; (1,0) = -OXA, +ATP; (1,1) = +OXA, +ATP; -OXA = tryptophanamide; +OXA = indolmycin.

area due to dimer formation is 3907.8 $Å^2$. Similar calculations using pymol yielded a buried surface area of 3815.5 $Å^2$. As is the case for the bacterial enzyme, a prominent feature of the dimer interface is the burial of a tryptophan side-chain (Trp 125) across the dimer interface into a space bounded by the specificity helix of the other monomer (Fig. 16B). A hydrogen bond between the carbonyl oxygen of Leu 76 and NE1 of Trp 125 helps stabilize the dimer interface. As measured from CH2, Trp 125 is 4.0 Å away from OG1 of Thr 159 and 4.1 Å from the Cα of Tyr 160. Both Thr 159 and Tyr 160 are part of the specificity helix and Tyr 160 stacks against the oxazolinone ring of indolmycin.

Superposition of the two monomers reveals structural differences in the region of loop 144-150 (Fig. 16C, D) that are presumably responsible, in part, for the inclusion of a dimer in the asymmetric unit. This loop is disordered in H_{mt}TrpRS monomer B, as evidenced by a lack of electron density, but well-ordered in monomer A. His 140 to Ala 144 of monomer A is helical and angled away from the active site compared to the helix formed by His 140-Thr 146 in monomer B. Residues from Thr 147 to Asp 152 form a helix in monomer A but cannot be placed in monomer B. This region contains a catalytically-relevant lysine residue, Lys 145, which is homologous to Lys 111 in BsTrpRS. The relative positions of Lys 145 in the two monomers differ by 5.1 Å as measured from the α-carbons following superimposition of monomer B onto monomer A (Fig. 16D). The NZ atom of Lys 145 is 9.9 Å away from the nearest gamma phosphate oxygen atom in monomer A but only 5.4 Å away in monomer B. While neither residue is in position to form direct interactions with ATP as is observed in the BsTrpRS pre-transition state and inhibited complexes, Lys 145 in monomer B does structurally align with BsTrpRS Lys 111. Loop 148-152 corresponds to residues 112-117 in BsTrpRS, which also was fitted with difficulty for some structures, depending on which ligands occupied the active site.

Kinetic analysis of mutants in this region in both TrpRS (20, 64) and TyrRS (64) show that residues from this loop contribute to ATP binding only in the transition state and imply that movement of the loop occurs during catalysis. In BsTrpRS Lys 111 competes with the catalytic Mg^{2+} ion for the same negatively charged gamma phosphate oxygen atom in the pre-transition state (2.9 Å) and inhibited state (3.4 Å) complexes. Mutation of Lys 111 to alanine affects k_{cat} but not K_M for ATP (20).

The H_{mt}TrpRS anticodon-binding domain is rotated ~5 degrees closer to the Rossmann fold domain than it is in the PreTS and inhibited BsTrpRS structures. Without knowing structures of tRNA complexes for either protein, it is possible only to speculate that this difference relates to differences between the respective tRNA structures.

Indolmycin interactions with active-site side-chains mimic those observed for BsTrpRS

The indole moiety of indolmycin is recognized by Asp 167 of the specificity helix as is observed for the homologous Asp 132 in BsTrpRS complexes (Fig 17B). Specifically, the side-chain of Asp 167 accepts a hydrogen bond (3.0 Å) from the pyrrole ring nitrogen. Phe 38 forms π-π stacking interactions while Ile 41, Val 74, Ile 168, Val 176 and Val 178 make van der Waals contacts with indolmycin. Side-chain atoms of His 77 and Gln 182 donate hydrogen bonds to the methylamino nitrogen (3.0 Å) and carbonyl oxygen (3.1 Å) atoms of indolmycin, respectively. The carbonyl oxygen accepts an additional hydrogen bond from a metal-coordinating water molecule, as does the oxazolinone nitrogen (Figure 17A, B).

H_{mt}TrpRS binds ATP in an extended conformation

H_{mt}TrpRS utilizes conserved residues for substrate recognition and binding. As was observed for the indolmycin-inhibited BsTrpRS complex, the negative charges of the triphosphate oxygen atoms form strong electrostatic interactions with a metal ion. In this

Data Collection	
Space group	C 1 2 1
Cell Constants	58.289 Å 78.087 Å 153.996 Å
a, b, c, α, β, γ	90.00° 96.55° 90.00°
Resolution (Å)	29.06 – 1.82
Completeness (%)[a]	98.5 (95.8)
Rmerge (%)[a]	7.7 (59.4)
Rmeas (%)[a]	9.8 (76.1)
Rpim (%)[a]	6.0 (47.0)
Mean I/σI [a]	8.1 (1.5)
Number of Observations	139667
Multiplicity	2.3
Refinement	
R_{work}/R_{free} (%)	17.2/20.7
Fo, Fc correlation	0.96
RMS (bonds)	0.004
RMS (angles)	0.92
Ramachandran favored (%)	97.0
Ramachandran outliers (%)	0.0
Average B, all atoms ($Å^2$)	28.8
Clash score	5.76
PDB Entry ID	5EKD

[a]Highest resolution shell is shown in parentheses.

Table 10: Data collection and refinement statistics for H_{mt}TrpRS inhibited complex. The H_{mt}TrpRS•Indolmycin•Mn^{2+}•ATP complex was determined to 1.82 Å resolution by molecular replacement using the BsTrpRS inhibited complex (PDB 5DK4) as a model. The final structure was refined to an R_{Work}/R_{Free} of 17.0/20.7%.


A

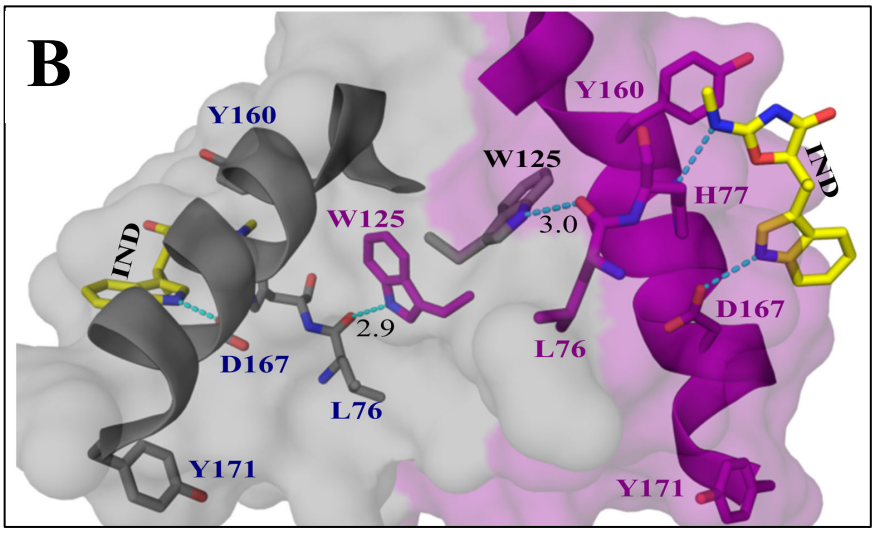
B
Y160
W125
IND
H77
3.0
W125
IND
D167
2.9
L76
D167
L76
Y171
Y171

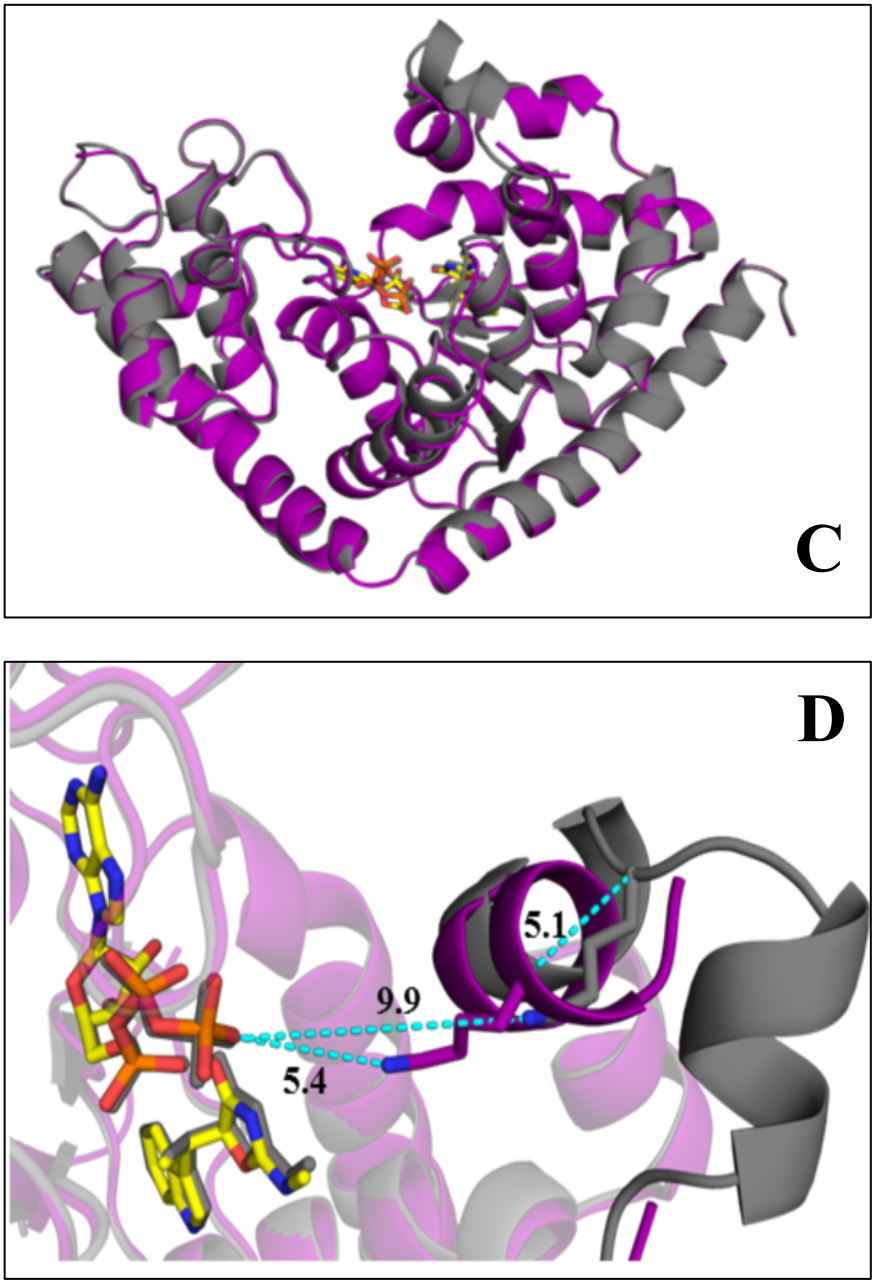

Figure 16: Dimeric H_{mt}TrpRS binds one molecule of ATP and indolmycin per active site. (A)Two monomers, A (grey) and B (purple), form the functional dimer. (B) A prominent feature of the dimer interface is the inter-monomeric burial of Trp 125, whose side chain is stabilized by a hydrogen bond to the carbonyl oxygen of Leu 76. This feature was also observed in several BsTrpRS structures. (C) Structurally, the two monomers are quite similar but show variation in the position of residues 140-150. (D) The importance of this difference to ligand binding is unknown. However, Lys 145 is analogous to Lys 111_{Bs}, which shows ligand-dependent structural variation.

case, Mn^{2+} is hexavalently coordinated by an oxygen atom from each phosphate group and three water molecules (Fig. 17A). The three phosphate groups are additionally stabilized by direct and water-mediated protein interactions. Gln 42 (2.8-3.0 Å), Asn 51 (3.1 Å) and Lys 229 (2.8 Å) form contacts with P_α, while Lys 226 (2.9 Å), Lys 229 (2.9 Å) and His 48 (2.9 Å) donate hydrogen bonds to P_β oxygen atoms (Fig. 17C).The backbone amide and side-chain hydroxyl groups of Ser 230 contribute to the stabilization of Pγ via two hydrogen bonds (3.2 and 2.6 Å). Thr 44, Lys 145 (B), Ser 228, and Lys 229 form additional water-mediated interactions with gamma-phosphate oxygen atoms.

The adenine 6-amino group donates a hydrogen bond to the backbone carbonyl oxygen atoms of Val 217 (2.9 Å) and Met 227 (2.9 Å) (Fig. 17D). The nitrogen atoms of the adenine ring accept hydrogen bonds from the amide groups of Val 217 (3.1 Å) and Gly 50 (3.1 Å) as well as from the side-chain NZ atom of Lys 226 (3.0 Å). The ribose moiety interacts with the conserved HIGH (48-51) and GxDQ (179-182) motifs. Specifically, the 2'OH group accepts a hydrogen bond from Gly 179 (3.0 Å) and donates a hydrogen bond to Asp 181 (2.7 Å) while Asn 51 donates a hydrogen bond to the ringed oxygen atom. The 3'OH group forms a close interaction (2.6 Å) with a water molecule (Fig. 17D). These interactions mimic closely those observed in BsTrpRS pre-transition state complexes (17, 22, 42).

Mutations to active site residues have greater impact on k_{cat} than K_M ATP

To confirm the functional equivalences with BsTrpRS inferred from the H_{mt}TrpRS structure, we chose to assess the impact of amino acid substitution at positions 42, 48, 145, 181, and 229. Gln 42, Asp 181 and Lys 229, which form direct polar interactions with ATP (Fig 17C, D) and are conserved at positions 9, 146, and 195, respectively, in BsTrpRS were individually mutated to alanine while His 48, which is analogous to BsTrpRS Thr 15, was mutated to

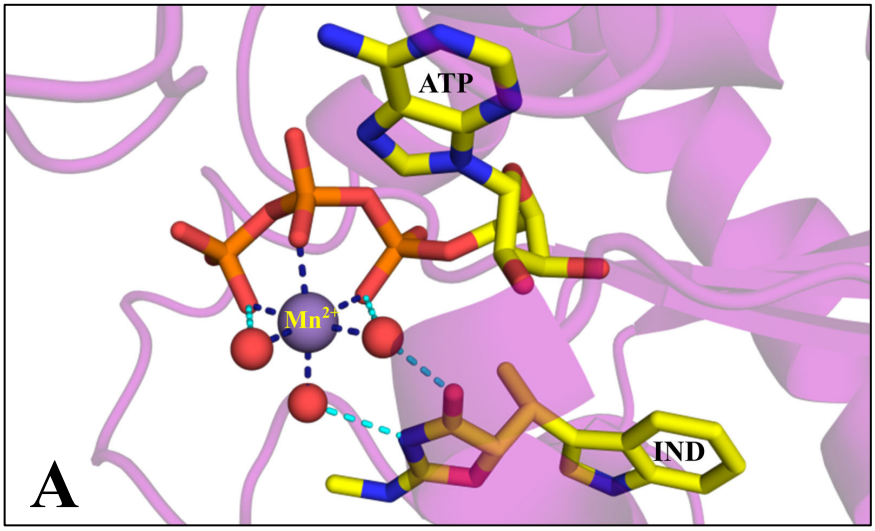
ATP
Mn2+
IND
A

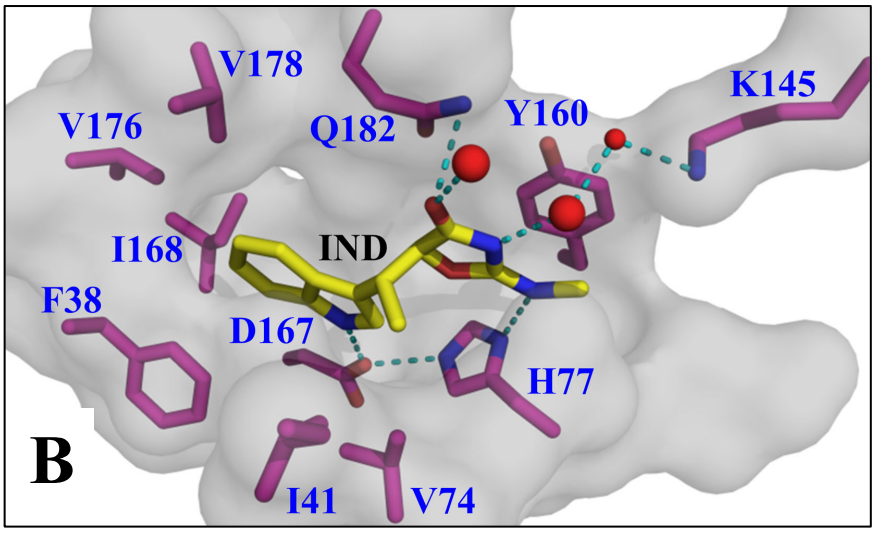
V178
V176
Q182
Y160
K145
I168
IND
F38
D167
H77
B
I41
V74

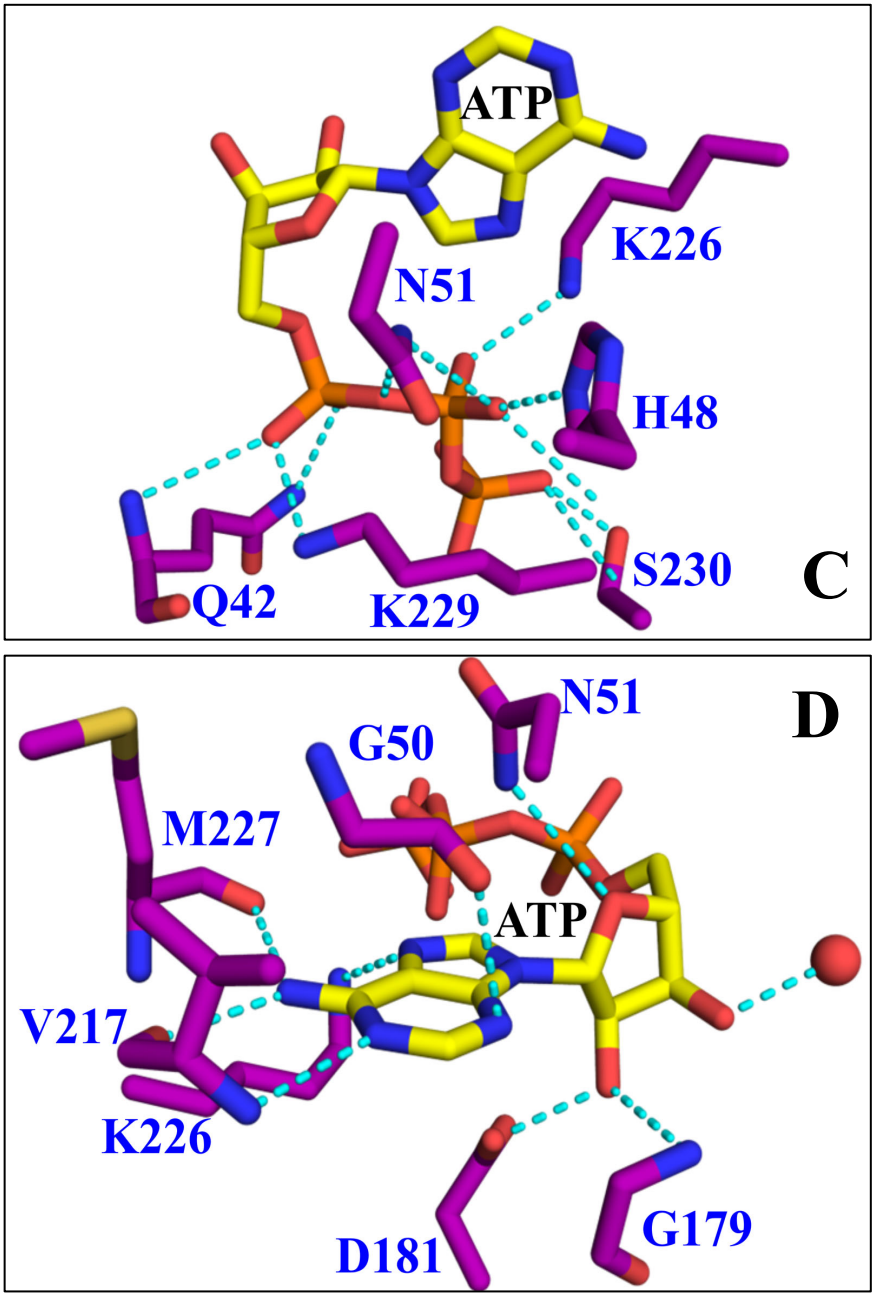

Figure 17: Molecular determinants of indolmycin and ATP binding are conserved in H_{mt}TrpRS and BsTrpRS. (A) Like BsTrpRS, the inhibited H_{mt}TrpRS complex involves a hexacoordinated-metal ion. (B) Binding of indolmycin involves hydrophobic, π-π, and hydrogen bonding interactions. The interactions with His 77, Asp 167, Gln 182 and two metal-coordinated water molecules mirror those observed in the inhibited BsTrpRS complex. (C) ATP binds in an extended configuration with the HIGH and KMSKS motifs stabilizing the triphosphate moiety. (D) The adenine and ribose moieties of ATP are recognized by the three signature sequences for class I aaRS enzymes; HIGH, GxDQ and KMSKS.

threonine. Although we did not observe direct interactions with ATP, we chose to substitute Lys 145 with an alanine due in part to the structural variation between monomers A and B as well as the 18.5-fold decrease in k_{cat} observed for the corresponding K111A BsTrpRS mutant.

In all, these amino acid substitutions cause less than a two-fold change in ATP affinity but vary greatly in their impact on k_{cat} (Fig.18, Table 11). The H48T variant retained the most catalytic activity with a modest 1.4-fold reduction in k_{cat} while substitution of alanine for Lys145 eliminated ~75% of the enzyme's catalytic efficiency. By comparison, the K111A BsTrpRS variant is 94% less efficient than wild-type BsTrpRS. Alanine substitution of Gln 42, which forms a hydrogen bond with each non-bridging alpha-phosphate oxygen atom of ATP, preserves the weak backbone interaction (3.4 Å) but eliminates the hydrogen bond formed between the side chain amide nitrogen and the metal-coordinated P_{α} oxygen (3.0 Å). The Q42A mutant has a relative catalytic efficiency of 0.15 due primarily to a 9.4-fold reduction in k_{cat}. Alanine substitution of either Asp 181 or Lys 229 disrupts the electrostatic environment of the active site as well as the hydrogen bonding network between the enzyme and ATP substrate. Removal of the negatively-charged Asp 181 results in a 50-fold reduction in k_{cat}. Alanine substitution of Lys 229 has an even greater effect on catalysis. The catalytic efficiency of the K229A mutant enzyme is only 0.5% that of wild-type H_{mt}TrpRS. Thus, as observed both for BsTrpRS (20) and BsTyrRS (64), active site interactions with ATP appear to manifest mutational effects only in the transition state affinity.

H_{mt}TrpRS	k_{cat} (s^{-1})	K_M (M)	k_{cat}/K_M (s^{-1} M^{-1})
WT	4.61 ± 0.03	3.59E-04 ± 2.23E-05	1.29E04 ± 7.34E02
H48T	3.28 ± 0.01	3.95E-04 ± 3.00E-06	8.30E03 ± 5.08E01
K145A	1.27 ± 0.13	4.38E-04 ± 1.24E-04	3.09E03 ± 1.09E03
Q42A	0.49 ± 0.01	2.55E-04 ± 2.52E-06	1.92E03 ± 2.05E01
D181A	0.09 ± 0.01	5.36E-04 ± 9.09E-05	1.60E02 ± 1.49E01
K229A	0.02 ± 0.01	3.71E-04 ± 7.33E-05	6.35E01 ± 2.37E01

Table 11: Reduced catalytic efficiency of active site mutants is driven by diminished k_{cat}. Amino acid substitutions to residues involved in ATP binding to H_{mt}TrpRS have a broader effect on k_{cat} than K_M ATP. Alanine substitution at either position 181 or 229 abolished ~99% of the catalytic efficiency while the K145A and Q42A variants lost 75% and 85%, respectively.

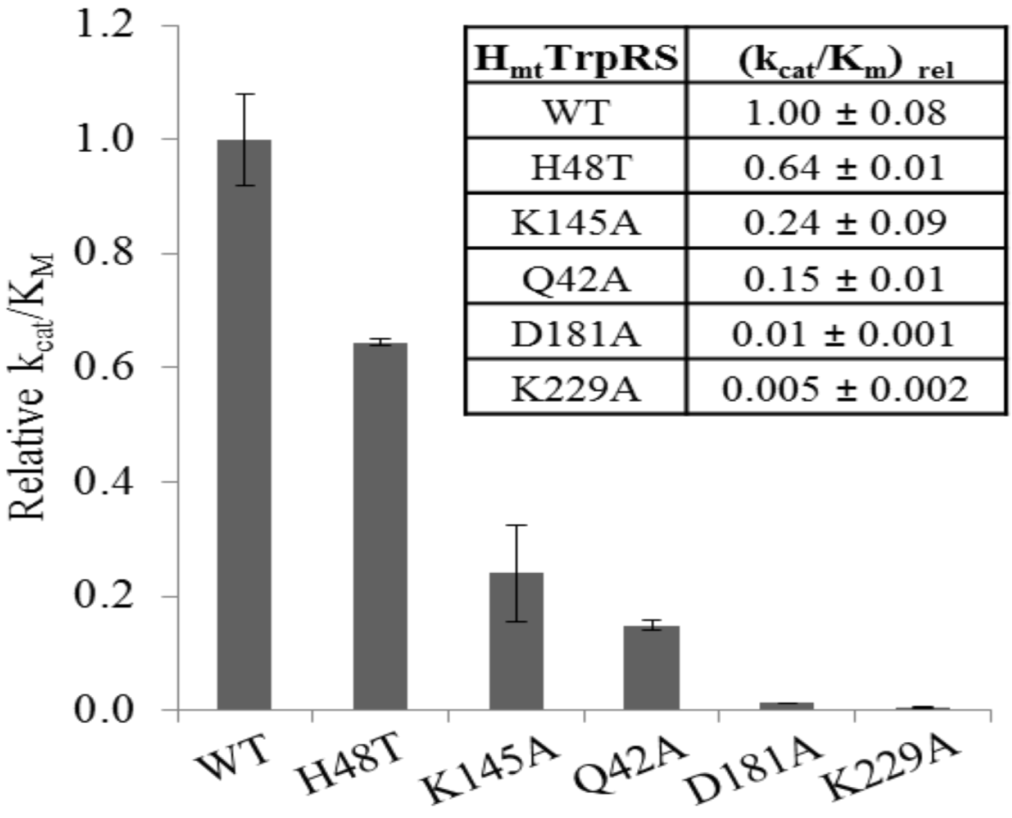

Figure 18: Mutations to active site residues have varying effects on catalytic efficiency. Data from steady-state Michaelis-Menten experiments were fitted by non-linear regression modeling to determine k_{cat} and K_M ATP for six H_{mt}TrpRS variants. The catalytic efficiency of each variant was determined and normalized to the wild-type Δ1-18 enzyme. The H48T and K229A mutants were the most and least efficient variants, respectively.

Discussion

There are distinctive evolutionary divergences between the eukaryotic and bacterial TrpRS enzymes (13, 58). Curiously, there is low conservation between the cytosolic, mitochondrial and bacterial TrpRS homologs at residues shown to form stabilizing interactions with tryptophan in H_cTrpRS. These sequence and structural variations affect the way these enzymes respond structurally following substrate binding, how they couple conformational changes to catalysis, the manner in which they hold the tryptophanyl-5' AMP intermediate as well as their ability to discriminate between tryptophan and other indole-containing compounds. This latter feature protects eukaryotic cytosolic TrpRS enzymes from inhibition by indolmycin while, as will be discussed, leaving mitochondrial and most prokaryotic TrpRS enzymes susceptible to inhibition.

Shared inhibition mechanism of BsTrpRS and H_{mt}TrpRS by indolmycin

Structural, kinetic and thermodynamic studies of BsTrpRS and H_{mt}TrpRS identify a shared mechanism for indolmycin inhibition of prokaryotic and mitochondrial TrpRS enzymes. Specifically, a conserved aspartic acid ($Asp132_{BS}$; $Asp167_{Hmt}$) in the specificity helix recognizes the indole nitrogen while recognition of the methylamino-nitrogen and carbonyl oxygen atoms of indolmycin by ND1 of His 77 ($His\ 43_{BS}$) and the side chain amide nitrogen of Gln 182 ($Gln\ 147_{BS}$), respectively, restrict the plane of the oxazolinone ring. Indolmycin is further stabilized by hydrogen bonding interactions via the carbonyl oxygen and oxazolinone nitrogen atoms with two metal-coordinated water molecules. The presence of the catalytic metal ion is required for the non-additive interaction energy between indolmycin and ATP. In the presence of Mg^{2+}, the oxazolinone-ATP interaction contributes ~-2.2 kcal/mol to the indolmycin binding energy. The additional contacts made with the oxazolinone moiety results in BsTrpRS and H_{mt}TrpRS each

having a higher affinity for indolmycin than its tryptophan substrate while the oxazolinone•Mg^{2+}•ATP interaction locks the enzymes in a stable, off-path inhibited state.

Conserved aspartic acid recognizes indole nitrogen

Human mitochondrial TrpRS has an aspartic acid residue in its specificity helix that is conserved among prokaryotic but not eukaryotic cytosolic TrpRS enzymes. The side-chain of this residue is used by prokaryotic TrpRSs to recognize the indole nitrogen of the tryptophan substrate and contributes to binding stability via a hydrogen bond. Eukaryotic cytosolic TrpRS enzymes, which lack this aspartic acid residue, rely on a tyrosine and glutamine that are closer to the N-terminus for recognition of the indole nitrogen. H_cTrpRS, which lacks a homologous aspartate in its specificity helix, undergoes induced fit rearrangement of its active site in response to tryptophan binding (23, 25, 27). This rearrangement relies on specific hydrogen bonding pattern between the tryptophan substrate and active site residues, allowing H_cTrpRS to better discriminate between tryptophan and other indole-containing compounds. Of the six H_cTrpRS residues that make direct contacts with tryptophan only one residue beside the strictly conserved glutamine of the GxDQ motif is conserved in H_{mt}TrpRS (Fig. 11). Tryptophan binding to BsTrpRS, promoted by a single hydrogen bond between the indole nitrogen of tryptophan and Asp 132 of the specificity helix, does not induce structural changes of the active site. Susceptibility to indolmycin inhibition, same mode of indole recognition, and high conservation of active-site residues imply a shared mechanism for tryptophan activation.

Role of active-site lysines in ATP binding and catalysis

The importance of positively charged active site lysine residues in stabilizing the negatively charged triphosphate oxygen atoms of ATP has been studied extensively in the case of BsTrpRS. Lysines 111 and 192 compete with the catalytic Mg^{2+} ion for stabilizing the

negative charge of the PPi leaving group, while Lys 195 interacts with a non-bridging alpha-phosphate oxygen as well as the oxygen atom bridging the alpha and beta phosphates. H_cTrpRS is missing lysines at analogous positions for both 111 and 195, the consequence of which is altered ATP configuration (bent instead of extended) and Mg^{2+}•ATP coordination. From the fully-liganded inhibited complex it is evident that H_{mt}TrpRS binds ATP in a conformation similar to that observed in all ATP-bound BsTrpRS structures with a catalytic metal forming electrostatic interactions with oxygen atoms from each phosphate group. Lysine 226 ($Lys192_{BS}$) competes with the metal for the same beta-phosphate oxygen, while Lys 229 ($Lys195_{BS}$) forms electrostatic and hydrogen bonding interactions with an alpha-phosphate oxygen atom. Both of these interactions mimic those observed in BsTrpRS. Indolmycin binding to BsTrpRS weakens lysine-ATP interactions while strengthening ATP-metal interactions. Part of a highly mobile loop, the positioning of Lys 111 varies depending on the ligands bound to the active site. The strength of the interaction with gamma-phosphate oxygen is weaker in the presence of indolmycin than tryptophanamide (and presumably tryptophan). This residue is conserved in H_{mt}TrpRS (Lys 145) but has great structural variation between the two monomers that make up the dimer in the crystallographic asymmetric unit. While neither lysine is close enough for direct interactions with ATP in the inhibited complex, our kinetic characterization of a K145A mutant shows that this residue contributes to the stability of the catalytic transition state as was observed for Lys 111 in BsTrpRS (20). Together, these data point to a shared role of active site lysines in the binding of ATP as well as the neutralization of negatively charged PPi leaving group following tryptophan activation between BsTrpRS and H_{mt}TrpRS. However, the contribution of Lys 145 to transition state stabilization of H_{mt}TrpRS is not as great as that of Lys 111 for BsTrpRS. The lack of additional structures for H_{mt}TrpRS showing conformational variation

prevents us from make conclusions on the possible parallel role of Lys 145 in the catalytic mechanism.

Overall structural agreement between H_{mt}TrpRS and BsTrpRS, but not H_cTrpRS

The inhibited H_{mt}TrpRS structure determined in this work is the only structure to date for a mitochondrial TrpRS enzyme. While it does not represent a catalytically-relevant state, it does allow us to make structural comparisons with BsTrpRS and H_cTrpRS, for which there are various structures deposited into the PDB. Superposition of the indolmycin-inhibited BsTrpRS and H_{mt}TrpRS structures gives an RMSD of 1.2 Å for 289 Cα-atom pairs. There is excellent agreement in the spatial positioning of the ligands within each active site (Fig. 19B). Comparison of these active sites, defined as residues within 6 Å of each ligand, revealed even greater structural similarity among active residues (0.5 Å RMSD). Similar comparison of the active sites of inhibited H_{mt}TrpRS and preTS BsTrpRS yielded an RMSD of 0.5 Å. Although the replacement of tryptophanamide with indolmycin in BsTrpRS results in weaker enzyme-ligand interactions, global structural changes are minimal. These two structures (preTS and inhibited) differ by 0.3 Å over 323 Cα-atom pairs (Fig. 19A).

As discussed in a previous section, H_cTrpRS uses N-terminal residues that are not conserved in prokaryotic or mitochondrial TrpRS enzymes to bind tryptophan. Additionally, the absence of two lysine residues involved in ATP binding to prokaryotic TrpRS results in H_cTrpRS binding an altered ATP configuration. Together, these differences result in an H_cTrpRS active site that greatly differs from that of BsTrpRS (3.0 Å RMSD) and H_{mt}TrpRS (2.6 Å RMSD). Superposition of the tryptophanamide indole moieties for the preTS H_cTrpRS and BsTrpRS structures illustrates the high degree of structural variation in the two active sites (Fig. 19C). It is immediately clear that, unlike for similar superpositions of H_{mt}TrpRS and BsTrpRS,

there is not good agreement in the placement of ligands relative to conserved HIGH and KMSKS signature elements; i.e. we cannot reasonably align all elements simultaneously (Fig. 19B, C). The greater structural similarity both overall (1.2 Å vs 5.0 Å RMSD) and at the active site (0.5 Å vs 2.6 Å RMSD), the utilization of conserved residues for indole recognition and ATP binding, and the shared mechanism for inhibition by indolmycin imply that the path to tryptophan activation employed by H_{mt}TrpRS better resembles that of BsTrpRS than H_cTrpRS.

Implications for tryptophanyl-5' AMP formation by H_{mt}TrpRS

Differences in the relative positioning of the tryptophan and ATP binding sites result in different conformers of tryptophanyl-5' AMP (TYM) occupying the BsTrpRS and H_cTrpRS active sites. The TYM bound to BsTrpRS is more extended, with the indole moiety CE3 atom being 1.6 Å further away from the 3'OH group than in the corresponding TYM of H_cTrpRS. Rigid-body fitting of TYM from H_cTrpRS into the H_{mt}TrpRS active site fitted by aligning its indole ring to that of indolmycin has the biggest difference in adenine/ribose placement compared to bound ATP (Fig. 20A). This conformer clashes with various residues including Gly 179 and Lys 215. When aligned to the adenine moiety of ATP this same conformer loses the interaction between Asp 167 and the indole nitrogen (Fig. 20B). Additionally, there are clashes with Gln 42 and Gln 164. H_{mt}TrpRS should hold onto the indole nitrogen during catalysis for continued assurance that the bound substrate is tryptophan. This appears to be the case for both H_cTrpRS and BsTrpRS as the enzyme-indole hydrogen bonding interactions are preserved in the pre-transition and product state structures of both enzymes. Rigid-body fitting of the BsTrpRS TYM product into the H_{mt}TrpRS active by superimposing either the indole or adenine rings maintains the Asp 167-indole nitrogen interaction (Fig. 20C, D). However, superimposition of the TYM indole moiety with that of indolmycin results in the loss of many of the observed H_{mt}TrpRS-ATP interactions,

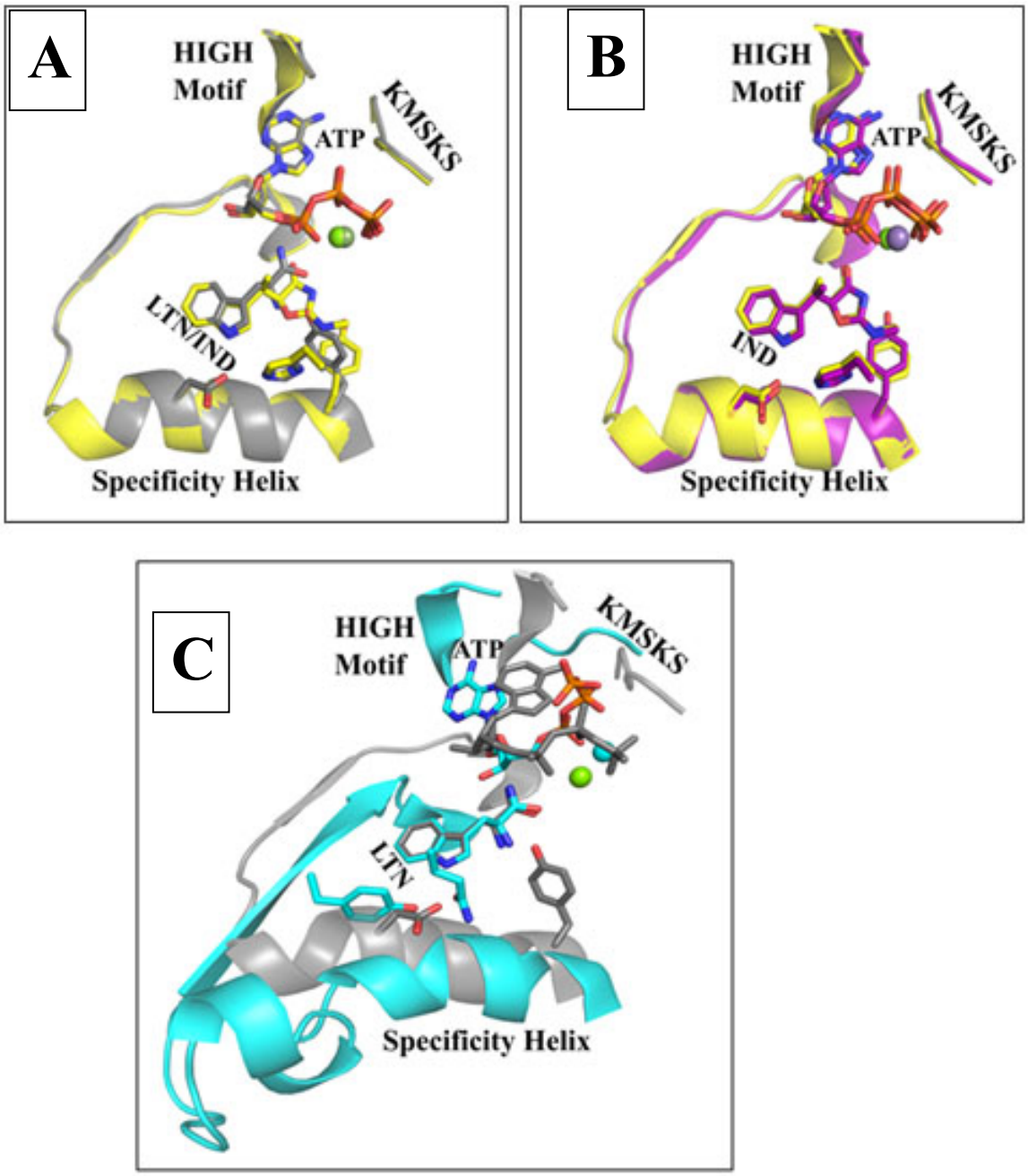

Figure 19: Comparison of BsTrpRS, H_cTrpRS and H_{mt}TrpRS active sites. A) Minor side-chain rearrangements and a shift in metal position (green spheres) accompany the replacement of tryptophanamide (LTN) in the preTS BsTrpRS structure (grey cartoon and sticks) for indolmycin (yellow cartoon and sticks). B) The active sites of H_{mt}TrpRS (purple cartoon and sticks) and BsTrpRS show great structural similarity in Cα atoms (0.5 Å RMSD), as conserved elements and bound ligands align well. C) The relative positions of LTN, ATP and Mg^{2+} in the H_cTrpRS active site (cyan cartoon, sticks and sphere) differs from that observed in BsTrpRS (grey).

including those with Asn 51 and Gln 42. Superimposition of the BsTrpRS TYM adenine moiety onto that of ATP maintains the Asp 167-indole interaction in addition to all but one of the H_{mt}TrpRS-AMP interactions observed in the inhibited complex without introducing steric clashes. This analysis suggests that H_{mt}TrpRS is likely to go from a preTS to product state via a transition mimicking that of BsTrpRS, with the TYM product adopting the more extended conformation observed in the BsTrpRS active site.

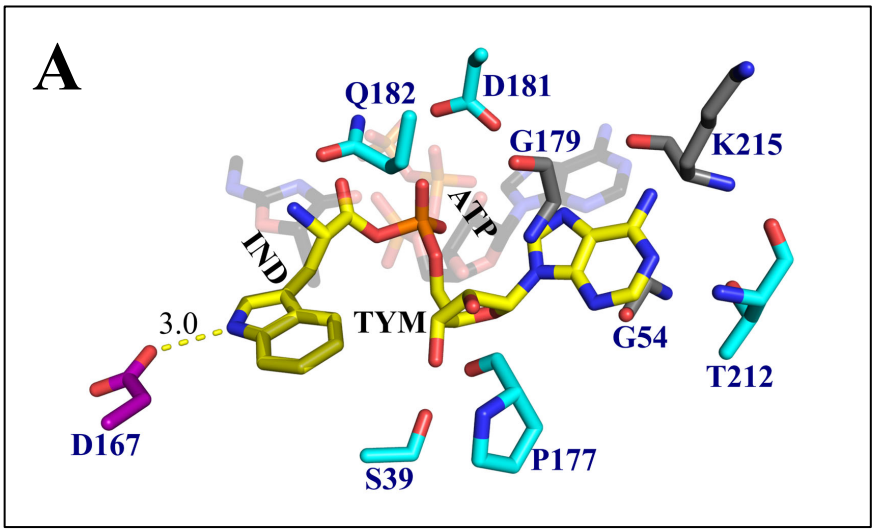

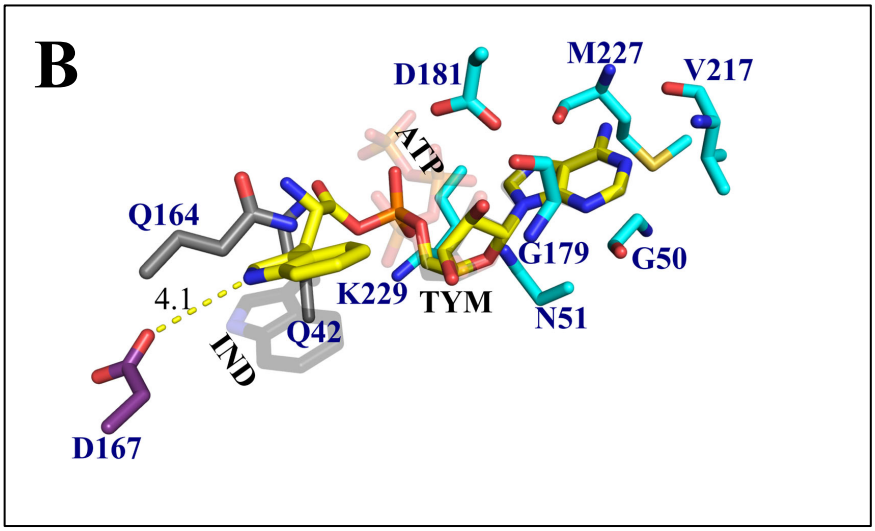

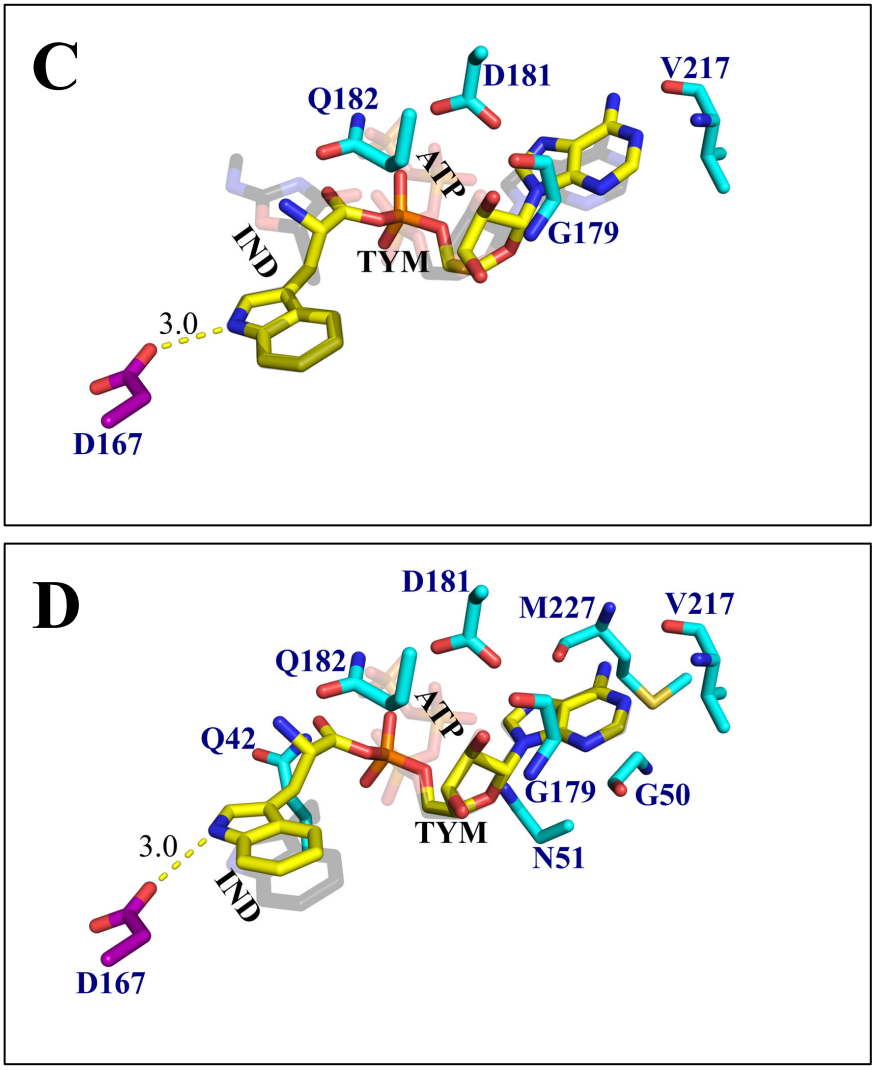

Figure 20: Rigid body modeling of TYM into H_{mt}TrpRS active site. The TYM (yellow sticks) product from H_cTrpRS (2QUJ) was modeled into the H_{mt}TrpRS active by superposition of indole (A) or adenine (B) moieties. Residues making hydrogen bonding contacts with TYM are shown in cyan while those that would clash are shown in grey. The more extended TYM conformer observed in BsTrpRS was similarly modeled (C, D). In all panels, Asp 167 is depicted in purple along with the distance to the NE1 atom and the original ATP/IND ligands are shown in the background.

Conclusion

In this work, we established conditions for heterologous expression of soluble, catalytically-active H_{mt}TrpRS in E. coli by co-expression with GroEL/ES chaperones. Our purification protocol routinely results in homogeneous samples in which 75 to 100% of the H_{mt}TrpRS molecules are competent for catalysis. We confirmed our hypothesis that conserved

elements, including Asp 167 and His 77, leave H_{mt}TrpRS vulnerable to inhibition by indolmycin. The 10^{-8} M inhibition constant is an order of magnitude weaker than that measured for BsTrpRS, consistent with K_M tryptophan values for the two enzymes. The 1.82 Å structure and the associated thermodynamic studies obtained by isothermal titration calorimetry validated our interpretation of the mechanism by which indolmycin inhibits BsTrpRS, specifically by simultaneously weakening enzyme-ATP and strengthening metal-ATP interactions to prevent metal activation. The structural data suggests that indolmycin binding should be tighter in the presence of Mg^{2+}•ATP. Isothermal titration calorimetry experiments validated this claim as pre-binding Mg^{2+}•ATP enhanced indolmycin binding to H_{mt}TrpRS ~80-fold. Interestingly, this potentiation effect could not be observed by differential scanning fluorimetry, where only indolmycin altered the thermal stability of H_{mt}TrpRS. The shift by ~9°C in the thermal transition to molten globule formation induced by indolmycin binding was independent of Mg^{2+}•ATP. Finally, this sole structure of H_{mt}TrpRS allowed us to determine that it employs conserved residues and structural elements to recognize the NE1 indole atom and to bind ATP in an extended conformation. Both of these features result in an active site arrangement mimetic of BsTrpRS but that varies substantially from that of H_cTrpRS. Together, work presented in this chapter imply a shared mechanism for tryptophan activation between H_{mt}TrpRS and BsTrpRS.

CHAPTER IV: CONCLUDING REMARKS AND FUTURE DIRECTIONS

Aminoacyl-tRNA synthetases are essential for accurate protein biosynthesis and the fidelity of the genetic code in all organisms. Divergent structural and mechanistic elements in aaRS enzymes across the three kingdoms of life make members of this enzyme superfamily attractive targets for novel anti-infective therapeutics. We were specifically interested in how the natural tryptophan analog indolmycin is able to exploit differences between prokaryotic and eukaryotic TrpRS enzymes such that it preferentially binds prokaryotic TrpRS 10^6-times more readily than eukaryotic homologs. The presented research i) provides a mechanistic basis for indolmycin inhibition; ii) accounts for the 10^3-fold tighter affinity that prokaryotic TrpRSs have for indolmycin over substrate tryptophan; iii) identifies the structural consequences of indolmycin binding; iv) accounts for the ability of eukaryotic cytosolic TrpRSs to evade inhibition by indolmycin; and v) establishes mitochondrial TrpRS enzymes as targets for inhibition by indolmycin via a shared mechanism with prokaryotic TrpRS. Ultimately, we hope this work will lay the foundation for rational design of novel anti-infective agents that exploit structural and mechanistic differences among cytosolic, mitochondrial and prokaryotic TrpRS enzymes such that these new compounds are maximally selective for prokaryotic TrpRS.

In Chapter II we uncovered the structural basis for the tight-binding inhibition of prokaryotic over eukaryotic cytosolic TrpRS enzymes by indolmycin as well as the 10^3-fold higher affinity for indolmycin over tryptophan observed for many prokaryotic TrpRS enzymes. Analysis of the structural rearrangements accompanying ligand binding to BsTrpRS allowed us

to identify subtle changes, including altered Mg^{2+} placement and coordination, which account for high-affinity inhibition by indolmycin. In order to experimentally confirm the role of metal "locking" in tight-binding indolmycin inhibition we propose conducting ITC experiments in which BsTrpRS pre-bound to either tryptophanamide or indolmycin is titrated with Mg^{2+}•ATP. As movement of the Mg^{2+} ion to assist in catalysis weakens the affinity of BsTrpRS for ATP in the transition state (V. Weinreb, unpublished result), if indolmycin prevents Mg^{2+} ion movement then we should not see weakened, but rather heightened ATP affinity in the presence of indolmycin compared to tryptophanamide.

DSF experiments confirmed the importance of Mg^{2+} in mediating stabilizing interactions between the oxazolinone moiety of indolmycin and ATP. While Mn^{2+} substitution for Mg^{2+} alters the kinetics of tryptophan activation, we did not examine the effects of this substitution on inhibition kinetics. Preliminary DSF experiments suggest that Mn^{2+} contributes comparably to Mg^{2+} in promoting the oxazolinone-ATP interaction; i.e. the presence of a divalent cation is more critical than the identity (Mn^{2+} vs Mg^{2+}). In addition to native enzyme, similar metal substitution experiments will be conducted using BsTrpRS variants bearing mutations to residues involved in long-range coupling to the catalytic metal ion. As discussed in Chapter II these BsTrpRS D1 switch variants showed altered ratios for tryptophan versus indolmycin selectivity. While extensive studies have been performed by the Carter group to uncover the kinetic and thermodynamic contributions of these residues, little has been done to study the structural effects of the D1 switch mutations. We have worked out the crystallization conditions for the ternary complexes with indolmycin and Mg (or $Mn)^{2+}$•ATP and collected datasets for a subset of the 15 combinatorial mutants. Structure determination and analysis is ongoing.

The robust stabilizing effect of indolmycin binding is considerably greater than that provided upon binding either tryptophan or ATP. While tryptophan alone is not enough to induce structural changes, high concentrations of ATP as well as simultaneous binding by ATP and tryptophan(amide) elicit induced-fit closing of the active site to form a pre-transition state. Indolmycin binding alone produces a structure that is more stable by 10°C than the closed preTS complex with tryptophanamide plus Mg^{2+}•ATP. This result suggests that indolmycin may promote global structural changes in the absence of ATP. In order to address this we are working to crystallize and determine the structure of BsTrpRS bound by indolmycin alone.

In Chapter III we determined that mitochondrial TrpRS enzymes are indeed susceptible to inhibition by indolmycin. Additionally, high-affinity binding is dependent on Mg^{2+}•ATP. Surprisingly, the potentiation of indolmycin binding by Mg^{2+}•ATP was not detected by DSF. In fact, we were unable to detect changes in the thermal stability of H_{mt}TrpRS in response to binding of any ligand other than indolmycin. While the thermodynamic cycle revealed a stabilizing interaction between the oxazolinone moiety and Mg^{2+}•ATP, we do not have experimental data showing the dependence of this interaction on the metal ion for H_{mt}TrpRS. This requires additional isothermal titration experiments in which we determine the dissociation constant for both indolmycin and tryptophanamide in the presence of bound ATP (metal free).

Despite differences in binding determinants and structural consequences of tryptophan binding, both BsTrpRS and H_cTrpRS bind tryptophan with comparable binding affinities of ~2 uM. In contrast, H_{mt}TrpRS, which has a high degree of similarity between active site residues with BsTrpRS, binds both tryptophan and indolmycin about an order of magnitude more weakly than does BsTrpRS. Examination of the tryptophan-binding pocket for the three enzymes did not identify any obvious reason for the weaker binding to H_{mt}TrpRS. Residues in this area are highly

conserved between BsTrpRS and H_{mt}TrpRS, as they use the same determinants for tryptophan recognition. The only difference we found that may account for the observed differential binding affinities is the replacement of a methionine in the specificity helix for a glutamine in H_{mt}TrpRS. In BsTrpRS the methionine sulfur atom is in position to interact with the aromatic ring of substrate tryptophan. To test if sulfur-aromatic interactions contribute to tryptophan binding I propose making and characterizing the tryptophan-binding behavior of M129Q BsTrpRS and Q164M H_{mt}TrpRS variants. If sulfur-aromatic interactions promote tryptophan binding I would expect the BsTrpRS mutant to have reduced affinity while the H_{mt}TrpRS mutant has increased affinity for tryptophan.

Shared characteristics between H_{mt}TrpRS and BsTrpRS include a mimicked ATP binding conformation as well as ATP-metal coordination. Additionally, there is a distinct lack of metal-H_{mt}TrpRS interactions which raises questions about metal-enzyme coupling. Specifically, is the catalytic metal coupled to a site remote from the H_{mt}TrpRS active site as has been demonstrated for the BsTrpRS enzyme? The D1 switch identified in BsTrpRS consists of Ile 4, Phe 26, Tyr 33, and Phe 37. Re-packing of these side-chains is coupled to movement of the metal into a catalytically-competent position and D1-Mg^{2+} coupling accounts for the increased tryptophan specificity over tyrosine of BsTrpRS primarily through effects on kcat (21, 65). Structure-based sequence alignment of the inhibited BsTrpRS and H_{mt}TrpRS structures identify the analogous H_{mt}TrpRS residues as Val 37, Trp 59, Tyr 66, and Tyr 71. Additional structures along the catalytic path are needed to identify side-chain rearrangements (re-packing) that occur as a consequence of substrate binding and catalysis in H_{mt}TrpRS. To that end, we are continuing our efforts to obtain X-ray crystal structures of H_{mt}TrpRS along its catalytic path.

Finally, although indolmycin targets H_{mt}TrpRS it does so ~40-times weaker than BsTrpRS. This selectivity ratio is higher than many commonly used therapeutics. The fact that there is a difference suggests that it may be possible to design novel compounds with increased selectivity for prokaryotic over mitochondrial TrpRS enzymes. In silico screening of a virtual compound library may identify such compounds, which can then be tested for inhibition of H_cTrpRS, H_{mt}TrpRS and BsTrpRS.

REFERENCES

1. Baroud M*, et al.* (2013) Underlying mechanisms of carbapenem resistance in extended-spectrum beta-lactamase-producing Klebsiella pneumoniae and Escherichia coli isolates at a tertiary care centre in Lebanon: role of OXA-48 and NDM-1 carbapenemases. *International journal of antimicrobial agents* 41(1):75-79.

2. Abraham EP & Chain E (1988) An enzyme from bacteria able to destroy penicillin. 1940. *Reviews of infectious diseases* 10(4):677-678.

3. Voulgari E, Poulou A, Koumaki V, & Tsakris A (2013) Carbapenemase-producing Enterobacteriaceae: now that the storm is finally here, how will timely detection help us fight back? *Future microbiology* 8(1):27-39.

4. Gao W*, et al.* (2010) Two novel point mutations in clinical Staphylococcus aureus reduce linezolid susceptibility and switch on the stringent response to promote persistent infection. *PLoS pathogens* 6(6):e1000944.

5. Pillai SK*, et al.* (2002) Linezolid resistance in Staphylococcus aureus: characterization and stability of resistant phenotype. *The Journal of infectious diseases* 186(11):1603-1607.

6. Floyd JL, Smith KP, Kumar SH, Floyd JT, & Varela MF (2010) LmrS is a multidrug efflux pump of the major facilitator superfamily from Staphylococcus aureus. *Antimicrobial agents and chemotherapy* 54(12):5406-5412.

7. Piddock LJ (2006) Clinically relevant chromosomally encoded multidrug resistance efflux pumps in bacteria. *Clinical microbiology reviews* 19(2):382-402.

8. Tangden T, Adler M, Cars O, Sandegren L, & Lowdin E (2013) Frequent emergence of porin-deficient subpopulations with reduced carbapenem susceptibility in ESBL-producing Escherichia coli during exposure to ertapenem in an in vitro pharmacokinetic model. *The Journal of antimicrobial chemotherapy* 68(6):1319-1326.

9. Fair RJ & Tor Y (2014) Antibiotics and bacterial resistance in the 21st century. *Perspectives in medicinal chemistry* 6:25-64.

10. Nakama T, Nureki O, & Yokoyama S (2001) Structural basis for the recognition of isoleucyl-adenylate and an antibiotic, mupirocin, by isoleucyl-tRNA synthetase. *The Journal of biological chemistry* 276(50):47387-47393.

11. Vogeley L, Palm GJ, Mesters JR, & Hilgenfeld R (2001) Conformational change of elongation factor Tu (EF-Tu) induced by antibiotic binding. Crystal structure of the complex between EF-Tu.GDP and aurodox. *The Journal of biological chemistry* 276(20):17149-17155.

12. Kirillov S*, et al.* (1997) Purpuromycin: an antibiotic inhibiting tRNA aminoacylation. *RNA (New York, N.Y.)* 3(8):905-913.

13. Ribas de Pouplana L, Frugier M, Quinn CL, & Schimmel P (1996) Evidence that two present-day components needed for the genetic code appeared after nucleated cells separated from eubacteria. *Proceedings of the National Academy of Sciences of the United States of America* 93(1):166-170.

14. Sutherland R*, et al.* (1985) Antibacterial activity of mupirocin (pseudomonic acid), a new antibiotic for topical use. *Antimicrobial agents and chemotherapy* 27(4):495-498.

15. Burbaum JJ & Schimmel P (1991) Structural relationships and the classification of aminoacyl-tRNA synthetases. *The Journal of biological chemistry* 266(26):16965-16968.

16. Ibba M & Soll D (2000) Aminoacyl-tRNA synthesis. *Annu Rev Biochem* 69:617-650.

17. Retailleau P, Weinreb V, Hu M, & Carter CW, Jr. (2007) Crystal structure of tryptophanyl-tRNA synthetase complexed with adenosine-5' tetraphosphate: evidence for distributed use of catalytic binding energy in amino acid activation by class I aminoacyl-tRNA synthetases. *J Mol Biol* 369(1):108-128.

18. Williams TL, Yin WY, & Carter CW, Jr. (2015) Selective Inhibition of Bacterial Tryptophanyl-tRNA Synthetases by Indolmycin is Mechanism-Based. *The Journal of biological chemistry*.

19. Werner RG, Thorpe LF, Reuter W, & Nierhaus KH (1976) Indolmycin inhibits prokaryotic tryptophanyl-tRNA ligase. *Eur J Biochem* 68(1):1-3.

20. Weinreb V, Li L, Campbell CL, Kaguni LS, & Carter CW, Jr. (2009) Mg2+-assisted catalysis by B. stearothermophilus TrpRS is promoted by allosteric effects. *Structure* 17(7):952-964.

21. Weinreb V, Li L, & Carter CW, Jr. (2012) A master switch couples Mg(2)(+)-assisted catalysis to domain motion in B. stearothermophilus tryptophanyl-tRNA Synthetase. *Structure* 20(1):128-138.

22. Retailleau P*, et al.* (2003) Interconversion of ATP binding and conformational free energies by tryptophanyl-tRNA synthetase: structures of ATP bound to open and closed, pre-transition-state conformations. *J Mol Biol* 325(1):39-63.

23. Shen N*, et al.* (2008) Catalytic mechanism of the tryptophan activation reaction revealed by crystal structures of human tryptophanyl-tRNA synthetase in different enzymatic states. *Nucleic Acids Res* 36(4):1288-1299.

24. Zhou M, Dong X, Shen N, Zhong C, & Ding J (2010) Crystal structures of Saccharomyces cerevisiae tryptophanyl-tRNA synthetase: new insights into the mechanism of tryptophan activation and implications for anti-fungal drug design. *Nucleic Acids Res* 38(10):3399-3413.

25. Yang XL*, et al.* (2007) Functional and crystal structure analysis of active site adaptations of a potent anti-angiogenic human tRNA synthetase. *Structure* 15(7):793-805.

26. Ilyin VA*, et al.* (2000) 2.9Å crystal structure of ligand-free tryptophanyl-tRNA synthetase: Domain movements fragment the adenine nucleotide binding site. *Protein Science* 9(2):218-231.

27. Yu Y*, et al.* (2004) Crystal structure of human tryptophanyl-tRNA synthetase catalytic fragment: insights into substrate recognition, tRNA binding, and angiogenesis activity. *The Journal of biological chemistry* 279(9):8378-8388.

28. Jorgensen R, Sogaard TM, Rossing AB, Martensen PM, & Justesen J (2000) Identification and characterization of human mitochondrial tryptophanyl-tRNA synthetase. *The Journal of biological chemistry* 275(22):16820-16826.

29. Ogilvie A, Wiebauer K, & Kersten W (1975) Inhibition of leucyl-transfer ribonucleic acid synthetasymol. *The Biochemical journal* 152(3):511-515.

30. Konrad I & Roschenthaler R (1977) Inhibition of phenylalanine tRNA synthetase from Bacillus subtilis by ochratoxin A. *FEBS Lett* 83(2):341-347.

31. Kanamaru T*, et al.* (2001) In vitro and in vivo antibacterial activities of TAK-083, an agent for treatment of Helicobacter pylori infection. *Antimicrobial agents and chemotherapy* 45(9):2455-2459.

32. Werner RG & Reuter W (1979) Interaction of indolmycin in the metabolism of tryptophan in rat liver. *Arzneimittel-Forschung* 29(1):59-63.

33. Studier FW (2005) Protein production by auto-induction in high density shaking cultures. *Protein expression and purification* 41(1):207-234.

34. Fersht AR*, et al.* (1975) Active site titration and aminoacyl adenylate binding stoichiometry of aminoacyl-tRNA synthetases. *Biochemistry* 14(1):1-4.

35. Francklyn CS, First EA, Perona JJ, & Hou YM (2008) Methods for kinetic and thermodynamic analysis of aminoacyl-tRNA synthetases. *Methods (San Diego, Calif.)* 44(2):100-118.

36. Schneider CA, Rasband WS, & Eliceiri KW (2012) NIH Image to ImageJ: 25 years of image analysis. *Nature methods* 9(7):671-675.

37. SAS (2013) JMP: The Statistical Discovery Software (SAS Institute, Cary, NC), 9.

38. Kabsch W (2010) XDS. *Acta Crystallogr D Biol Crystallogr* 66(Pt 2):125-132.

39. Adams PD*, et al.* (2010) PHENIX: a comprehensive Python-based system for macromolecular structure solution. *Acta Crystallogr D Biol Crystallogr* 66(Pt 2):213-221.

40. Emsley P, Lohkamp B, Scott WG, & Cowtan K (2010) Features and development of Coot. *Acta Crystallogr D Biol Crystallogr* 66(Pt 4):486-501.

41. Cleland WW & Northrop DB (1999) Energetics of substrate binding, catalysis, and product release. *Methods Enzymol* 308:3-27.

42. Doublié S (1993) 2.9 Å Crystal Structure of *Bacillus stearothermophilus* Tryptophanyl-tRNA Synthetase Complexed to its Adenylate, Tryptophanyl-5'AMP. Ph. D. (University of North Carolina at Chapel Hill).

43. Retailleau P*, et al.* (2001) High resolution experimental phases for Tryptophanyl-tRNA synthetase (TrpRS) complexed with Tryptophanyl-5'AMP. *Acta Crystallographica* D57:1595-1608.

44. Yin Y (1995) Crystallographic study of Bacillus stearothermophilus tryptophanyl-tRNA synthetase in its catalytic reaction. PhD (University of North Carolina at Chapel Hill).

45. Calvin M, Hermans J, Jr., & Scheraga HA (1959) Effect of Deuterium on the Strength of Hydrogen Bonds. *J. Chem. Phys.* 81:5048-5050.

46. Matulis D, Kranz JK, Salemme FR, & Todd MJ (2005) Thermodynamic Stability of Carbonic Anhydrase: Measurements of Binding Affinity and Stoichiometry Using Thermofluor. *Biochemistry* 44:5258-5266.

47. Niesen FH, Berglund H, & Vedadi M (2007) The use of differential scanning fluorimetry to detect Ligand interactions that promote protein stability. *Nature Protocols* 2(9):2212-2221.

48. Weber PC, Wendoloski JJ, Pantoliano MW, & Salemme FR (1992) Crystallographic and Thermodynamic Comparison of Natural and Synthetic Ligands Bound to Streptavidin. *Journal of the American Chemical Society* 114:3197-3200.

49. Jencks WP (1981) On the attribution and additivity of binding energies. *Proc. Nat! Acad. Sci. USA* 78(7 (July)):4046-4050.

50. Kapustina M, Weinreb V, Li L, Kuhlman B, & Carter CW, Jr. (2007) A conformational transition state accompanies tryptophan activation by B. stearothermophilus tryptophanyl-tRNA synthetase. *Structure* 15(10):1272-1284.

51. Laowanapiban P, *et al.* (2009) Independent saturation of three TrpRS subsites generates a partially assembled state similar to those observed in molecular simulations. *Proceedings of the National Academy of Sciences of the United States of America* 106(6):1790-1795.

52. Kitabatake M, *et al.* (2002) Indolmycin resistance of Streptomyces coelicolor A3(2) by induced expression of one of its two tryptophanyl-tRNA synthetases. *The Journal of biological chemistry* 277(26):23882-23887.

53. Hurdle JG, O'Neill AJ, & Chopra I (2004) Anti-staphylococcal activity of indolmycin, a potential topical agent for control of staphylococcal infections. *The Journal of antimicrobial chemotherapy* 54(2):549-552.

54. Vecchione JJ & Sello JK (2009) A novel tryptophanyl-tRNA synthetase gene confers high-level resistance to indolmycin. *Antimicrobial agents and chemotherapy* 53(9):3972-3980.

55. Ali KS (2002) Bascillus stearothermophilus tryptophanyl-tRNA synthetase: mutations leading to indolmycin resistance.

56. Gangjee A, Vasudevan A, Queener SF, & Kisliuk RL (1996) 2,4-diamino-5-deaza-6-substituted pyrido[2,3-d]pyrimidine antifolates as potent and selective nonclassical inhibitors of dihydrofolate reductases. *Journal of medicinal chemistry* 39(7):1438-1446.

57. Smith C & Teitler M (1999) Beta-blocker selectivity at cloned human beta 1- and beta 2-adrenergic receptors. *Cardiovascular drugs and therapy / sponsored by the International Society of Cardiovascular Pharmacotherapy* 13(2):123-126.

58. Yang XL, *et al.* (2003) Crystal structures that suggest late development of genetic code components for differentiating aromatic side chains. *Proceedings of the National Academy of Sciences of the United States of America* 100(26):15376-15380.

59. Varga ZV, Ferdinandy P, Liaudet L, & Pacher P (2015) Drug-induced mitochondrial dysfunction and cardiotoxicity. *American journal of physiology. Heart and circulatory physiology*:ajpheart.00554.02015.

60. Lewis W, Simpson JF, & Meyer RR (1994) Cardiac mitochondrial DNA polymerase-gamma is inhibited competitively and noncompetitively by phosphorylated zidovudine. *Circulation research* 74(2):344-348.

61. Kalghatgi S, *et al.* (2013) Bactericidal antibiotics induce mitochondrial dysfunction and oxidative damage in Mammalian cells. *Science translational medicine* 5(192):192ra185.

62. Winn MD, *et al.* (2011) Overview of the CCP4 suite and current developments. *Acta Crystallogr D Biol Crystallogr* 67(Pt 4):235-242.

63. Lee B & Richards FM (1971) The interpretation of protein structures: estimation of static accessibility. *J Mol Biol* 55(3):379-400.

64. Fersht AR (1987) Dissection of the structure and activity of the tyrosyl-tRNA synthetase by site-directed mutagenesis. *Biochemistry* 26(25):8031-8037.

65. Weinreb V*, et al.* (2014) Enhanced Amino Acid Selection in Fully Evolved Tryptophanyl-tRNA Synthetase, Relative to Its Urzyme, Requires Domain Motion Sensed by the D1 Switch, a Remote Dynamic Packing Motif. *The Journal of biological chemistry* 289(7):4367-4376.